Politecnico di Torino

Master of science in Mechanical Engineering

Master's Degree Thesis

Scale-up of a solar-driven modular desalination device for remote areas

Academic Supervisor:
Pietro Asinari

Research Advisor:
Matteo Morciano

Candidate:
Gabriele Baiamonte

Academic Year 2018-2019

Alla mia famiglia,
la cosa che amo di più al mondo.
Ad i miei amici,
del quale non potrei mai fare a meno.
A questa vita imprevendibile,
che non vedo l'ora di continuare a percorrere.

Contents

Abstract

More than 700 million people around the world suffer from severe water scarcity. Desalination is one of the most promising solution to contrast this problem. In particular, passive desalination is considered the most suitable expedient to mitigate water scarcity where this problem is striking the most, namely in remote areas. These passive technologies, although historically considered energy-intensive, are particularly appealing when powered by renewable sources such as solar energy. The goal of this thesis is then to develop a scaled-up version of the innovative passive solar high-yield seawater desalination technology, developed at Politecnico di Torino. The latter is able to operate without the use of any active components and it is based on a smart combination of low-cost materials. The work is organized according to different sections. First, an overview of the most common active desalination techniques operating at industrial level is addressed. Subsequently, the state-of-the-art of technologies able to passively produce freshwater is reported. Among these, the scaled-up version of the proposed passive device shows the best performance relying on a multi-stage process that enables latent heat recovery. Then, the design and prototyping activities have been extensively discussed. The guidelines imposed by a modern world wide contest (namely *Oman Humanitarian Desalination Challenge*) have been followed to develop the device. In detail, a cross-flow configuration has been exploited to overcome the limited capillary-driven water transport on each hydrophilic layer exasperated by the increased size of the unit. Numerical simulations are carried out by means of COMSOL Multiphysics® software to figure out the best configuration. Finally, results of an extensive in-field experimental campaign, conducted on the roof of Politecnico di Torino, are reported and discussed. The latter are in agreement with the model predictions obtained by the already developed theoretical approach. The described promising results lead the proposed desalination technology one step closer towards public distribution.

List of Figures

List of Tables

Nomenclature

Symbol	Description
a	Water activity
a_c	Water activity at the condenser
a_e	Water activity at the evaporator
c	Molar concentration
c_0	Initial molar concentration
d	Membrane thickness
d_{air}	Air layer thickness
$d_{air,top}$	Air layer thickness between PMMA and TiNOX
D_{eff}	Effective diffusion coefficient
d_{gap}	Gap thickness between evaporator & condenser
d_m	Hydrophobic membrane thickness
d_{PMMA}	PMMA panel thickness
D_{wa}	Molecular diffusion coefficient of vapor
$D_{wa,air}$	Molecular diffusion coefficient of vapor in air layer
D_{wK}	Knudsen diffusion coefficient
ε_m	Membrane porosity
ϕ_{rel}	Relative humidity
h	Convective heat transfer coefficient
$h_{conv,top}$	Convective heat transfer coefficient at top surface
h_{top}	Total convective heat transfer coefficient at top surface
Δh_{LV}	Latent heat of vaporization
η	Device efficiency
J	Produced specific mass flow rate of freshwater
K	Permeability
k_{air}	Air thermal conductivity
$k_{microfiber}$	Microfiber thermal conductivity
$k_{eff,g}$	Thermal conductivity in the gap between air and membrane
k_{gap}	Gap between evaporator and condenser thermal conductivity
k_{hphi}	Hydrophilic membrane thermal conductivity
k_{PMMA}	PMMA thermal conductivity
k_{PTFE}	PTFE thermal conductivity
λ	Lagrangian multiplier
M_{H_2O}	Water molar mass
M_{NaCl}	Sodium chloride molar mass
μ_w	Chemical potential of water vapour
$\mu_{w,pure}$	Chemical potential of pure water vapour
N	Distilled flow rate expressed in $[mol\ s^{-1}]$
N_{ion}	Particle's number of ions

P	Total pressure
p_a	Arithmetic mean of the air partial pressure
p_v	Water vapor pressure
Δp_v	Difference in water vapor pressure
ρ_{max}	Maximum amount of water for 100% relative humidity
$Q_{boundary}$	Boundary heat source
Q_{solar}	Solar heat flux
Q'_{solar}	Solar heat flux diminished from the optical losses
q_1	Lateral specific heat loss
R	Ideal gas constant
r	Average pore radius of the membrane
T	Temperature
T_C	Temperature at the condenser
T_E	Temperature at the evaporator
τ	Tortuosity
x_w	Water mole fraction
Y	Salt mass fraction
Y_C	Salt mass fraction at the condenser
Y_E	Salt mass fraction at the evaporator

Table 1: Symbols

Glossary

Acronym	Description
AD	Adsorption Desalination
AGMD	Air gap Membrane Distillation
BMED	Bipolar Membranes Electrodyalisis
CB	Carbon Black
CP	Concentration Polarization
DCMG	Direct contact Membrane Distillation
ED	Electrodyalisis
EDR	Electrodyalisis reversal
FM	Freezing-Melting
FO	Forward Osmosis
FO-LPRO	Forward Osmosis-Low Pressure Reverse Osmosis
LDPE	Low-Density Polyethylene
MD	Membrane Distillation
MED	Multi-Effect Diffusion
MED	Multi-Effect Distillation
MEDAD	Multi-Effect Distillation Adsorption Desalination
MSF	Multi-Stage Flash
MVC	Mecanical Vapour Compression
NESMD	Nanophotonics-enabled Solar Membrane Distillation
NTU	Nephelometric Turbidity Unit
OHDC	Oman Humanitarian Desalination Challenge
PP	Polypropylene
PV	Photovoltaic
RE	Recovery Efficency
RO	Reverse Osmosis
RR	Recovery Rate
SGMD	Sweeping gas Membrane Distillation
SWRO	Seawater Reverse Osmosis
TVC	Thermal Vapour Compression
TDS	Total Dissolved Solids
TW	Tilted Wick
VMD	Vacuum Membrane Distillation
WHO	World Health Organization
ZTIMD	Zero Thermal Energy Input Membrane Distillation

Table 2: Acronyms

Chapter 1

Introduction

1.1 Water scarcity around the world

Nowadays technology develops rapidly aiming to make everyone's life easier, however, some basic historic issue for mankind still remain unresolved. One of the most striking ones, is the availability of water all around the world. Latest data shows the situation is far from improving, rather it looks always more concerning. Climate change greatly influences water scarcity, causing warming and droughts in many areas [1]. One third of the world's population faces "high baseline water stress", whereas one quarter faces even "extremely high baseline water stress" [2]. These terms have been used by hydrologist to define the lack of water in whole regions, by using the "population-water equation". It simply consists of comparing the available water resources per year with the population dwelling the same area. Typically when the annual available water per person is below 1,700 m^3, experts already consider people experiencing water stress. When such threshold drops below 1,000 m^3 or even 500 m^3, people are experiencing high water scarcity or extremely high water scarcity [3]. A definite solution still remains far from reality, as the number of people lacking the right amount of water per day is still growing. Forecast do not leave space to much hope for an improvement, unless the world scenario will soon change drastically for the better. In figure 1.1, a study showing results regarding the last 50 years and future estimations is depicted [4].

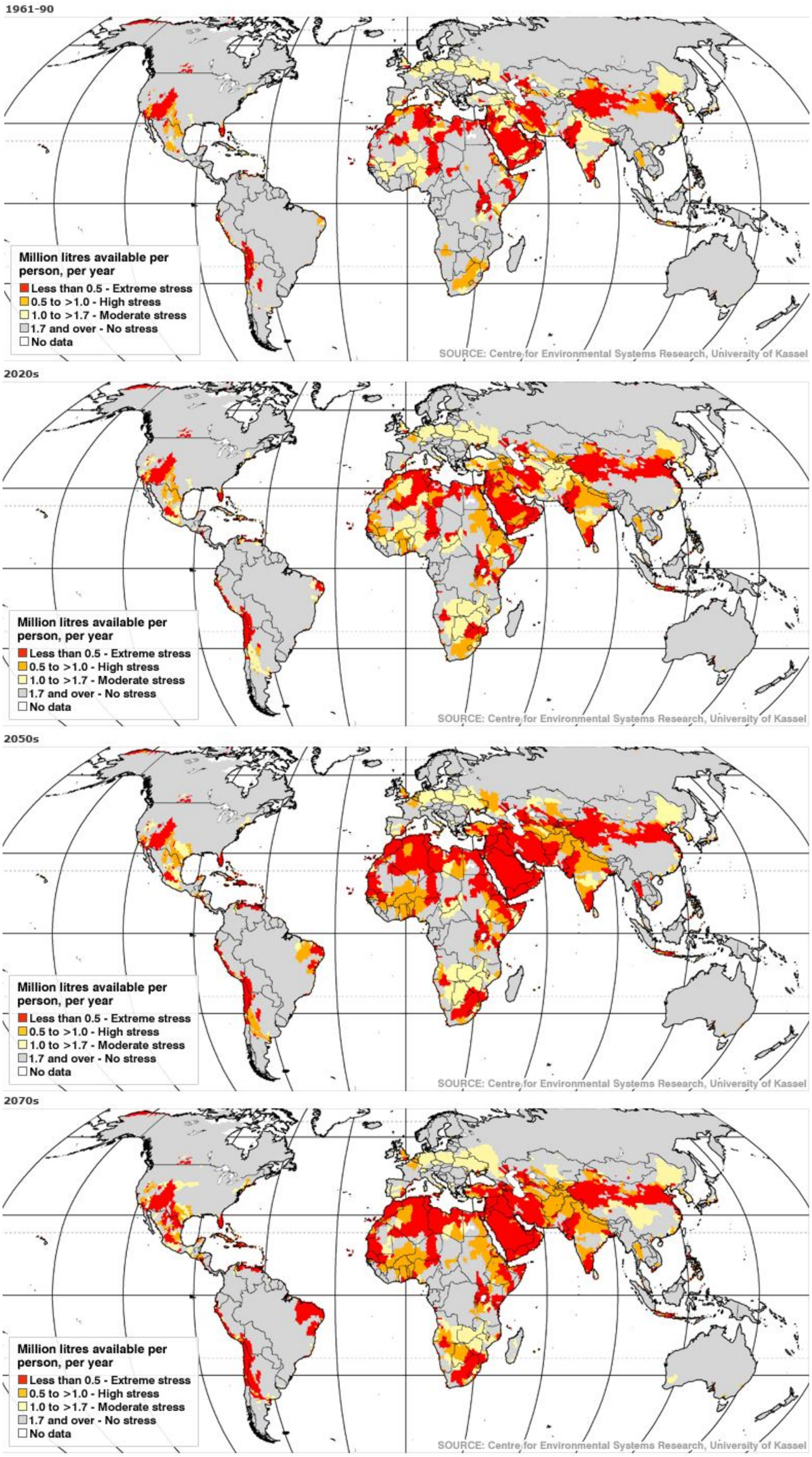

Figure 1.1: World Water Stress Projection in a time span of 100 years [4]

Water scarcity can occur due many different causes. These can be divided into two macro-groups, economical and physical causes. Whenever a country is not able to satisfy the water population demand due of a lack of natural resources, it is said there is a *physical water scarcity*, whereas a country that has the right amount of resources, but it still can't provide enough water due a poor management of them foresees an *economical water scarcity*. Both cases implement an unsatisfied high water demand, which is not only covering the drinkable water, but also the one needed for agriculture, industries and personal uses.

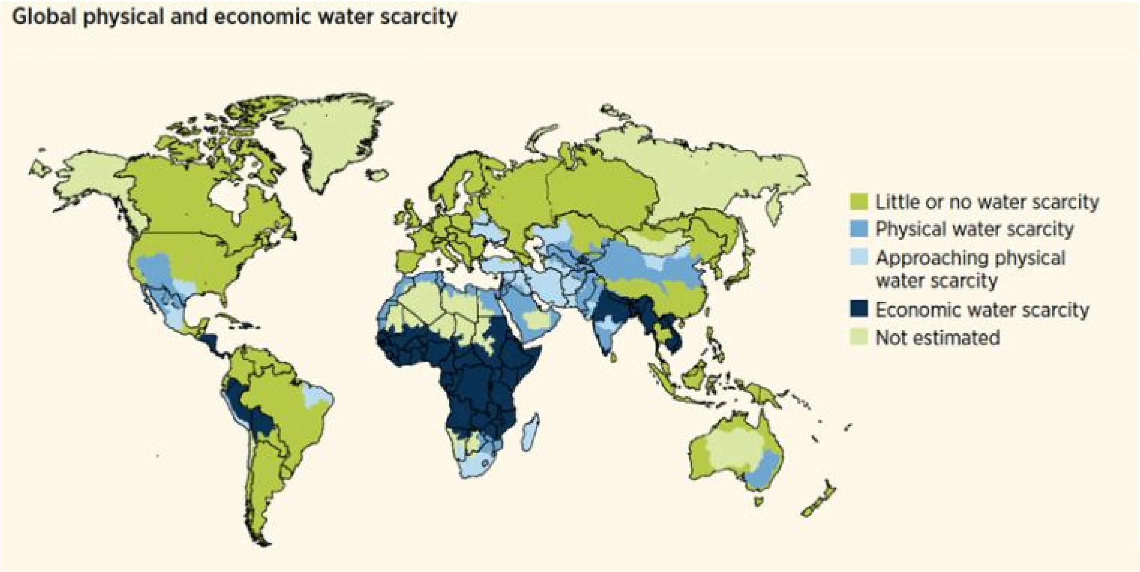

Figure 1.2: World division in physical and economical water scarcity [3]

1.1.1 Economical water scarcity

As shown in figure 1.2 large parts of Africa, north India, Peru and Bolivia suffer from this phenomenon. Economical water scarcity is in fact often linked to high poverty condition. It is mostly caused by a lack of infrastructure and workforce. These countries would in fact have the right resources to meet the population water needs within 2025 [5], but a lot of investments should be made on water projects and infrastructures at enormous social and economical costs.

1.1.2 Physical water scarcity

Physical water scarcity is met when there is no primary resource to satisfy the population needs. The regions more affected are arid regions, which mostly spread along the equator. Physical water scarcity can be further categorized into two smaller groups: demand-driven scarcity, which causes *water stress* and population-driven scarcity, which causes *water shortage* [6]. The first is accounted by computing the annual withdrawal from the natural resources, the second is computed by the "Falkenmark water stress index", which describes the crowding of people sharing a single water source [7]. While it is more difficult to make forecast for economical water scarcity (it depends on socio-political aspects), it is easier to do it for physical water scarcity. Factors as the demographic growth and the climate change are reliable reasons to believe this issue will just get more problematic, as figure 1.1 attests. In many water resources around the world it is extracted water at an higher rate than the time to regenerate it [8]; it thus seems more impelling to find solutions to this radical problem.

1.2 Water supply

To satisfy the world water demand, it is necessary to employ the so-called *water resources*. It is defined, as a water resource, any arrangement of water, regardless of its actual technical and economic exploitation. The total water resource on earth accounts for ~1.4 billion cubic kilometers. As table 1.1 testifies, ~97% of the total water available comes from the sea. Of the remaining ~3%, almost all of it is inaccessible because in the form of polar ice, deep ground water and vapor in the atmosphere. Only ~0.027% is then available to humans and other living organisms [9].

Source	**Phase**	**Volume** *[1000 km^3]*	**Volume %** *[global %]*	**Fresh Water Volume %** *[global %]*
Atmosphere	Gas	12,900	0.001	0.04
Earth	Liq. & Sol.	47,965	3.459	99.96
Ocean	Liq. & Sol.	1,338,000	96.54	/

Table 1.1: How water resources are spread around the world [10].

Source	**Phase**	**Volume** *[1000 km^3]*	**Volume %** *[global %]*	**Fresh Water Volume %** *[global %]*
Biological tissues	Liq.	1.12	<0.0001	0.003
Rivers	Liq.	2.12	0.0002	0.03
Swamps	Liq.	11.47	0.0008	0.04
Salty lakes	Liq.	85.4	0.007	/
Fresh lakes	Liq.	91	0.007	0.26
Permafrost	Sol.	300	0.022	0.86
Soil	Liq.	16.5	0.001	0.05
Fresh groundwater	Liq.	10,530	0.76	30.1
Salty groundwater	Liq.	12,870	0.93	/
Polar ice	Sol.	24,060	1.74	68.6

Table 1.2: How earth water is spread in natural resources [10].

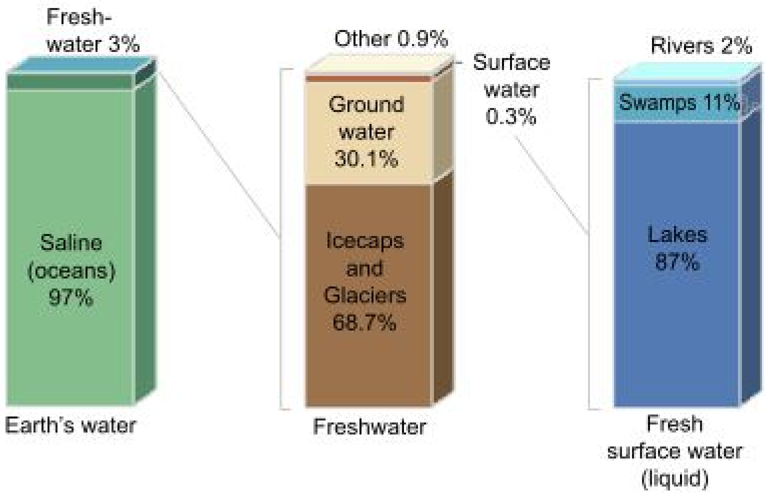

Figure 1.3: Earth's water distribution [10]

Looking at table 1.2 it can be noticed water supply can be mainly processed by using water resources of suitable quality, coming from the ground or underground level. Depending on the type and nature of the water resource to be used and according to the methods and times of operation, appropriate works must be prepared, amongst which: intake works, derivation works, accumulation works, wells, etc. Water coming from the ground level is usually taken from rivers, streams or lakes. Water can also be taken from the underground and in this case, it is called *groundwater*. Most of the groundwater present on the planet, undergoes a closed cycle called *hydrologic cycle*. This cycle comes in different steps where water changes phase twice, by evaporation and by condensation. The process of vapor formation is activated by solar energy, while the formation of outflows are initiated by essentially the gravitational force. The hydrologic cycle is important, amongst many things, to distinguish the *renewable water resource* from the *non-renewable water resource*. It is considered as a renewable water resource, whatever water resource is able to regenerate in a short time span; a good example would then be all the water participating to the hydrologic cycle, so all the ground level water and the shallow groundwater. On the other hand, the non-renewable water resources are all the water resources able to regenerate, but in a long time span; a good example are polar ice and deep groundwater [11].

The part of a water resource useful to the living of organisms is called *water reserve*. Therefore, just a very small part of the water resources can be so considered. Many researches have carried on new studies and ideas in order to expand the concept of water reserve to a wider piece of the world water resources [12, 13]; the most commons are groundwater extraction and desalination. However, extracting groundwater usually results inconvenient, as it implies the use of very expensive pumps. Thus, the most popular field of research is the development of desalination system. Some recent new discoveries have lead these type of techniques to become more affordable and efficient on a global scale.

1.3 Water desalination systems

Desalination is the process through which minerals, most commonly salt, are removed from water. When the goal is to make drinkable water, desalination must be designed so to produce water with a contamination level below the World Health Organization's drinking water limit of 500 ppm [14], otherwise it can also stand to lower standards. Nowadays, desalination systems are responsible for 1% of the world potable water [15], even more is produced, accounting also for systems finalized to agriculture purposes. This technique is not a primary water source yet, because it historically pollutes and it requires an high energy consumption (in high-pressure reverse osmosis plant, on average, to supply 300,000 people in a day, 31 MW are required [16]), but with the invention of new technologies, it seems a more and more promising viable water supply alternative. In 2015 more than $97.5 \times 10^6\ m^3 day^{-1}$ were produced by desalination systems, and this number is expected to increase till 192×10^6 $m^3 day^{-1}$ by 2050 [17, 18]. In some countries like Kuwait and Qatar, already 100% of the water comes from desalination. To counteract the environmental issue, integration of renewable energy into desalination plants is also becoming more diffuse.

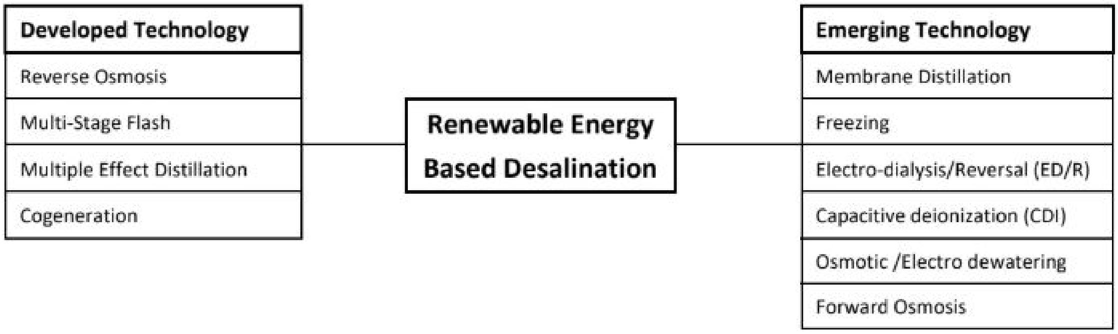

Figure 1.4: Technique relating to renewable energy [19]

Water produced by desalination systems has generally an higher cost (2,000$ an acre foot, ~1620$ per 1000 m^3 [20]), about twice the one of water coming from natural resources. This aspect is a consequence of the high energy consumption that desalination systems usually require. For this reason, one of the challenges of today studies is to cut down such cost. Moreover, some desalination system are meant to desalinate brackish water, which usually has a content of no more than 10 mgL^{-1} [15]. These operations are much less expensive, although the world resources of brackish water account for less than 1% of the water on earth, making this research field less appealing.

Generally speaking, desalination system can be divided into **direct** and **indirect** techniques. The technique is said to be direct whenever collectors are connected internally with the condensers; it is instead said indirect, when collectors and condensers are externally integrated within the plant. Indirect desalination yields generally higher productivity; however, direct techniques are still very diffused as they get competitive in small production systems, due to their low capital cost requirement and their simplicity [21].

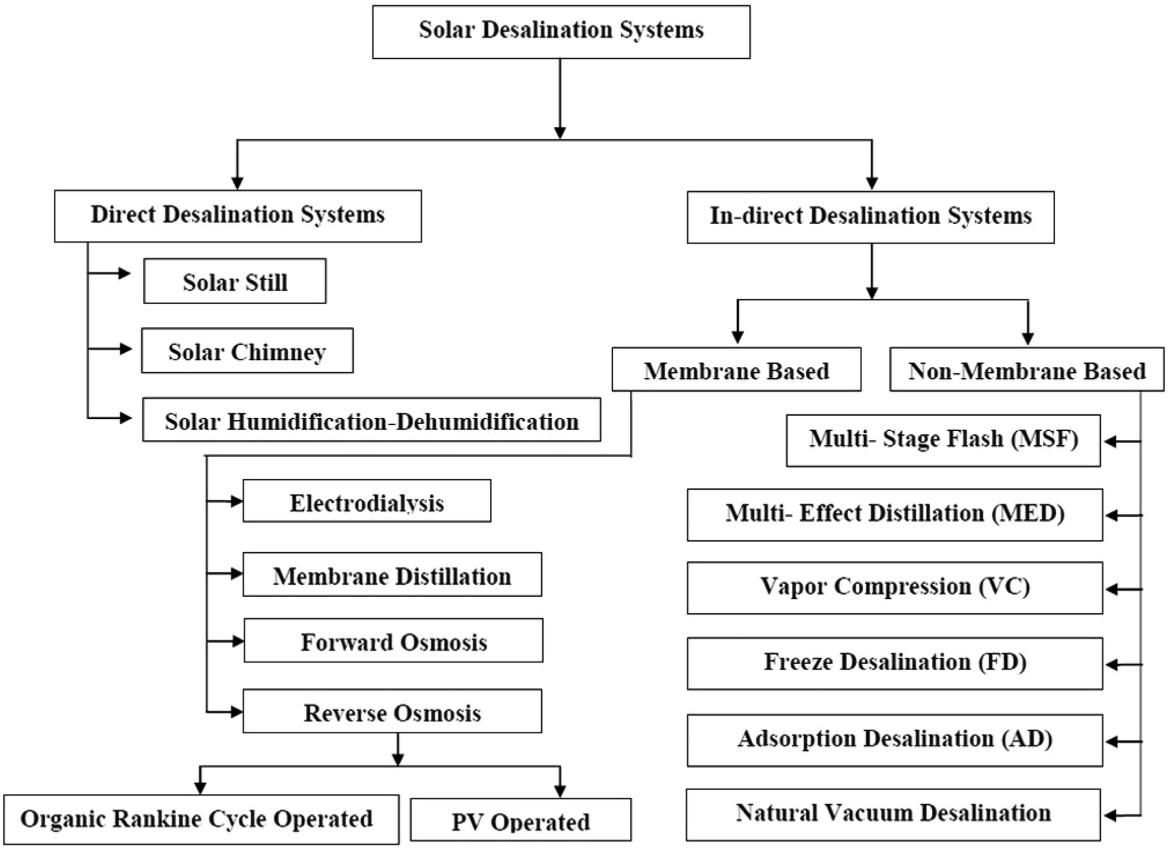

Figure 1.5: Overview of solar desalination systems (adapted with permission) [22]

Another important desalination system distinction regards the working principle. Mainly the desalination processes can be either *thermal-based* or *membrane-based*. Thermal-based technologies use an heat source to evaporate water and then condensate it, leaving the minerals in the brine; membrane-based technologies instead, use membranes and high pressure gradients to filtrate the water from the salt. Thermal-based process are more commonly used in regions with high salinity water and low energy cost, as in the Middle-East [23]. However, these processes require high establishment and operational cost, and they are considered high-energy intensive due to their reliance on thermal energy which mainly comes from fossil fuels [24]. For these reasons, membrane-based technologies have been considered much more of interest in the last years; thanks to their high energy efficiency, low space requirement, operational simplicity and ease of automation they are now starting to replace the thermal systems even in low energy cost regions [25, 26]. Furthermore, desalination systems can also be divided into *active* and *passive* systems. The first is so defined whenever it is implied the use of some external energy sources. Passive systems, instead, base their working principle on mainly solar absorption and insulating materials, avoiding thus the help of any electrical or mechanical external power source.

For the sake of simplicity, it will now be described the state of the art of just some of the most common and innovative different desalination techniques, by diving them in active systems, which usually aim to big scale production (e.g. industrial applications), and passive systems which mostly aim to small scale production (e.g. small community use).

1.4 Active systems

1.4.1 RO - Reverse Osmosis

RO is currently considered as the most reliable state-of-the-art technique for desalination[27]. It is the most common used technique around the world, accounting for 61% of the world desalinated water produced [28].

When two solutions characterized by a different solute concentrations are separated by a semi-permeable membrane come to contact, it is created a *chemical potential difference*. Due to this difference in the solute concentration, the solvent crosses the membrane from the low concentration region to the high concentration region; as shown in figure 1.6a. Being the membrane semi-permeable, it allows only water to pass through, rejecting the solute and reducing the chemical potential difference. This phenomenon is called *osmosis*. It continues until the chemical potential difference is balanced by the *osmotic pressure* (π), as shown in figure 1.6b, in this case a state of osmosis equilibrium is reached. If instead it is applied an opposite pressure gradient, higher than the osmotic pressure difference across the membrane, such process can be inverted and water is forced to flow in the opposite unnatural direction figure 1.6c; such phenomenon is called *reverse osmosis* [29]. In a real RO plant each flow is continued, thus there are 3 flows overall: an inlet feed water source, and two outlets flows represented by the produced water and the rejected water carrying salts, or also called *brine*. Furthermore, due to the high resistance of the membrane and the flows through the channels, the external pressure applied needs to be much higher than the osmotic pressure. For example, for RO plant's pump using water at 35 ppm, even 100 bar may be required [30]. The need of high pressure pumps and then high operational cost is inevitable.

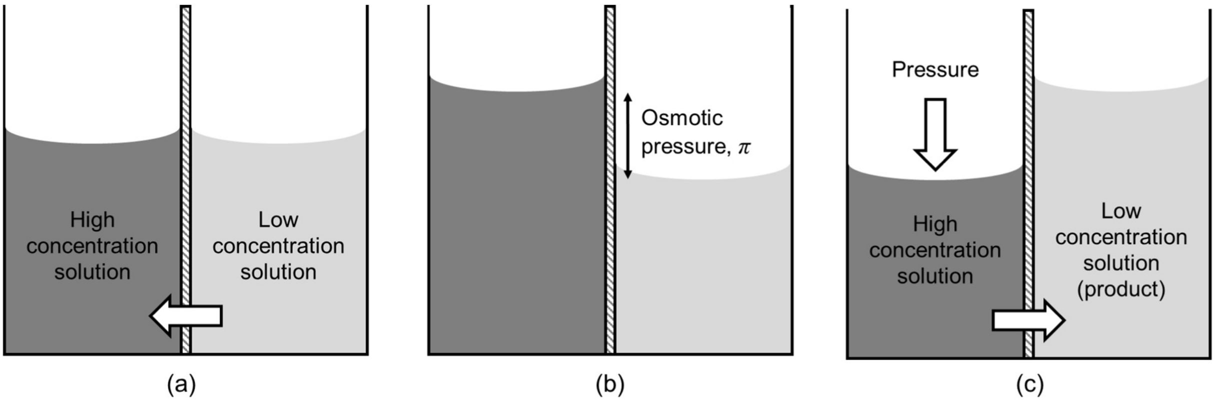

Figure 1.6: **a**) Osmosis **b**) Osmosis equilibrium **c**) Reverse Osmosis (adapted with permission) [29].

To make use of the high pressure pumps, it is necessary to remove any possible inorganic suspended solid from water [31]. Doing so, salt precipitation and microbial growth are avoided, otherwise they would increase fouling in the RO membranes. Therefore, some pre-treatment processes are always needed, as they also allow to facilitate membrane operationes. Overall, a simple RO plant schematic will look as in figure 1.7.

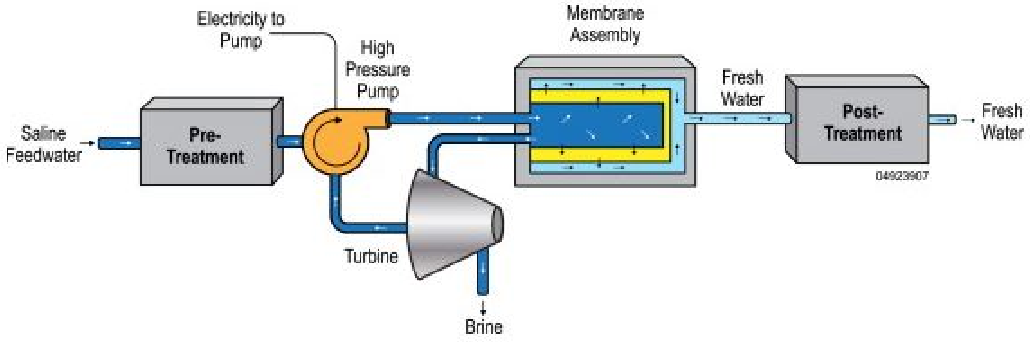

Figure 1.7: Schematic of a RO plant (adapted with permission) [32].

A few components are then needed to make an RO plant working properly. As pre-treatment processes, some common are typically coagulation, sedimentation and send filtration; otherwise, also micro- and ultra-filtration can be used [33]. After pre-treatment, pumps generally supply water at a pressure of 17-27 bar for brackish water, while it gets typically around 69-80 bar for seawater [34]. Membranes exist of many types, among which *hollow fiber*, *spiral wound*, *plate* and *tubular*. The first two are generally the most commonly used for their versatility, and their cost related to the performances [35]. They usually consist of a pressure vessel with an interior semi-permeable membrane, usually made of materials such as cellulose triacetate or polyamides and polysulfones. Pores in the membranes are wide enough to let water through but enough small to also block salts particles. Generally speaking, membranes selection is based on pH stability, working life, mechanical strength, pressurization capacity and selectivity for solutes. After passing through the membrane, water is divided into two flows; one is the rejected water, full of wastes, the other is the desalinated water. The latter may at the end need some post-treatment, depending on the future purpose of the produced water. Some common post-treatment processes are pH adjustment, disinfection, and remineralization [31, 35].

RO technology is so widely used technique thanks to its many advantages [31]. Some of them are:

- Simplicity in plant design and operation.
- Modular nature of the plant, which yields easy plant's dimension amplifications.
- Low maintenance requirement.
- Both organic and inorganic unwanted elements can be removed by the same membrane in RO.
- It is possible to recover waste water streams as with a turbine (see figure 1.7.
- Waste streams volume is reduced.

- Plants operate at ambient temperature, reducing problem of corrosion and then decreasing maintenance activity.
- The process is adaptable to solar panels, as it is mainly driven by electricity.
- Specific energy required is lower than other technologies: 3 - 9.4 kWh/m^3

However, RO systems have also some drawbacks. An important parameter to evaluate each desalination technique is the *recovery efficiency* (RE) or *recovery rate* (RR). This is defined as the *"ratio of the volume of desalinated water produced to feed water"* [36]. For RO plant, the RE does not get higher than 45% when treating seawater; it gets as low as 30% for very salty water as 40,000 ppm. It is in fact much lower than the one for systems using thermal-based desalination (where for example it gets as high as 97% for MVC), but on the other hand these latter, result even more energy costly respect RO. When referring to small-scale production, RO looses its advantages though, and it is considered much more expensive. An other drawback regards the environmental impact. Problems are mostly associated with the construction and operation of intake systems, and the disposal of concentrate; but from this point of view, many solutions, as ideal geographical position of the plant and velocity-cap intakes, have been made [37]. However, the main drawback of RO regards the high amount of energy needed to function. Many components as the intake feed, the pre-treatment and other possible auxiliary system, require in fact also an high amount of energy [38].

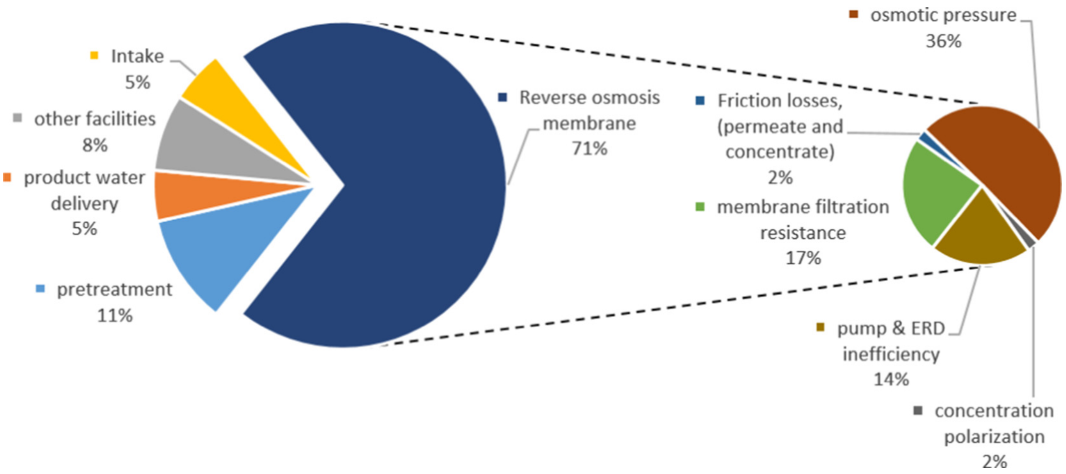

Figure 1.8: Energy consumption division in a SWRO system (adapted with permission) [29].

Moreover, the energy needed for all these operations is often coming from fossil fuel, an unsustainable costly energy source, both environmentally and economically. It has been estimated, in rich countries suffering from water-stress, as Saudi Arabia and Kuwait, even 50%-70% of the fossil fuel used, is intended for desalination plants [39, 40]. For these reason many progress have been made in the last decade, to substitute fossil fuel with wind and solar power, in order to fuel desalination plants. Nowadays, among all the desalination plants using renewable energy, RO makes 52% of them. 40% are PV RO plants, 8% are PV-wind RO plants and 4% are solar Rankine RO plants [41]. Some plants also use: *forward osmosis*, to combine wastewater with seawater, to reduce the specific energy required [42, 43]; *pressure retarded osmosis*, which uses the difference in the osmotic pressure to drive a flow to power a turbine[44], as shown in figure 1.7; and even *waves energy* exploited in seashore plants[45].

The cost of RO desalinated seawater keeps dropping due the many technological improvements; Wilf and C. Bartels estimated a cost of $\$0.5/m^3$[46]; however, researches have forecast even more optimistic estimations in the near future [47]. On the other hand, PV powered SWRO plant can achieve a total water production at the cost of $\$0.825/m^3$, with a payback period for the addition of the PV technology within ~23 years [48].

1.4.2 MSF - Multi-Stage Flash

MSF is the most worldwide spread thermal-based technology for desalination; 26% of the total desalinated world water production comes from MSF systems [28].

When a saturated liquid enters an environment, through a throttling device, at a substantial lower pressure, a portion of the liquid evaporates instantaneously. Such phenomenon is called *flash evaporation*. MSF plants functioning is based on this simple concept. A schematic of the plant is shown in figure 1.9. Through a feed intake pump, seawater is withdrawn into the plant. It passes through an heat exchanger system, divided in stages, where the salty water is heated up while the fresh water, coming from the end-cycle, condensates. After, the temperature of the seawater is further increased, by an external heating source (which could be either a fossil-fuel boilers, a power-plant waste heat, anuclear reactor or a renewable energy source), till it reaches 90°-110° C. The hot brine then enters a lower pressure and lower temperature environment, to which follows a flash evaporation. Such phenomenon is enhanced by a multistage process where at each step pressure and temperature slightly drop. A typical MSF system has between 4 and 40 stages. Vapour then condenses again on the heat exchanger tube bundles, thanks to the new colder seawater coming in. At the last stage, the concentrated brine will have a very high salinity, thus it is treated as a waste and it is finally discharged [32].

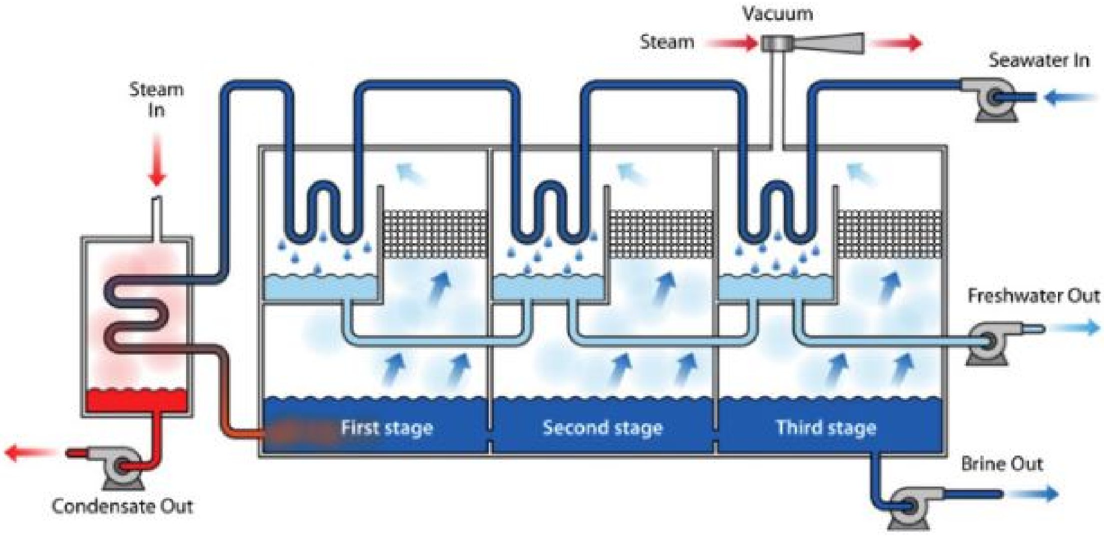

Figure 1.9: Schematic of a MSF plant (adapted with permission) [32].

Overall the plant needs electrical energy and thermal energy to work. Thermal energy is used through the medium-pressure steam, in the ejectors, to generate vacuum in the vessels; moreover it is also used as the external heating source, which further heats up the hot brine. In the most modern plants, the heating source is represented either by PV or solar collectors to reduce the system climate impact. Electrical energy is instead used to power the many pumps present in the plant; their purpose is manly related to recycling, cooling water, treating the produced water, blowing down the brine and condensating [49]. Some of the biggest advantges of MSF are [50]:

- Simple working principle.
- Ideal for large scale productions

- PV and solar collectors can be easily integrated to supply eletric and thermal energy.
- Also high temperature waste heat can sometimes be used as an heat source.
- It is reached an high quality of desalinated water, it contains no more than 10 ppm
- Differently from RO, feed water quality is not important; the only pretreatment technique required is filtration, to remove any solids.
- It is the most cost-effective process in areas where energy cost is low.

In MSF plant, RE does not get generally higher than 25%. This technique is also strictly related to a high level of maintenance. Flashing produces scales and deposits usually at the entrances of the flash chambers and in the heat exchangers tubes; for such reason periodic cleaning is needed, which causes higher operational costs [51]. Another problem related to MSF is the discharge of the brine. Being the waste full of salt, it can change the water salinity, lowering oxygen in the disposal site, and then risking to cause damage to flora and fauna. To solve this problem studies have been carried on, about brine concentration recovery system; their aim is to convert the brine into salt, which could then possibly be used to maintain the salinity of the solar ponds ("pool" of saltwater which collects and stores solar thermal energy) [52].

MSF is a proven technology especially in gulf regions because of its ease of operation and because there is less reliance on raw water quality. Many MSF plants there located, have been employed in cogenerations plants [53], having long service life of over 30 years. That is also because MSF technology is very suitable for large capacities; and in the middle-east many countries are greatly dependent on desalination technologies. For example, for the last 50 years, Kuwait has fully depended on MSF [54]. It is in fact not surprising the largest desalination plants in the world use this technology.

The related specific energy consumption is between 10-16 kWh/m^3 [47], with production ranging from 1000 m^3/h to 22,000 m^3/h. At the end, water produced has a more than competitive price, costing between 0.52 $\$/m^3$ and 1.75 $\$/m^3$ [55]. A comparison between MSF and SWRO water cost over the years is shown in figure 1.10.

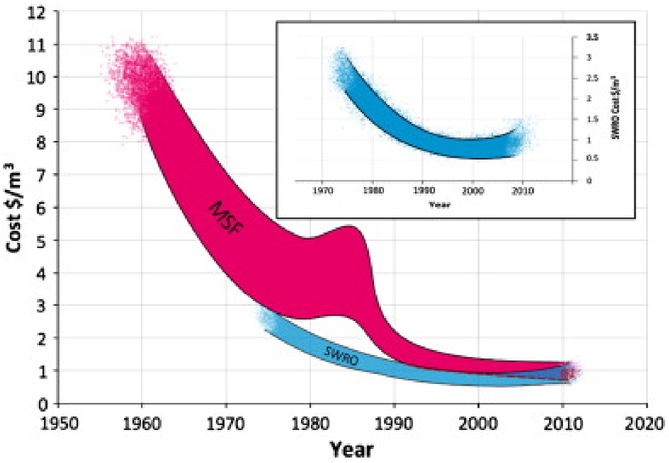

Figure 1.10: SWRO vs MSF unit water cost (adapted with permission) [47].

It then looks more inconvenient than RO, due higher energy consumption and higher fresh water cost, however, it is still a very competitive technology thanks to the large scale production.

1.4.3 MED - Multi-Effect Distillation

MED is an older technology respect MSF, it was in fact first used for water desalination. Nowadays it is still the second most diffused thermal-based technology around the globe; 6% of the total desalinated water comes from MDE [28].

Its principle of function is simply based on exploiting the different volatilities of the water components, so to let evaporate only the fresh water content. Through a feed intake pump, seawater is extracted to enter the plant. At first it is slightly preheated by some vapour coming from the last stage of the system (preheated multi-effect distillation process). The seawater is then sprayed over heated pipes, in each stage. In the first one, the pipes are heated by an external source (fossil-fuel boilers, power-plant waste heat, nuclear reactor or renewable energy source), at a temperature lower than 70°C; for higher temperature, the scaling problem is in fact enhanced. Most of the sprayed seawater than evaporates, thus becoming fresh water vapour. Such vapour passes to the next stages through a new set of pipes.

As at each stage, water needs to evaporate at a slightly lower temperature, also the pressure needs to be slightly lower. The hot water vapour is then used to heat the new sprayed seawater, while it condenses itself, becoming freshwater. The brine is collected at the bottom vessels. The process is repeated at each stage, progressively lowering temperatures and pressures, as shown in figure 1.11. In the last stage the vapour condenses by heating the whole new amount of seawater coming in, as t is designed for a prehated MED. The usual number of stages ranges from 2 to 16 [32].

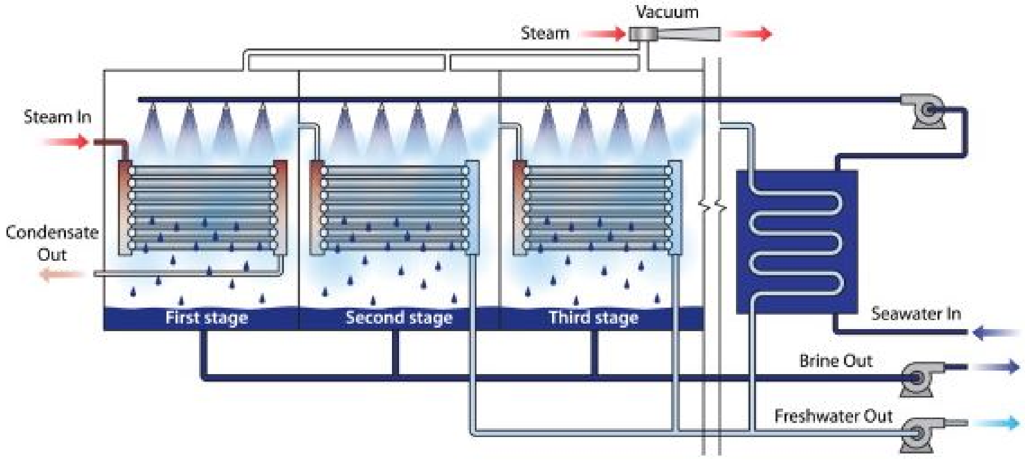

Figure 1.11: Schematic of a preheated MED plant (adapted with permission) [32].

As MSF, also MDE requires thermal and electrical energy to work. The two technique have in fact different similarities and the way energy is used is one of them. Thermal energy is used once again used in the ejectors, to create lower pressure environments, and to heat up the first stage. Electrical energy is instead needed to power the various pumps within the system.

The first world desalination plants used MDE, altough MSF has historically taken over as the preferred thermal-based technology. The latter in fact provides less scaling and fouling problems of the evaporation tubes surface; moreover, it usually guarantees a lower fresh water cost [56]. MDE has in fact nozzles, located in the spraying system, which can clog when raw water is too turbid. However, the interest in MDE technology has lately been renewed as it is recently been adapted to some new modifications. Some of the biggest advantages of MDE technology, especially over its thermal-based counterpart, are [50]:

- Less tube corrosion respect MSF, as MDE operates at lower maximum temperatures.
- It is better for low scale production respect MSF.
- It has a better compatibility with solar desalination auxiliaries than MSF.
- For each *kg* of distillate required, it is needed less steam than in MSF; there is then an higher *performance efficiency* which can eventually lead to a lower product cost.
- Power consumption is generally lower, due to the lower temperatures reached.
- Differently from RO, feed water quality is not important; the only pretreatment technique required is filtration, to remove any solids.

MDE recovery efficiency is gets to about 30%-50% [57], so performing similiary to RO and better than MSF. However, MDE has still been considered a past away technique for long, because of some of its disadvantages. For example, the plant construction is quite complex due to its many components, thus a scale down is difficult to realize. Moreover, due the scaling problem at high temperatures, not all the heat source are suitable to heat the first stage [58]. But the most important MDE technology drawback is probably its physical limitation imposed by the first and last temperature in the plant sequence. As already mentioned, the input temperature can not be higher than 70°C due to scaling problems. On the other hand, the output temperature needs to be at least as low as the ambient temperature to let freshwater condense. Such temperature can even reach 40°C in hot areas as in the middle-east, which are usually the regions where desalination is most needed. There is then a maximum number of stages that can stay in between, or either a maximum temperature difference between each stage. However, one of the reason why MDE is becoming once again more popular, is the addition to the system of a hybrid technology that allows to break such limit. Such technology is the *Adsorption desalination* technique (AD), which with MED makes up the *Multi Effect Distillation Adsorption Desalination* (MEDAD).

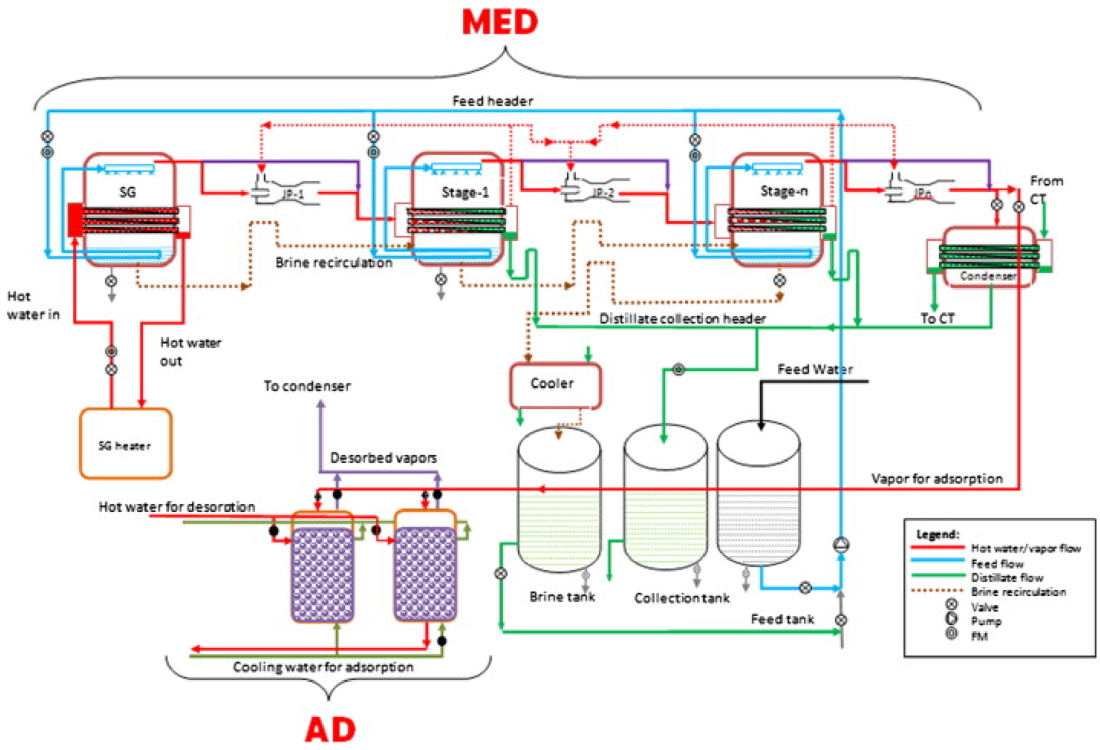

Figure 1.12: Detailed schematic of a MEDAD plant (adapted with permission) [59].

It consists in the addition of one last particular stage where it is contained a silica gel which can absorb water at a temperature as low as 5°C [59]. It is then increased the maximum and minimum temperature difference in the plant, thus allowing more stages or a higher temperature difference in each stage. This gel is particular because it has a unique property for which it is hydrophilic at low temperatures and hydrophobic at higher temperatures. After absorbing water at 5°C it is then heated up above ambient temperature (between 80°C and 55°C) so it can release the water previously adsorbed, which then is able to condense in the very last stage. The energy used to heat the gel can be easily provided by renewable energy resources or wasted heat sources. Doing so, the production of the system can even double without theoretically adding any additional energy input [60].

Coupling MED with also other techniques has allowed to further increase the importance of MED technology in today's scenario. A very widespread solution consists of the hybrid between MED and thermal vapour compression (MED-TVC). The system guarantees the best performances amongst all steam-based thermal desalination technologies [61]. This solution is convenient whenever it is possible to use medium-pressure steam and when not just low sensible heat sources are available. It allows to optimize the use of thermal energy and to reduce the electrical consume of the system by adding a steam jet ejectors which uses the steam coming from the external source to compress a portion of the steam coming from last stage of the system. Such steam is then reinserted in the first stage, so enhancing the system efficiency [62, 63]. Other MDE improvements are the *Boosted Multi-Effect Distillation* (B-MDE), and the *Flash-Boosted Multi-Effect Distillation* (FB-MDE). The first solution is very useful when the heat source reaches low temperatures. It in facts adds an additional evaporation unit, which uses the still hot liquid heat source, after being used, to let the feed water evaporate in an additional stage. The heat source fluid then has an higher temperature drop than in a normal configuration. The second solution allows to exploit the maximum thermal energy from the waste sensible heat. It uses multiple flashing chamber, as in MSF, to make a further use of the waste energy to create additional steam [62].

For what concerns energy use, MDE result better of MSF, as it has a specific energy consumption of 5.5–9 kWh/m^3. Water price results slightly higher though, ranging from 0.7 $\$/m^3$ to 1.2 $\$/m^3$. However, in terms of capital and running cost, thanks to advanced material and technology available, MED results better than MSF. Finally, it is likely MED will overtake MSF in the future, some studies even states it could even be competitive with RO in areas where very polluted and/or salty water is present [47].

Overall, as the main industrial technologies have been analysed, it is interesting to sum up and compare some of the most important production parameters:

Process	**Thermal energy** $[kWh/m^3]$	**Electric energy** $[kWh/m^3]$	**Total energy** $[kWh/m^3]$	**Water costs** $[\$/m^3]$
SWRO	/	3-4	3-4	0.5-1.2
MSF	7.5-12	2.5-4	10-16	0.7-1.2
MDE	4-7	1.5-2	5.5-9	0.8-1.5

Table 1.3: SWRO vs MSF vs MDE: energy consumption and water costs [47].

1.4.4 ED - Electrodialysis

As RO, MSF and MED produce the 93% of the world desalinated water, any other technology may seem just secondary respect to them. However, some are still very relevant as they can eventually result as the best choice depending on the resources and the applications. One of the most diffuse of such technologies is with no doubt *electrodyalisis*. After RO, it is probably the most important membrane-based technology, as it is one of the most diffused for the desalination of brackish water.

Its working principle is based on the ions separations, and it is described in figure 1.13. The technique exploits the dissolution of salt in water, through which it is broken up into positive ions (Na^+) and negative ions (Cl^-). Such ions can then be separated using respectively a negative and an positive charged electrode. In particular the system is made up by a feeding system, electrodes, a direct current supply, ion selective membranes, solvents and electrolytes [64, 32]. The feeding system, brings seawater in the circuit by usually employing low-pressure pumps. The water is then brought in a container where ion exchange membranes are positioned in parallel so to form different channels. The electrodes, electrically charged through the external direct current supply, are located at the sides of the container. As the membranes closer to the negative electrode are cation-permeable while those closer to the positive charged electrode, the salt ions are able to travel separately through the respective membranes. More in particular, positive ions travel through the cation-permeable membrane attracted by the negative electrode, and negative ions travel through the anion-permeable membrane attracted by the positive electrode. The water passing through the central channel results then desalinated, while the one passing through the external channel will contain the brines [32].

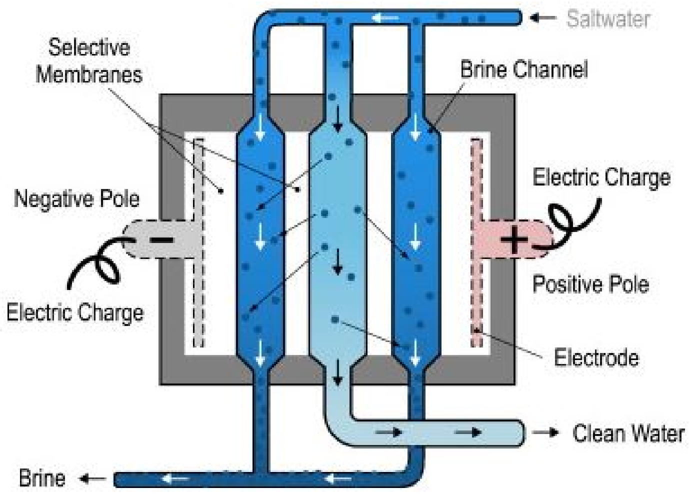

Figure 1.13: Schematic of a ED plant (adapted with permission) [32].

Pretreatment and post-treatment operations are usually also required in series with the system. These are respectively mainly aiming to remove floating corps which risks to create fouling on the membranes, and to allow to withstand the water standards required. ED is in fact not optimal when extremely low salinity water is needed, as it is not able to completely remove particles not tending to mobile [65]. As the process goes on, always more ions deposits on the membranes, thus, some cleaning operation is also needed in order to keep a costant efficency and to increase membranes life [32]. Such operation is usually accomplished through *electrodyalis reversal* (EDR). The technique consist in switching the electrodes polarity; doing so the concentrate stream and the feed stream get inverted, and the ions are guided away from the membranes. As shown in figure 1.14, the advantage of such method consist in not having the need to reduce the plant treatment capacity during cleaning operation.

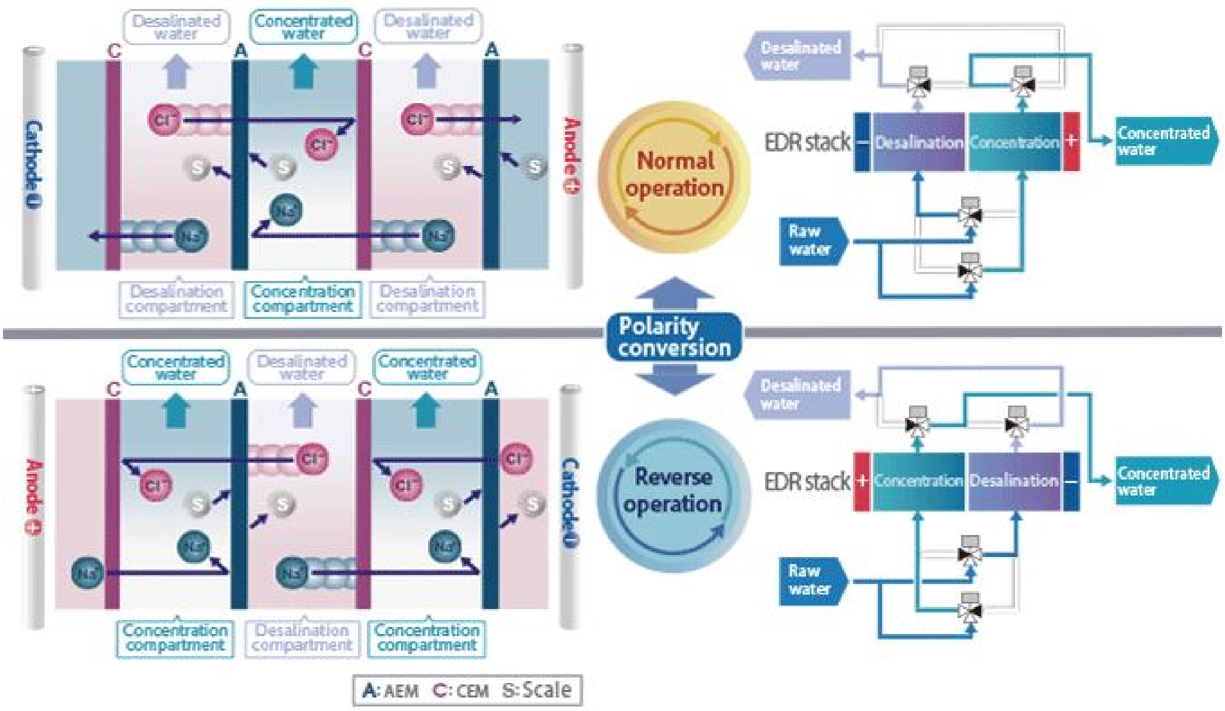

Figure 1.14: Working principle of EDR [66].

Membranes are usually made of crosslinked polystyrene that has been previously sulfonated (cation-permeable), and matrix fibers with quaternary ammonium groups (anion-permeable); electrodes are instead mainly made of niobium or titanium with a platinum coating [67].

Even if RO is widely the most diffuse desalination methods, when treating brackish water, ED can sometimes be more convenient due to some of the following advantages [68, 67, 69]:

- Better than RO in tunable areas; meaning that in sites where inflow water salinity may change (for example due to tides), it is easy to adjust the system energy required to maintain the same output.

- Uses a low-pressure feed intake system over the high pressure pumps needed in RO. It is then not needed the presence of special valves and pipes able to withstand high stresses.

- Easy maintenance respect RO. While an RO plant suffer from a decrease in treatment capacity when it is offline, ED does not.

- Cleaning is carried out through EDR which operates with the previously discharged liquid, having it an high salt concentration. On the other hand, RO requires the addition of acids which generates a waste which may need to be treated before any discharging in the environment.
- To improve water quality it is possible to just add more stages in series. Moreover, at each stage it can be applied a different suitable potential difference, so resulting in a optimization of energy consumption.
- Less sensible to preatreatment than RO. ED can in fact still function with lower feed water quality.
- ED membranes live up to 7-10 years, while RO membranes can be mantained for about 5-7 years.

On the other hand, limitations of ED can also be quite relevant, especially for high desalination standards. For example, particles which are not charged, or have a high molecular weight, or are generally not easily mobile, are less likely to be removed; for such reason the process becomes more expensive as more strict is the removal of minerals (more stages are required) [65]. ED plants are in fact mainly employed for brackish water only or to slightly improve the quality of drinkable water. For instance, the biggest ED plant in the world, located in Abrera, Spain, desalinates brackish water, and has a capacity of 220,000 m^3/day [67]. Moreover, despite its many advantages, ED is still considered too much energy expensive respect RO; it is mainly for this reason that ED technology is not supposed to treat seawater and it is still not as much widely diffused [69]. However, its research field is still of interest thanks to some new configurations that have allowed better performances. One of this is *electrodialysis with bipolar membranes* (BMED). This techniques consist in using membranes composed by both a cation-exchange layer and an anion-exchange layer. Doing so, it is possible to split the solvent to gain some advantages such as the absence of byproduct gas generation, lower voltage descrease, maximal energy use, lower encumbrance and easier installation [64]. Furthermore, ED can be integrated with pressure-driven membranes operations, which can be used as pretreatments, in order to decrease any membrane pollution [64].

Energy consumption of ED treating seawater would amount to about 10-25 kWh/m^3 [70]. However, as already mentioned, because such values are too high to be competitive with other desalination technology, ED plants treat mainly brackish water. The system becomes in fact more expensive as higher is the level of water salinity, and thus, in these cases, it looses its competitiveness. For such reason, parameters as the general energy consumption or the water cost must not be compared with other seawater desalination techniques, because they strongly depend on the initial water salinity level. For example, for an ED system treating brackish water at 2000-10,000 mg/l the energy consumption amounts to 0.4–4 kWh/m^3; while the water cost gets around ~0.25 $\$/m^3$ [70].

For what instead concern treatment capacities, ED plants are able to space over a wide range of production; they are typically able to produce from 2 to 145,000 m^3/day [32].

Although ED is historically energy expensive, future improvements may lead to make it more competitive, even for seawater desalination. For example, a study lately made by Doornbusch et al. attests it is possible through a multistage ED system, operating at limiting current density condition, to get desalinated water close to WHO standards [71], at 3.6 kWh/m^3, which is basically the energy consumption of a modern RO system [69].

1.4.5 MD - Membrane Distillation

Membrane distillation is an important thermal-based technology to desalinate water with high salt concentration. Desalination is just one of its possible (and most common) use as it can also be employed in the treatment of wastewater and in the production of concentrate liquid. Its advantages have been neglected for long, in favour of the lower operational cost that RO, MSF and MED guarantee. However, MD has recently gained interest again, thanks to the development of modular component, which allow the use of the technology also in remote areas, and auxiliary systems which helped reducing the thermal and electric energy consumption as well as maximising water recovery [72]. It is still not considered by all a proper industrial desalination technology though [73]. There is some disagreement in the literature about MD potentiality and applications; other researches attest in fact the opposite, affirming that the energy consumption is comparable with the one of MSF and MED [74].

The general principle of functioning of MD is shown in figure 1.15. The purpose is to exploit water evaporation to get rid of any non-volatile solutes . As the seawater is extracted by the feeding system, it enters into a channel tangentially bounded by a foil on one side, and an hydrophobic micro-porous membrane on the other. Then, as the foil is heated up by an external source, water quickly evaporates. The hydrophobic micro-porous membrane does not let any water pass through it, but at the same time it is also highly permeable to vapour. The latter is then guided through the membrane by a driving force which originates from the difference in partial pressure (which in turn is caused by the thermal difference) that coexist between the two sides of the membrane. As vapour reaches the other side of the membrane it is able to condense due to the presence of another colder foil. Overall the membrane is then confining on one side with evaporating seawater and on the other with condensing vapour. The latent heat of vapour is then reused to initiate to a new stage [75, 76]. There can be as more stages as higher is the amount of heat provided by the heating source.

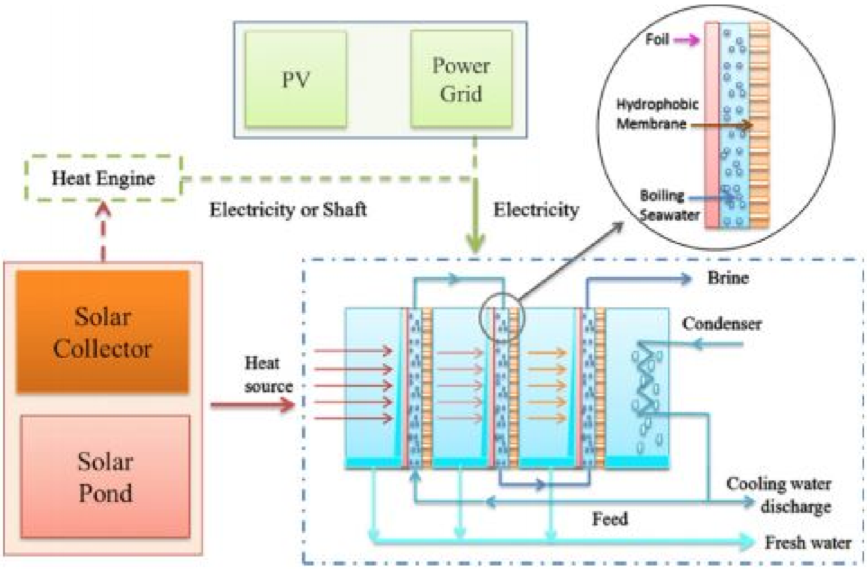

Figure 1.15: Schematic of a MD plant coupled with PV and Solar Collectors (adapted with permission) [76].

Generally speaking, MD technology can generally be of four types; they are reported in figure 1.16 [74]:

- **DCMD** - Direct contact membrane distillation: It is the simplest and most widely diffused configuration. Both the vaporizing and the condensing fluid are in contact with the membrane. Vapour is then driven through the membrane by the pressure difference, from the hot side to the cold one, where it can finally condense. The problem of this configuration is the high heat loss caused by conduction.

- **AGMD** - Air gap membrane distillation: The vaporizing fluid is still in contact with the membrane but the condensing one is not. The cold side is in fact separated from the membrane by an air gap layer. Vapour can still pass through it but there is a lower mass transfer as the air gap acts as a resistance. The advantage of this configuration is the reduction of the conductive heat loss.

- **SGMD** - Sweeping gas membrane distillation: It is considered as an improvement respect AGMD. A cold gas passes tangentially through the permeate side, the vapour then diffuses in it and it is brought away to condense outside of the device. Doing so, the conductive heat loss are further reduced respect DCMD; moreover, also the mass transfer resistance created by the gas is less relevant respect the AGMD case. The drawback of this configuration is that due to the diffusion of vapour in the gas, a larger condenser will be needed.

- **VMD** - Vacuum membrane distillation: As in SGMD, also for VMD condensation takes place out of the membrane module. However, in this case, instead of a gas it is used vacuum. The heat loss are then brought to a minimal negligible value but the use of an additional pump is requested. Capital and operational costs will then increase as well.

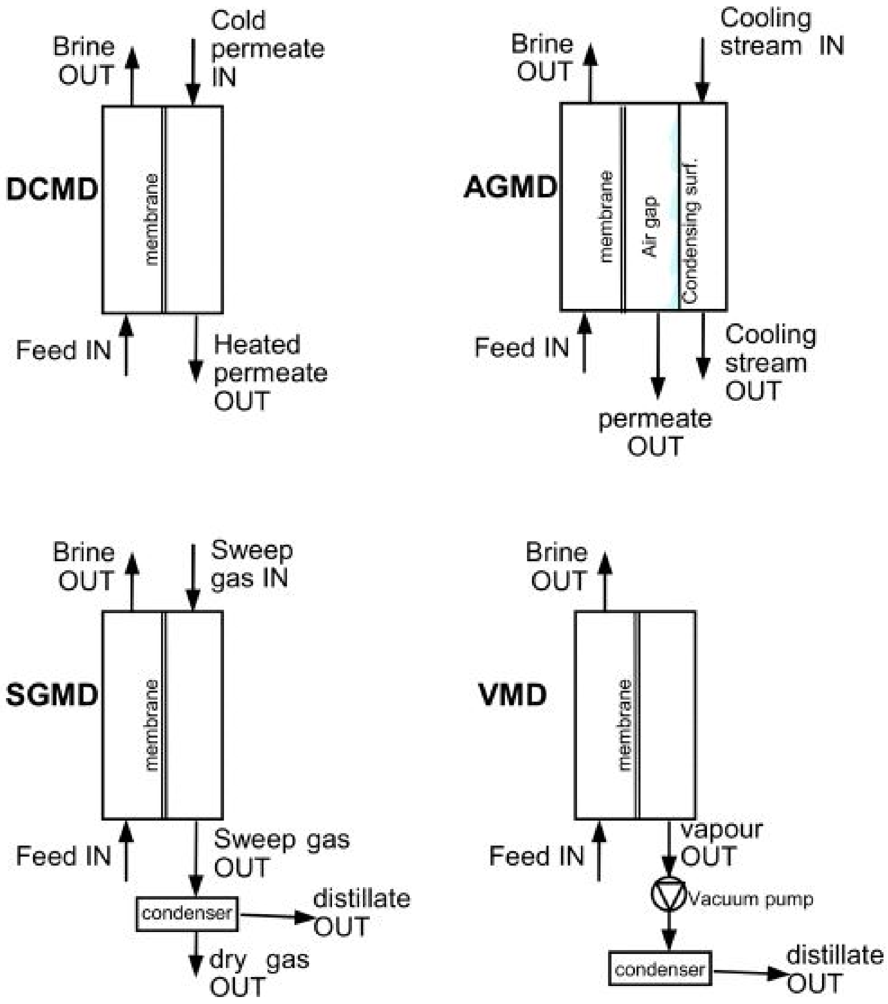

Figure 1.16: Schematic of the various MD configurations [75].

Overall, DCMD and AGMD have both the advantage of not needing any external device; while the first guarantees higher mass transfer and lower thermal efficiency, the second has lower transport of vapour and lower heat loss. SGMD and VMD overcome both these problems (in particular VMD guarantees the highest vapour flux) but they also have to pay an higher complexity of the system.

Generally speaking, as for all the thermal-based technology, also MD configurations needs both thermal and electrical energy to work. On this matter, one of the main reason why MD is considered so interesting is the ease of satisfying the energy demand by means of renewable energy resources. MD plants do not usually reach temperatures higher than 80°C; thus low grade heat can be easily obtained through the help of either solar ponds, wasted heat or solar collectors . In particular, modelling of the latter one has shown higher permeate flux through the membrane [77]. On the other hand, electric energy can be supplied by means of PVs or heat engines which use the solar renewable energy coming from the thermal energy supply [76]. Summarizing, it follows a list of MD advantages which make this technology so attractive, especially for further studies [75, 76]:

- MD membranes are cheap and robust. Fouling and scaling are then less likely to occur, while costs related to chemical usage and pretreatment are less relevant when compared to RO technology.
- There are no corrosion problems.
- All non-volatile components are theoretically fully removed from water.
- During operation, the electrical consumption is low.
- The modularity of the system yields a low complexity apparatus.
- The system requires minimal maintenance.
- Temperatures and pressures are low when compared to those of other desalination technologies.
- The technology is ideal to be coupled with renewable energy resources.

Despite these many advantages, MD applications are still uncommon at an industrial level because of its drawbacks. For instance, although a low grade heat is required, the amount of thermal energy needed is still relatively high. Moreover, respect RO the permeate flux is much lower. These characteristics make the process expensive; an aspect which is considered important enough to make all the positive attributes unworthy. However, many efforts are being made to make this technology more competitive; for example, it is expected to make large progress on the systems membrane and module design, which is in fact still considered not optimized [75]. Some of the latest research go even further: one speculates a membrane distillation which does not require external thermal energy: the *zero thermal* *energy input membrane distillation* (ZTIMD). This technique is supposed to exploit the thermal difference between the ambient temperature at the sea surface (~30°C) and the one at the sea bottom (~10°C) to use it as the process driving force [78].

For what concerns energy consumption, as already mention, for MD it is much higher than for typical industrial techniques. According Ullah et al. the thermal energy required amounts to about 100 kwh/m^3, while the eltric energy needed is much lower, accounting for 1.5-3.65 kwh/m^3. On the other hand, the RE is higher than common desaliation technologies, it reaches a range of 60-80% [57]. There are instead not many resources in the literature mentioning MD seawater desalinated cost. It is considered a technology which will be able to lower it, but today there is still a big gap with prices offered by the more affirmed techniques. A study from Banat et al. estimated a cost of $15\$/m^3$ for a plant producing 100 l/day, using membrane of 10 m^2 and powered by panel collectors [79].

1.4.6 FO - Forward Osmosis

Despite RO, MSF and MED are widely the most affirmed technologies, they are still considered too much energy intensive or environmentally dangerous. For such reasons many studies have been carried on about technologies which potentially require lower energy and that can yield less pollutants discharges [80, 81, 82]. As MD, an other method which is recently gaining more interest and it is considered a valid alternative to conventional methods is *forward osmosis* (FO).

As described in page 10, FO desalination bases its principle of function on a simple process of natural osmosis. It uses the passage of solute, from a higher concentrated solution (higher osmotic pressure) to a solution with lower concentration (lower osmotic pressure), through a permeable membrane; a process which continues until the chemical potential in the two solution reaches equilibrium. However, a proper FO plants uses some auxiliary systems as it is shown in figure 1.17. The overall process can be separated in two parts. In the first one the feed intake brings seawater into the circuit and then into the membrane system. Here the feed water is in contact with the semi-permeable membrane, which is in turn confining on the other side with a solution at a higher concentration, generally called *draw solution*. Forward osmosis is then possible and the draw solution is diluted. After, this is brought into a recovery system where the fresh water can finally get separated from the draw solution by means of either a low grade heat source, a secondary membranes, physical separation or a of combination these methods. The draw solution is then recovered and it is able to begin a new cycle [81].

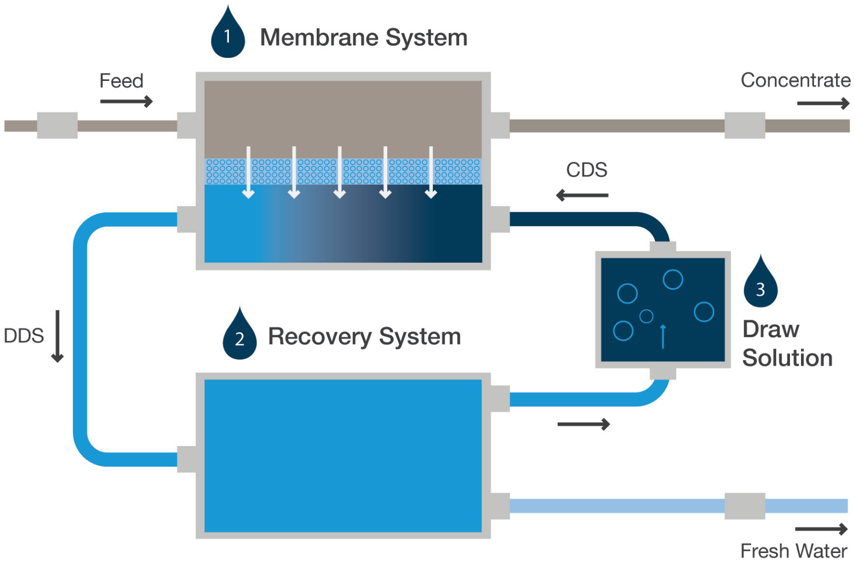

Figure 1.17: Schematic of a FO plant [83].

The efficiency of the technique depends quite relevantly on the role played by the draw solution and the recovery method. The first one should be able to guarantee an high osmotic gradient, an high water flux, the possibility to be recovered at low energy costs, zero toxicity and low costs of the solution itself [80]. A variety of draw solutions have been considered over the years and many improvements have been made [84]. One of the most affirmed technology involves the use of hydrophilic nano-size magnetic particles [85]. On the other hand, for what concerns recovery methods some of the most popular ones are ultrafiltration, which takes place by mean of a membrane, and magnetic separation, which is needed to separate magnetic particles. However, depending on the nature on the draw solution, recovery methods could have not even been needed over the years, as it can be seen from table 1.4.

As it can already be noticed, FO technology does not require neither high temperatures or

Year	Draw solution	Recovery technology
1965	SO_2	Heated gas stripping operation
1975	Glucose	Not required
1989	Fructose	Not required
2005	NH_4HCO_3	Moderate heating up to 60°C
2007	Dendrimers	Adjusting pH
2011	Polymer hydrogels	Pressure and thermal stimuli
2013	Thermo-sensitive polyelectrolytes	Hot UF
2014	Dimethyl ether	Exposure to air
2015	Electric-responsive polymer hydrogels	Electric field

Table 1.4: Summary of some of the historically used draw solution and recovery method [81].

high pressures for its correct functioning. For such reason, it is considered a very attractive research field. It was in fact embedded also in other types of applications, such as: wastewater treatment [86], power generation [87], food processing [88] and even healthcare [89]. Some of the most important advatnges of FO are in fact [80, 81, 90]:

- High water recovery.
- Minimal fouling and scaling phenomena.
- Potentially lower energy consumption. Forward osmosis occurs spontaneously, so the consumption depends mostly on the recovery step.
- Low pressures and temperatures. They also leads to a simpler equipment, especially for membrane support.
- Hybrids of FO are able to desalinate water also with particularly high salt concentration (even 5 times normal seawater salinity: 150,000 ppm TDS); something that RO itself cannot do.
- The high water recovery also leads to a reduction in the production of brine.
- High rejection of most contaminats.

Although FO is considered one of the most prospective technologies, it is still not affirmed as an industrial method due to some of its challenges which still remain unresolved.

For example, even if a lot of improvements have been made on the choice of the draw solution, a proper ideal one has not been found yet. Moreover, the energy consumption of the recovery system does not allow to this technology to become competitive respect the more conventional ones. As always, in fact, the biggest obstacle to overcome is the economic feasibility of the system. Other than that, *concentration polarization* and *reverse salt flux* are still important issues [81]. CP can be either an internal or an external phenomenon, whether it is taking place in the support membrane layer or in the active one; it is responsible for the decrease in the water flux through the membrane [91]. On the other hand, reverse salt flux is caused by the non perfect solute rejection of the membrane; thus, it seems unavoidable, but it can still be certainly improved.

To overcome many of such challenges many hybrids have been developed. For such reason, it is difficult to find in the literature precise data concerning important parameters such as the energy consumption and the water cost. These are in fact greatly influenced by the many variables which change from a hybrid configuration to another. However, it results interesting to analyze some particular cases of study which have yielded some important results. One regards the hybrid between FO and RO, where the reverse osmosis technology is implemented in the system recovery step. The brine of the RO would then act as the recovered solution. According a study carried by Tzahi Y Cath et al. it has been proven that such configuration can achieve an energy consumption lower than a RO standalone system; in particular it was estimated an energy consumption of about 1.3–1.5 kWh/m^3 [42]. For what concerns the desalinated water cost, it is interesting to highlight a case of study carried by Linares et al. concerning FO-LPRO (forward osmosis-low pressure reverse osmosis). For such system, they have estimated a water cost which can achieve even a 16% reduction with respect an other commonly diffused technology, such as RO [92].

1.4.7 Other types

It is important to notice the desalination techniques mentioned so far are not the only one existing. Water scarcity is in fact considered a primary problem on a world scenario; thus, the methods tried out and the fields of research are multiple. The techniques hitherto described are those which are either the most diffused or that represent one of the most reliable future solutions. However, there are other relevant processes which are worth mentioning.

Cogeneration

Probably the most diffused and classical technique not yet noted is *cogeneration*. It consist in using fuel to produce both power and desalinated water. Moreover, it can be employed in a variety of configurations, each with its own capital costs and energy requirement [53]. This solution allows to increase the thermal efficiency of single-purpose power plant; typically from 35% to 65-82 % [93]. Some countries particularly suffering from chronic water shortage like Israel, have introduced even the idea of using cogeneration in nuclear power plants [94].

VC - Vapour Compression

Desalinated water can be produced also by means of *vapour compression*. As water vapor is compressed, it is in fact able to provide the heat needed to evaporate salt water. In particular, this is achieved by means of two similiar techniques; one is *mechanical vapour compression* (MVC) and the other is *thermal vapour compression* (TVC). A general schematic valid for both cases is shown in figure 1.18. The feed water first passes through a heat exchanger, here its temperature increases while the fresh water condenses. The salt water is then sprayed into a chamber where it is heated up by some old compressed vapor, in order to evaporate. After, the new vapor is gathered into a channel and it is compressed mechanically (trough a mechanical compressor) or thermally (through a steam ejector), so that it is able to raise its temperature. Then, the vapor is able to heat up the new sprayed seawater coming in. The brine left in the vessel is pumped away and divided into two streams: one is recirculated within the new feed water, while the other is pumped away as a waste [32].

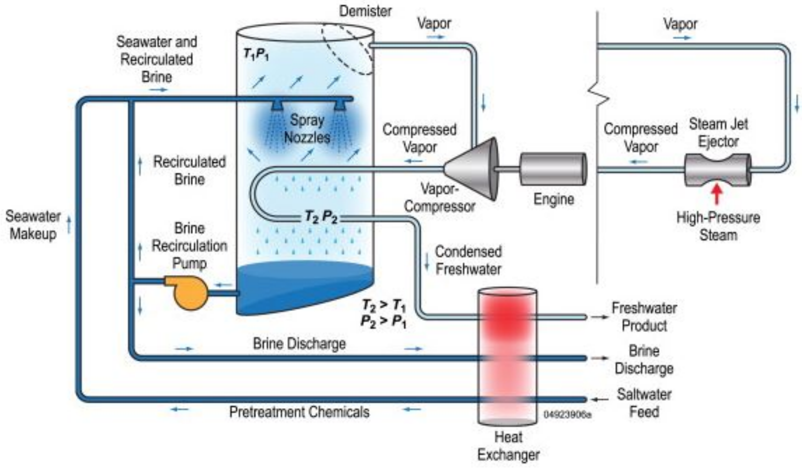

Figure 1.18: Schematic of a MVC (and TVC) plant (adapted with permission) [32].

While MVC is generally built in a single stage, TVC usually has multiple. That is because only TVC thermal efficency can increase by adding new stages [95].

Generally speaking, these techniques are used for small-medium productions: MVC can produce up to 100-3000 m^3/day, while TVC arrives to about 10,000-30,000 m^3/day [32]. Moreover, this technology allows to reach the highest RE amongst all the desalination methods; it in fact amounts to ~85-97%. The energy costs are also usually lower than MSF and MED. Lastly, it is interesting to point out that although this technology best suites feed water with low TDS, it is possible to use it also for high TDS water, as long as corrosion resistant materials are employed in the plant construction [50].

Freezing

Although nowadays *freezing* process (or also *freezing-melting* process) is more diffused for the treatment of industrial wastes [96], it has been for long considered a potentially interesting desalination technique. Its principle of work is opposite respect the one of thermal-based plants: to get rid of salt the goal is no more to evaporate water, but to freeze it . When water freezes, in fact, salt and other minerals are yet unable to crystallize, so the final result will be only fresh ice. Anyhow, the freezing process is actually stopped right before the whole mass of water freezes. Doing so, it is possible to wash the ice before any attachment of salt occurs; the salt is then concentrated in a brine which is brought away. As a final step it is finally possible to melt the water, so to produce the final fresh water [97].

Freezing has historically been a very interesting technique for desalination; theoretically it in fact requires a very low energy consumption. That is because the ice latent heat of fusion is almost one seventh of the water latent heat of evaporation [98]. FM has also been considered attractive for long thanks to other of its advantages. For example, it is important to point out it operates at very low temperatures, which is a condition that minimizes scaling and fouling phenomena, and it allows to work with cheaper materials. Moreover, the technique does not generally require use of any chemicals, and thus, it ensures no pollution problem. However, although it may seem very convenient, there are also drawbacks difficult to ignore. Probably the most striking one is the large capital and operational cost that the plant requires. Not only growing of ice must be considered in fact, but also ice handling (which is mechanically complicated) and washing costs. The system results then complicated and usually inconvenient to build up.

Ion Exchanger

Nowadays, ion exchange is an affirmed mean to desalinate both brackish and seawater. This technology is mainly employed in the production of *ion exchange membranes*, which are generally used for industrial purposes [99]. However, also proper ionic exchanger plants have historically been able to desalinate seawater. They work by mean of electrically charged resin beads, contained in a vessel, in which seawater is introduced through an inlet pipe, located at the top of the container. The water is then able to flow towards the bottom, crossing the pores between the beads. At the same time, as the beads are electrically charged, they are able to remove salt from water. At first, on the surface of the resin beads, there are in fact positively and negatively charged counterions (H^+ and OH^-); however, as the ionic strength of the sodium (Na^+) and chloride ions (Cl^-) is higher than that of the counterions, they are able to replace H^+ and OH^- on the beans surface. Hydrogen ions and hydroxide ions can then merge to form a new water molecule. The phenomenon is also depicted in figure 1.19.

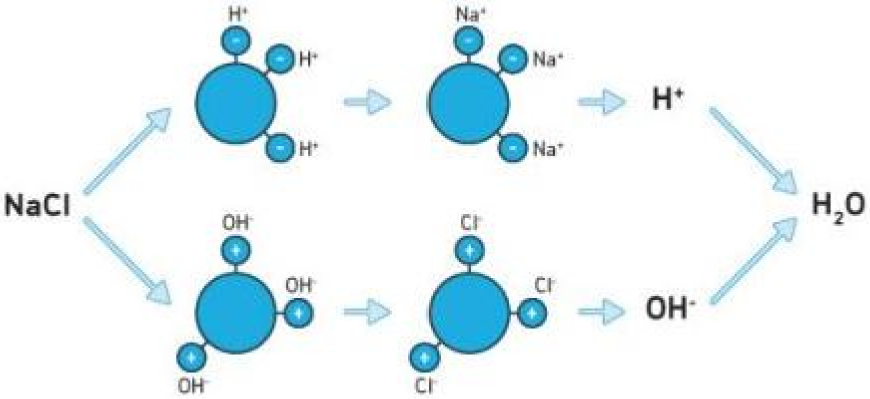

Figure 1.19: Ion exchange on the beads surface [100]

By means of this process, salt is progressively removed from water, until, at the bottom of the container, it is forced to pass through a filter and it is finally ejected as freshwater. Once the beads cannot accept anymore ions, a cleaning operation is required. The process is then reversed using an acid and a base, to regenerate respectively the cation and the anion exchangers.

Ion exchanger allows to reach very high water quality; however, the use of strong acid and alkaline causes a grave environmental impact. Moreover, the capital and operational costs of the system are generally too high to make this technology consistently competitive [97].

1.5 Passive systems

1.5.1 Solar still

Solar still is the most antique desalination method, its working principles is in fact very simple: it is a direct process which uses solar energy to evaporate water. In particular, it exploits the greenhouse effect. The simplest configuration of solar still consist of a container, having at the bottom an insulated layer covered by some shallow seawater, and a tilted (or sometimes double-tilted) lid of clear glass. Solar radiation is then able to pass through the glass and water is able to evaporate. As the vapor raises, it comes to contact with the glass and it then condenses. After, the drops of fresh water can finally flows along the tilted glass so to be collected apart.

During the years, there have been many progresses concerning solar still configuration that have greatly improved its performance. Nowadays in fact, there exist many types of solar still; some of the most common are depicted in figure 1.20.

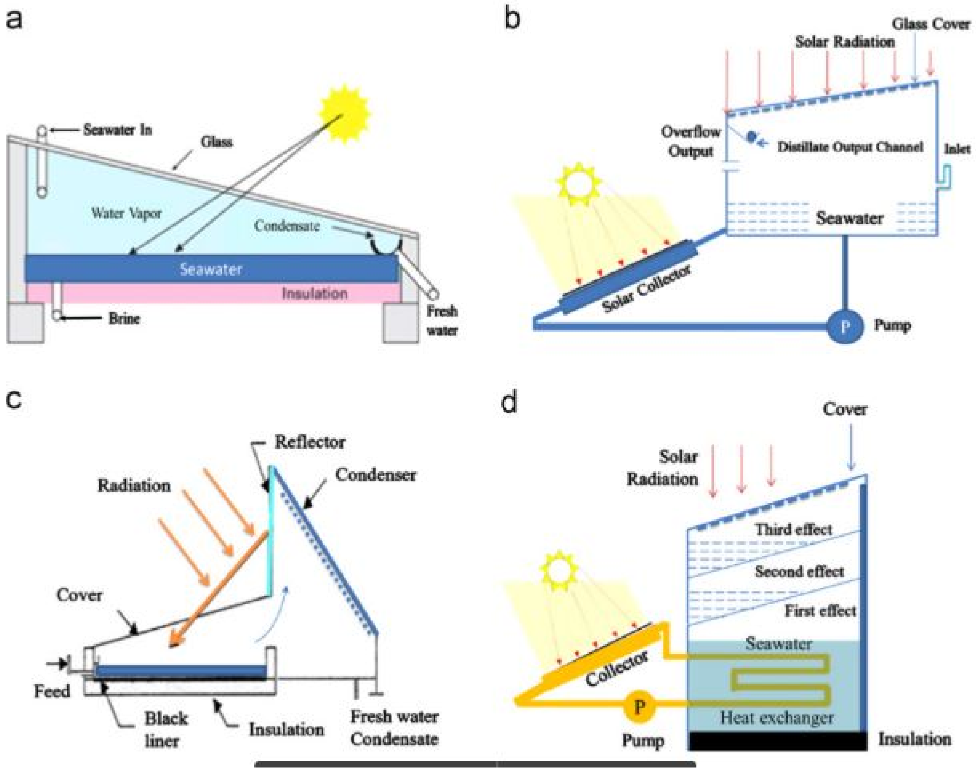

Figure 1.20: **a)** Single stage device; **b)** Coupling with collector; **c)** Coupling with condenser; **d)** Multi-stage device (adapted with permission) [76].

There are both active and passive configurations of solar stills, but this technology is rarely employed at an industrial level because of its relativity low freshwater capability. The daily production depends in fact on the device area, and unless very big plants were built (which results inconvenient), the productivity is very limited. Nevertheless, solar stills are still considered very beneficial for remote area applications. This technology is in fact able to provide high quality water without causing any pollution. Moreover, the set-up and operational costs are relative low, which makes this technique ideal especially for arid regions, which are rich of sunshine and with a limited water availability [101].

Due to the variety of devices exploiting this technology, it results difficult to give a general idea of the performances which solar stills are able to provide. It seems then convenient to analyse a particular case of study, which serves also as a glimpse on the state-of-the-art of this technology. The study carried on by Hiroshi Tanaka & Koji Iishi is very interesting; it had proved the validation and feasibility of the coupling of two solar still configurations: the multiple-effect diffusion still (MED) and the tilted wick still (TW). A schematic of these two diffuse technologies is shown is figure 1.21.

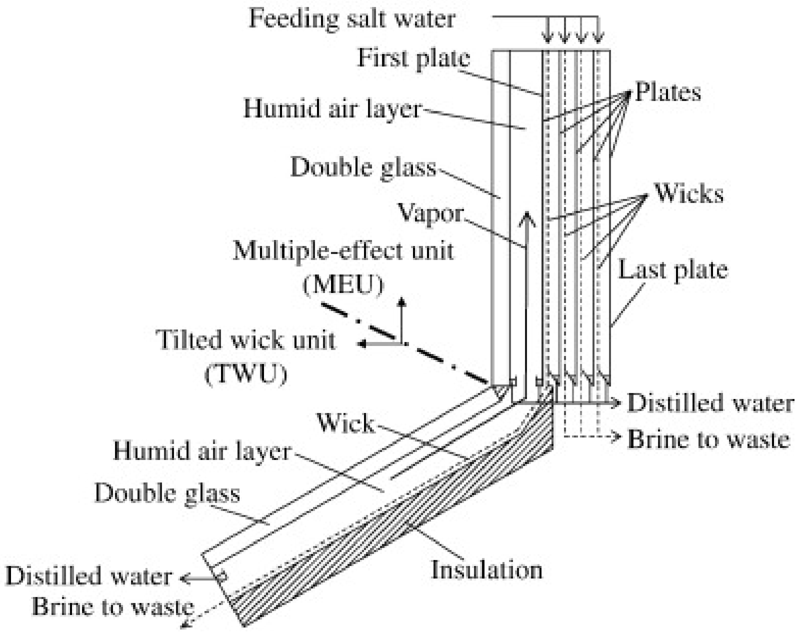

Figure 1.21: Schematic of the coupling of a MED and a TW still devices (adapted with permission) [102]

.

Saltwater enters in the system from the top of the ME unit, through the wicks. It is important to notice, of all the MEU wicks, only the first one is connected to the TWU wick. Through solar radiation, water in the TWU is able to evaporate. As the humid air layer bewteen the two units is connected, such vapor condenses mostly when coming in contact to the TWU double glass, while a part of it is brought up by natural convection. This vapor then condenses in the MEU, and the latent heat of vapor helps out the solar radiation, to provide the energy to cause evaporation in the first stage of the MEU. Here it is then started a multi-stage process, in which each plate of the MEU works both as an heating and condensing surface. The evaporation at the n stage, occurs by exploiting the latent heat of vapor of the $n-1$ stage. At the end, the brine is ejected from the base of both the TW and MED units [102].

The relevancy of this study dwells on the performance reached by the system. As no more industrial active system are being treated, parameters as the "cost of water" or the "energy consumption" loose interest. Passive device will mostly be exposed to the solar irradiance, which can only vary depending on the location and the weather condition. "Cost of water" becomes more senseless as these devices aims to produce water for private use, in regions where water is not accessible at all. An interesting parameter becomes then the productivity of the system; now the main goal is in fact to produce as more water as possible in a day, so to satisfy the water needs of the most people in a community. On this matter, this device has shown very good performances respect other solar still plants [103]. It was proved experimentally that with natural exposure at an average irradiance of 700 W m^{-2}, it could be obtained an average mass flow rate per meter square of 0.936 L m^{-2} h^{-1} [102].

1.5.2 Direct irradiation + MD

An overview of MD technology has already been proposed in the relative section, on page 26. As it is already been discussed, membrane distillation has the big advantage to work at low temperatures and pressures, but the big drawback to require a relatively high energy consumption. Due to this aspect this technology is not widespread on an industrial level yet, but with research advancing it may be one of next generation one. However, in applications for use in remote areas MD has already been widely used, especially when the passive system were required. In this cases, sunlight is exploited as the system external energy source. This is used to evaporate seawater, which is then able to pass through the porous membrane, driven by the difference in the vapor pressure.

In direct MD technology an important objective is to maximize the water vapor flux. To do so, it is possible to increase the vapor pressure difference, which in turn depends on the temperature difference across the membrane. Thus, it is important to maximize such gradient in order to have an higher productivity of fresh water. It results then important to provide additional heating to the feed water. This could be achieved by coupling the system with industrial processes (but the solution would not be passive anymore), or using solar absorbers to couple with the feeding system [104, 105].

However, a more interesting solution has been proposed by Dongare et al. They have proposed to further locally heat the feed membrane, in order to reduce unwanted heat transfer phenomena such as *temperature polarization*, which is responsible for causing the bulk temperatures at the intake and the distillate, to do not be consistent with those at the membrane surfaces. [106]. To accomplish this task, *nanophotonics-enabled solar membrane distillation* (NESMD) was employed, a variation of conventional direct MD technology. Here, light absorbing nanoparticles have been embedded in the membrane hot surface to enhance solar absorption. Water vaporizes on the hot side, then, free of salts, it can condense on the other side of the membrane. With this solution vapor flux is remarkably higher. A schematic of the two techniques is shown in figure 1.22 [107].

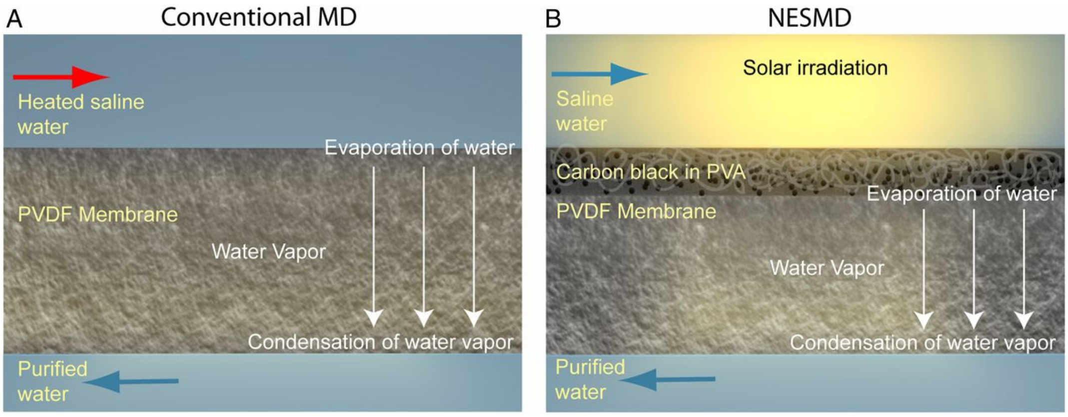

Figure 1.22: Comparison of a conventional direct MD process vs a NESMD process [107]

.

The adsorbing layer is made of carbon black nanoparticles. It is important to notice there exist an ideal concentration of CB in the polyvinyl alcohol (PVA). In fact, it is intuitive that a too low concentration yields less sunlight absorption, but also a too high concentration is not optimal. It in fact would cause most of the adsorption to be only on top of the PVA, so the membrane would not get heated up and the temperature gradient would not be maximized.

Generally speaking, NESMD not only has presents an higher vapor flux respect MD, but also a better solar efficiency and a salt rejection of over 99.5%; for such reasons, it is a very interesting technique to look at, also for scale-up studies. Neverthless, this technology has shown very good performance: undergoing a solar irradiance of 700 W m^{-2}, the productivity had reached 0.5 L m^{-2} h^{-1} [107].

1.5.3 Low-cost solar steam generator

Solar steam generation is a smart way to desalinate water as it uses only renewable energy and it does not release any pollutants. However, this technology is not suitable to produce large quantity of fresh water; therefore, many studies have been carried on about improving this process efficiency and productivity. One of the most striking reason for the limited solar steam efficiency dwells in most devices design. Solar steam generator are usually built assuming a direct contact between the solar absorber and the bulk water. This solution makes inevitable to have thermal losses throughout the bulk water; these are as more relevant as higher is the quantity of water treated. The energy transferred from the solar absorber to the bulk water is in fact not all used to evaporate the top layer of water but some is also "dissipated" through the bulk water standing below. The scalability of the system is then limited, as if more water wants to be desalinated, the efficiency drops. To avoid this phenomenon Li et al. have proposed a smart solution, presented in figure 1.23**B**.

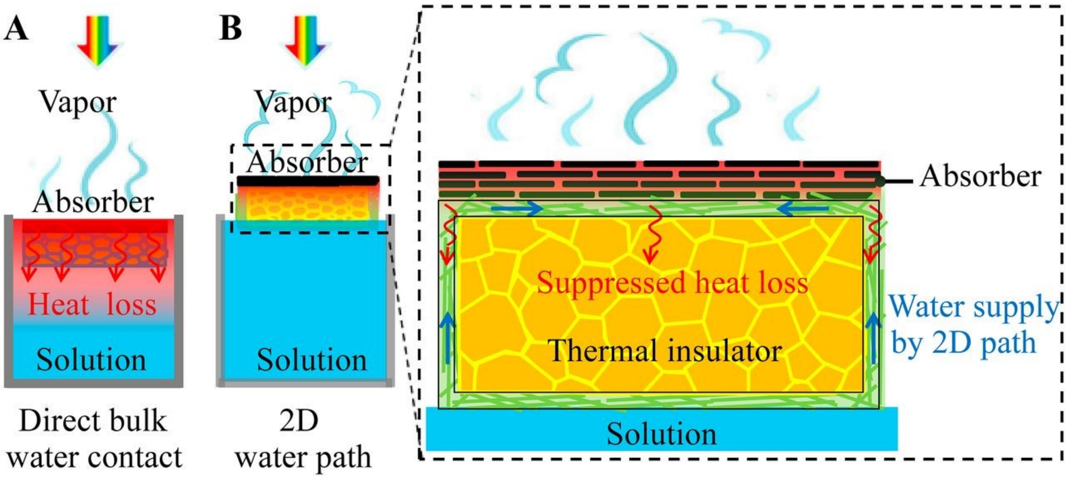

Figure 1.23: **A)** Conventional diret contact steam generator **B)** Li et al. solution of a 2D water path [108]

.

The goal of this device is to create a 2D water path, to suppress heat loss and provide an efficient way to produce water. A floating thermal insulator stands upon the bulk water. This component is wrapped in an hydrophilic foil. Water is then pumped into this foil by capillary forces and when it reaches the top, it spreads over a 2D layer. As water reaches the top of the device, it is able to exploit the solar energy gathered by the absorber to vaporize. The solar energy used is maximized, as all of it is employed in water evaporation. The absorber is made of a graphene oxide layer, a low-cost material, with a porous structure, ideal to let water and vapor pass through it. It also has a very low thermal conductivity in the normal direction (an aspect which allows to further minimize the thermal losses) [109]. The hyrdophilic foil is instead made of cellulose, which can be naturally attached to graphene oxide. The thermal insulator chosen is instead a polystyrene foam, able to float over the bulk water. The overall construction of the device is then shown in figure 1.24.

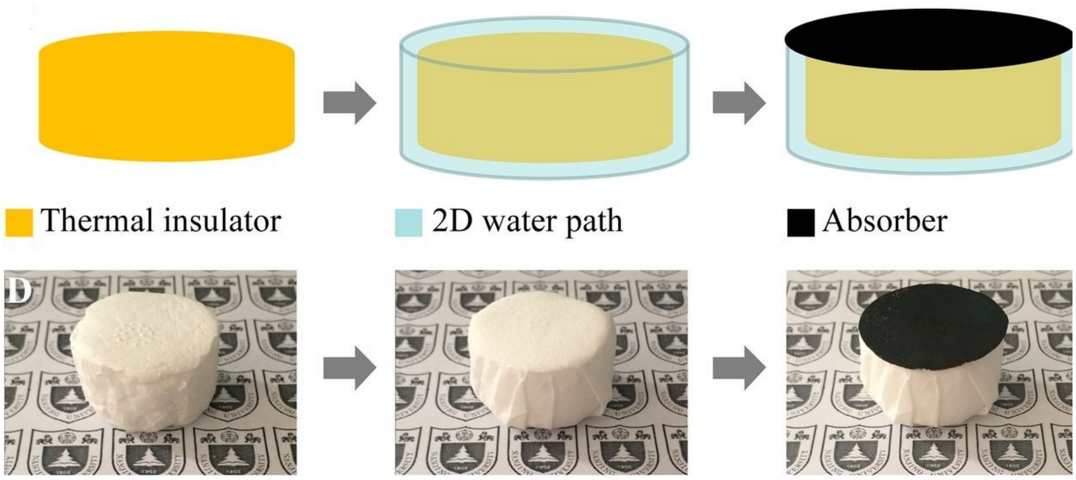

Figure 1.24: Device fabrication [108]

.

Having overcome the obstacle of scalability, this method is very interesting to be considered also for larger productivity employment in future applications, maybe even at an industrial level. The productivity of the system under one sun (1000 W m^{-2}), is in fact much higher than the one of many other passive technologies; this system has reached productivity as high as 1.45 L m^{-2} h^{-1}. Moreover, the energy efficiency resulted to be ~80% and it is now independent of the amount of water treated; an aspect which is very rare to find in any desalination technology [108]. The low-cost and high performance characteristic of this device makes it then an ideal solution to be employed in remote areas which lack of water infrastructures.

1.5.4 Advanced solar steam generator

Other passive solutions aiming to produce steam by means of solar energy, usually require the employment of a cavity or a surface to absorb sunlight. The heat can then be transferred directly or via a fluid to the bulk water, which then evaporates. However, this type of technologies are limited by a low energy efficiency. These systems often require high optical concentration, to which it follows an higher complexity, capital and operational cost of the system. Moreover, they suffer from various types of energy losses. Another possibility would then be to use lower optical concentration, reducing also convective heat losses through the use of vacuum, but this solution would still generate an higher cost of the plant [110]. Finally, a state-of the-art technique which employs low optical concentration, exploits the use of *nanofluids*, which work as volumetric absorbers, in order to anneal surface energy loss. However, even in this case, the thermal efficiency, does not get higher than 24% [111].

A big step forward on the resolution of this matter has been brought by Ghasemi et al. who have reported the development of a new device, able to overcome most of these problems. They promoted a double-layer structure, able to float on water. The layer in contact with the bulk water is insulating, hydrophilic and porous; the top layer has also the same properties but rather than insultating, it is absorbing. The property of hydrophilicity ensures a constant flow of water upwards due to the capillarity forces. The absorbing layer, does not require the need of high optical concentration, making the system simple and not very costly. Lastly, the insulating layer is able to suppress most of the thermal losses, allowing to employ most of the solar energy for water evaporation. A schematic of the system is shown in figure 1.25, where it is also depicted a gradient of the temperatures.

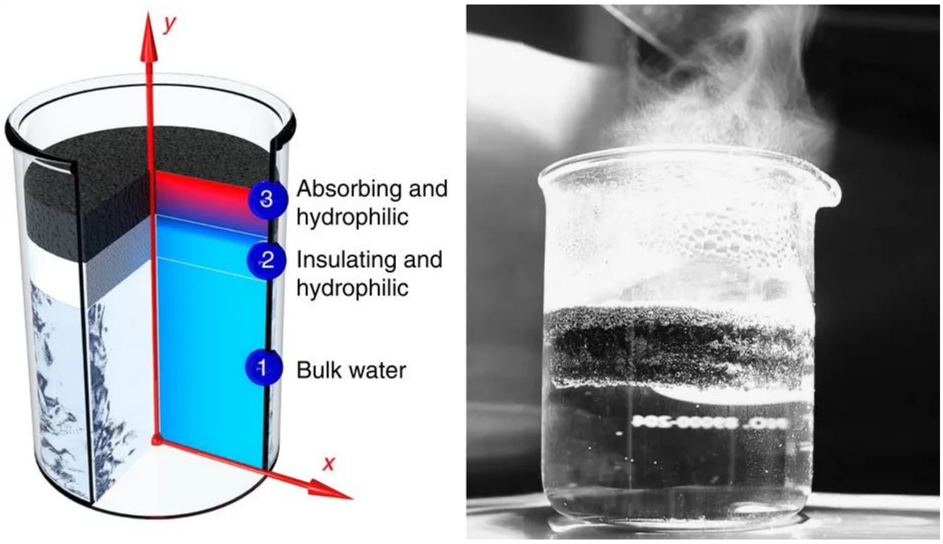

Figure 1.25: On the left a schematic of the structure cross section approximating the temperature distribution. On the right a picture from the experimental campaign (adapted with permission) [112].

.

More in particular, the insulating material used is a carbon foam with small pore size, suitable for the passage of water. On top of it, it is deposited the adsorbing layer, made of exfoliated graphite, which on the other hand, it has larger pore size, as it needs to allow vapor to pass through it. Exfoliated graphite is an ideal, material for this type of application because, other than attaching to the carbon foam and having suitable pore size, it guarantees a reflectivity lower than ~3%, which translates into the possibility of adsorbing more than 97% of the solar power, greatly enhancing then the overall process thermal efficiency [112]. An illustration of the double-layer structure is proposed in figure 1.26.

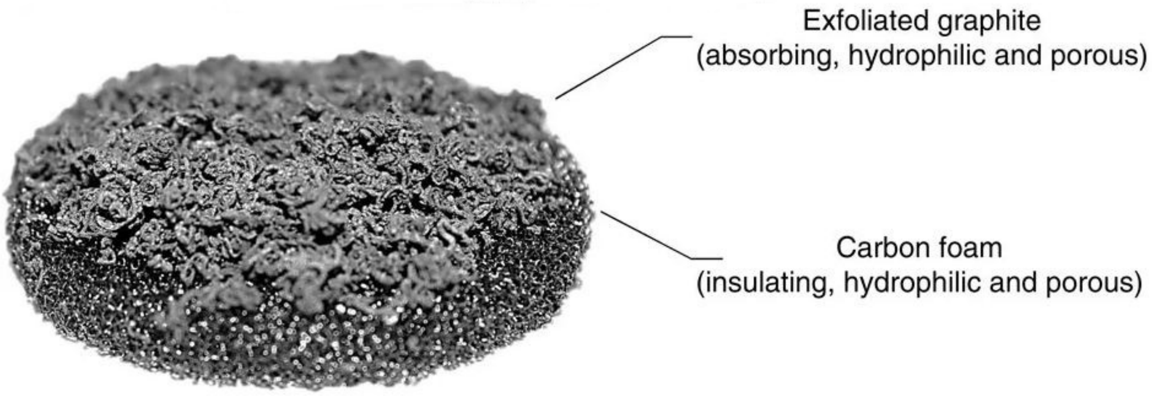

Figure 1.26: Double-layer component (adapted with permission) [112].

.

This technology allows to maintain as low optical concentration as the one in open air, keeping also relatively low costs. But the most interesting result of this study is the incredibly high thermal efficiency that it has been reached: as high as 85%. Moreover, Ghasemi et al. attests these performances may be even further improved, by using a more insulating material than the carbon foam and by optimizing the thickness and the porosity of each layer. Furthermore, this device was tested under different irradiance levels and so it was detected a range of different production rates depending on it. Under one sun, this technology was able to achieve production rates of about 1.076 L m^{-2} h^{-1}, while at 10 kW m^{-2} the productivity even reached 12 L m^{-2} h^{-1} [112].

1.6 Thesis outlines

The work of this thesis is organized into different sections. After having provided a detailed analysis of active desalination technologies and some state-of-the-art passive desalination technologies in **Chapter 1**, the scaled-up version of the innovative passive solar-driven device, objective of this thesis, is illustrated in **Chapter 2**. Here, designing and prototyping processes are extensively illustrated, and the the theoretical model supporting the system functioning principle is also discussed. In **Chapter 3**, numerical simulations results, obtained by means of the COMSOL Multiphysics® software, are explored to figure out the best configuration of the device. The results brought up by the in-field experimental campaign are reported as well. Finally, in **Chapter 4** a summary of this work is presented along with the most important conclusion drawn in this thesis and suggestions concerning future works.

Chapter 2

Methods

2.1 Introduction

A problem which has not yet been mentioned, common to most passive desalination technologies, is the inability of the passive devices to recover latent heat of condensation when fresh water returns to its liquid phase. A considerable amount of energy usually gets wasted into the environment, while it could instead be exploited to improve the thermal efficiency of the system [113]. Some attempts have already been executed historically [102], but they always ended up employing also active components, thus loosing all the advantages belonging to passive technologies. The *SMaLL Laboratory*, a scientific research group working at the Department of Energy of Politecnico di Torino, have recently developed a multi-stage solution to solve this problem, which allows the system to overcome the thermodynamic limit that a single-stage desalination device needs to withstand. That would be the solar power (considering one sun) related to the latent heat of vaporization of water at 20°C; such limit amounts to about $1.471\ \mathrm{L\,m^{-2}\,h^{-1}}$. This study is the first one to present very innovative concepts, such as the multi-stage complete distillation process and the passive feeding water system. Moreover, it keeps all the advantages of passive desalination technologies, eventually bringing them even further. During testing in fact, the device showing the best performance had shown a productivity which was considered so far prohibitive for passive technologies; that is 3 L m^{-2} h^{-1}, up to for times of the usual state-of-the-art performances. Results brought by theoretical model are even more relevant as they showed a potentially higher productivity: 6 L m^{-2} h^{-1}. This result could practically be achieved by optimizing some of the device features, amongst which the most important regard improving the thermal insulation layer and optimizing the materials and thicknesses employed. However, these improvements would probably increase also the cost of the device, while one of the main initial goal of this research was to keep it low [113]. Nevertheless, because such promising performances were reached, a step forward needed to be done. To make the system practicable to use in remote areas, where it could actually satisfy the daily drinkable water needs of a person (2 L per day [114]) or a whole family, a scale-up of the system needed to be made. That is the main objective of this work: to build a scaled-up version of the innovative passive solar high-yield seawater desalination technology, developed at Politecnico di Torino, based on a smart combination of low-cost materials. The main goal of this chapter is then to provide a full explanation of the steps which had to be crossed for the realization and experimentation of the new scaled-up prototype. The designing process along with the guidelines, which had to be respected throughout, are exposed. Furthermore, it will carefully be analyzed the experimental set-up built in the laboratory, with the problematics encountered and the new resolutive configurations conceived. Finally to the description of the theoretical model will be reported at last.

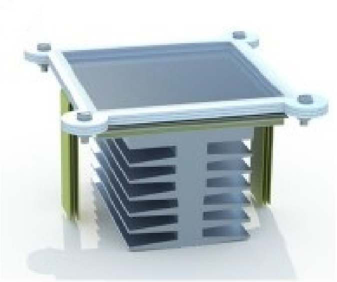

Figure 2.1: CAD of the small modular solar high-yield seawater desalination device (adapted with permission) [113].

.

2.2 Working principle

The working principle of the scaled-up device is very similar to the one of its smaller counterpart. The main idea is to reduce the characteristic distance between the two thin hydrophilic layers in order to enable a more efficient multiple complete evaporation/condensation cycle. A schematic of the system is shown in figure 2.2. The feeding system is simply composed by some hydrophilic membrane strips, which protrude from the evaporator at each stage. Seawater can thus be pumped into the system by exploiting the related capillary forces. After, it continuous its path within the membrane aided by gravity. Respect the smaller device, a cross-flow configuration has been devised, in order to overcome the limited capillary-driven water transport exasperated by the increased size of the unit. The system was in fact designed over an inclined support (tilted about 16°). The hydrophilic membranes are attached to some thin aluminum sheet (with area 56x38 cm^2) by means of either silicon or some double-sided tape. In the first stage, the upper part of the aluminum sheet is covered by a spectrally selective solar absorber. In detail, it is made of TiNOX®, a suitable material to absorb solar radiation primary due to its optimus characteristic of high solar absorbance (about 0.95), low emissivity (about 0.04, thus limiting radiative thermal loss), and relatively low cost (5 \$ m^{-2}, not considering scale economy). At the very top of the device, covering the solar absorber, it is disposed a PMMA panel, which helps reducing convective heat transfer. The material was chosen because it allows to guarantee high transparncy to sunlight (about 0.93), low cost (1.80 \$ m^{-2}, again not considering scale economy) and good mechanical strength to protect the TiNOX® from any external damage. As the aluminum layers are really thin (1 mm), it is possible to approximate a 1D thermal conduction along its cross section. Conductive heat losses at the panel borders are then negligible. Overall, through solar irradiance and thermal conduction, the aluminum sheet is heated up with a very high efficiency. Thermal energy is thus transferred to saltwater, which is then able to evaporate. For the same working principle governing the MD technology, the vapor flux is driven by a difference in vapor pressure (which is in turn given by the difference in temperature and water activity) through the hydrophobic membrane. A schematic of this principle is shown in figure 2.3. The membrane hydrophobicity is given by both the geometrical structure and chemical composition of the surface. Vapor is then able to condense on the colder side of the stage, and it is gathered in a new hydrophilic membrane as distilled water. This latter can then flow within the condenser membrane. Finally, it is guided, along some protruding strips, into a freshwater basin. At the same time, strips protruding from the evaporator lead the brine out of the system. Both of these processes are aided by gravity. The latent heat of condensation released by water in the last part of the stage is re-used as the input for the new stadium. This last principle is fundamental to overcome the thermodynamic limit current passive desalination devices are used to front. Overall, a total of 3 stages were implemented in the scaled-up version, in order to withstand the allowable costs and encumbrance of the device. In the very last stage, the condenser is left in contact with open air, so to make it work as an heat sink. Convection is then enhanced, in order to increase the system thermal gradient and thus its vapor flux .

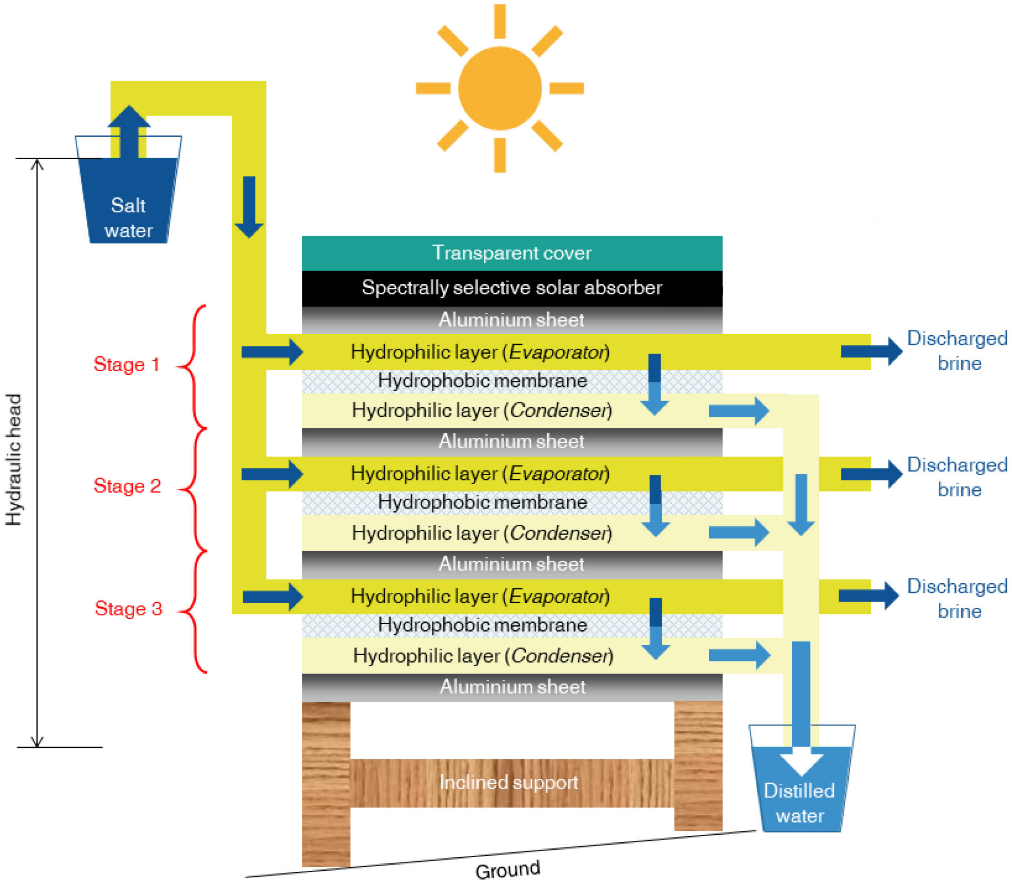

Figure 2.2: Schematic of the scaled-up modular solar high-yield seawater desalination device.

.

The cross-flow configuration implies the presence of an hydraulic head. Exploiting Young-Laplace law, which describes the capillary pressure difference between two static fluids at the interface, it was in fact estimated that saltwater should not be located at the feet of the device, to allow the capillary forces to drive it into the system. Then, a basin needs to be placed and fulfilled upstream, at the top of the device. This procedure, makes this preferable to work in remote areas rather than above the sea. An external operator is then also required, although to perform very simple operations.

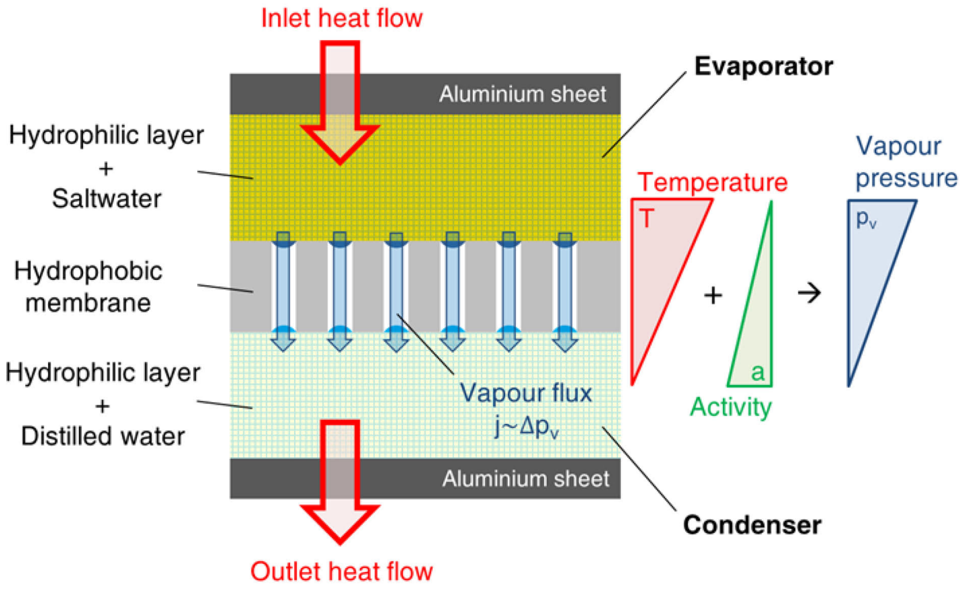

Figure 2.3: Working principle of the scaled-up modular solar high-yield seawater desalination device.

.

The smaller version of the distiller has an area of 12x12 cm^2. Hydrophilic and hydrophobic membranes, solar absorber and aluminm sheets are employed as in the same way just described. Contrary to the first realization of the device, te scaled-up version exploits a cross-flow design. For the smaller system, in fact, the capillary forces are sufficient to promote a continuous water flux; namely, by working with smaller areas, the aid of gravity is not necessary, as the capillary forces are enough to wet the whole membrane layers. Furthermore, in this case, a brine discharge apparatus is not present. Moreover, in this older configuration, rather than a PMMA panel, a 3D printed structure is used to avoid convection at the top layer. [113].

2.2.1 Salt removal

During the distillation process, as water evaporates from the hydrophilic layers, salt is just partially drained out by the outgoing brine; the remaining part remains in fact trapped in the layer, thus increasing its salt concentration. This phenomenon has an effect on the overall system productivity, as water activity (defined as ratio between vapor pressure in a substance and vapor pressure in pure water) is inversely proportional to salt concentration. Thus, the productivity decreases when the salinity increases as indicated by the Raoult's law, which describes how the salinity and the temperature of the solutions affect the vapor pressure:

$$\Delta p_v = a(Y_E)p_v(T_E) - a(Y_C)p_v(T_C) \tag{2.1}$$

Δp_v is the difference in water vapor pressure at the two sides of the hydrophobic membrane; p_v is respective water vapor pressure, depending on the temperatures T_E and T_C; a is the water activity, which instead depends on the salt mass fractions Y_E and Y_C. The subscripts indicates respectively the evaporator and the condenser region.

To ensure durable desalination performances, the salinity of the hydrophilic layers acting as evaporators must be regenerated. This can be done by rinsing the membrane with some additional seawater (at its typical salt concentration of 35 g L^{-1}), at the end of each working day. Although this procedure is very simple to perform, it requires some external activity from an operator.

2.3 OHDC

Throughout most of the device design and development process, the guidelines imposed by a modern world wide contest have been followed as a method to guarantee the device appealingness, respect the other state-of-the-art solutions, on different levels. This expedient not only made possible to actually compete on a proper challenge, thus having the chance to benefit from an eventual succeeding, but it also permitted to get some external opinions, thus having the possibility to gain prospective feedbacks for any possible prototype future improvements.

In particular, the *Oman Humanitarian Desalination Challenge* (OHDC) was chosen as the most suitable competition to this purpose. This challenge was initiated by the cooperation of MEDRC Water Research and the Oman Research Council. It does not surprise that one of the most active countries promoting desalination competitions is Oman. According the World Resource Institute, in fact, Oman was ranked as the 16th country in the world, which is suffering the most from water scarcity [2]. However, the competition's goal is to achieve the realization of a new product that can be quickly distributed, at affordable costs, to people living in those regions which are suffering mostly from water scarcity; mainly remote areas. Devices must also be conceived in order to be used in other critical scenarios. For instance, after a natural catastrophes (as a tsunami or a hurricane), when seawater may be submerging entire cities and people may be wandering on life rafts in lack of drinkable water. Furthermore, it becomes also important to have a small single-use device, that can fulfil its purpose of taking bacteria and viruses as well as salt, out of water, to produce not just distilled but also drinkable water.

In detail, there are 9 general guidelines that have been considered by the OHDC necessary characteristic of the ideal desalination device. They are used as a meter to judge the various competing technologies. These are listed as follows:

1. **Low Cost** - Because the device needs to be distributed on a large scale, especially in those areas considered the poorest, the maximum production cost needs to withstand

within a 20$ budget.

2. **Handheld-size** - The device needs to be small and easily transportable, as it may be moved every day to a close water source by a single person; or when employed for rescues purposes, it may be carried around in critical conditions by a lone individual.

3. **Easy to use** - The system must be very easy to operate. The average user will in fact most likely be an ordinary person, with no technical background knowledge.

4. **Robust** - The apparatus must be resilient and corrosion resistant. It should also minimize the employment of assembling components, in order to avoid the loss of any parts which would make the device inoperable. Thus, the shelf-life itself should be maximized.

5. **Easily transportable** - The overall system should be very light and ergonomic. To transport it by hand, even for long distances, should not result an issue.

6. **Minimum rate of production** - The device is supposed to produce a minimum of 3 litres of freshwater per day, a bit more then the average drinkable needs of a single person.

7. **Stand-alone** - The system needs to be passive. No addition of chemicals, fuel, or other external materials other than the seawater, is allowed. It should thus result possible for the system to be employed in remote areas, at almost zero operational costs (a rare maintenance may always be required) with null polluting discharges.

8. **Water quality** - The device needs to be able to purify 100 NTU (Nephelometric Turbidity Unit), so to bring water from a 35 g L^{-1} concentration to a maximum 1 g L^{-1} TDS. This level falls within WHO maximum contaminant levels [71].

9. **Short-term use** - The device should be able to operate for a minimum of 30 days.

2.4 Experimental set-up

As already mentioned, the design of the prototype was based on the already tested smaller working device. The differences previously highlighted (mainly concerning the cross-flow configuration, the brine discharge and the PMMA panel), were taken into account to devise the new scaled-up version, and the proper changes were adapted during the prototyping process. Therefore, it follows now a description of the components that were needed to realize the prototype, along with their fabrication and assembling. After, auxiliary instruments, employed in the experimental campaign for the data acquisition, will also be examined. Lastly, some of the device most important features, concerning its characteristics and its proper use will be discussed.

2.4.1 Device composition

After the designing process, the realization of the prototype was here executed manually. In detail, the components employed for the realization of a single device are the following:

1. **Transparent cover**: PMMA panel of dimensions 59.5x42x0.25 cm.
2. **Solar absorber**: aluminum sheet of dimensions 59.5x42 cm coated by a TiNOX® layer on one side.
3. **Aluminum sheets**: (x3) of dimensions 56.5x38x0.1 cm.
4. **Hydrophilic layers**: made of microfiber, they were acquired as standard sized wicks of dimensions 34.5x34.5 cm.
5. **Hydrophobic membranes**: (x3) made of polytetrafluorethylene (PTFE), of dimensions 63x52 cm, with pore sizes ranging from 0.1 μm to 3 μm .
6. **Plastic components**: polypropylene (PP) was used to shield the protruding strips of hydrophilic layers in order to prevent water evaporation, which would otherwise increase the salt concentration layers; (Low-Density Polyethylene) (LDPE) was used

to cover the evaporator side of the aluminum sheets, in order to avoid any corrosive phenomena, as the metal might have otherwise come in contact with saltwater.

7. **Adhesive aluminum tape**: cut in strips which were then attached partially overlapped, so to form an adhesive flexible sheet of dimensions 41x25 cm.
8. **Inclined support**: crafted plywood supports, tilted at an angle of ~16°. The supports dimensions are 27x4.3x4.3 cm (rear) and 16.3x4.3x4.3 cm (fron).
9. **Bolts**: (x14) M5 bolts, A2-70 (austenitic, cold worked acid proof stainless steel), and respective nuts of the same material.
10. **Seawater basin**: simple plastic with internal dimensions of 46x9.5x8.5 cm.
11. **Brine basin**: simple plastic container with internal dimensions of 29.5x23.8x9 cm.
12. **Fresh water gathering bag**: (x3) some catheters were adopted as freshwater basin.
13. **Elastomeric component**: rubber was carved in hollowed rectangles, chracterized by an external geometry of 59.5x42 cm and an internal one of 55.5x38.5 *cm*; and in strips of dimensions of either 56.5x2 cm or 38x2 cm.

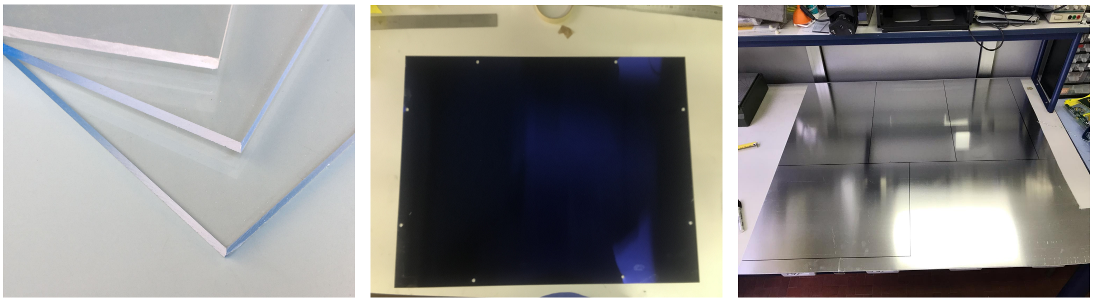

(1) Transparent cover (2) Solar panel (3) Aluminum sheets

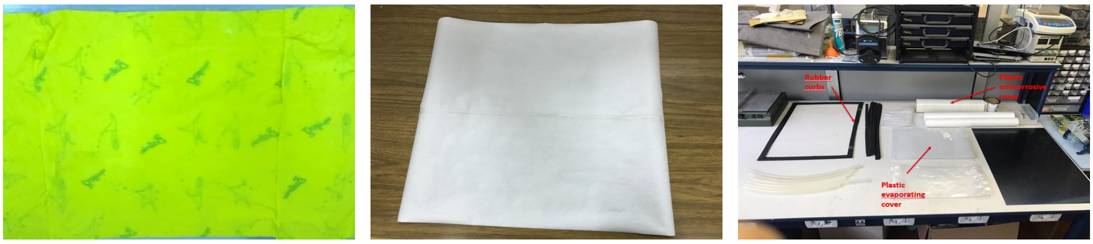

(4) Hydrophilic membrane (5) Hydrophobic membrane (6) Plastic and rubber components

(7) Adhesive aluminum shield (8) Plywood supports (9) M5 Bolts

(10) Seawater basin (11) Brine basin (12) Freshwater bag

Figure 2.4: Representations of all the components employed in the prototype construction.

As a first step, most of the previously described components were properly customized accordingly to their purpose. The PMMA panel, for example, was shaped through a jig saw. The aluminum layers were cut through the help of both a shear for iron (able to yield a more accurate cut, but also causing a foil inflection), and a grinder (less accurate cut, but no inflection). The hydrophobic and hydrophilic membranes were modified as well. As the first were available in rolls wide 27 *cm*, to get the desired shape, each membrane was crafted by overlapping two of them and then attaching them together by means of some biadhseive tape. The hydrophilic membranes, on the other hand, had initial dimension of 34.5x34.5 *cm*. Therefore, they needed to be carved and stock together, in order to obtain the desired shape of both the protruding strips at the evaporator and the condenser. The geometries realized are depicted on figure 2.5:

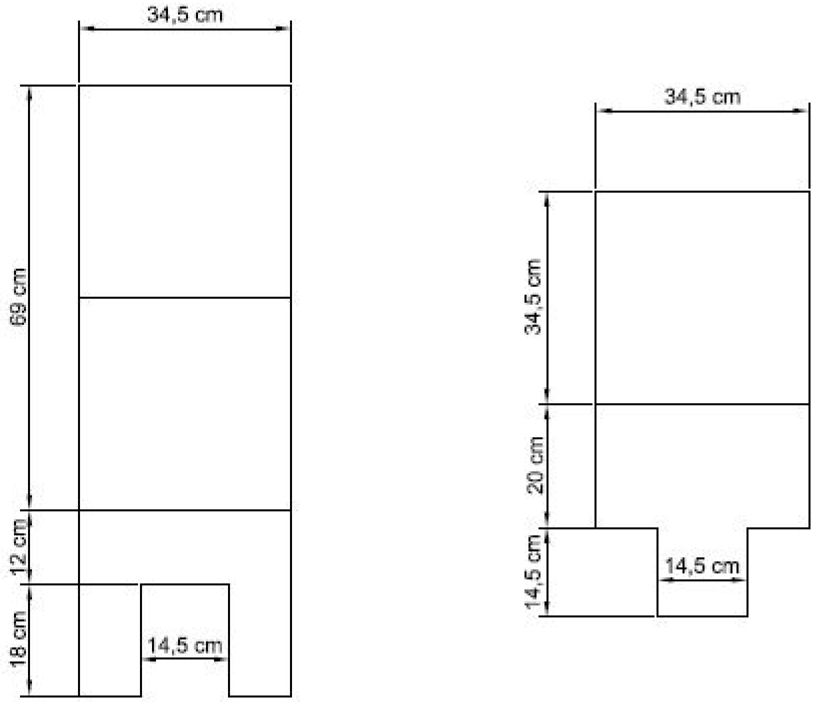

Figure 2.5: Sketch of the evaporator (left) and condenser (right) hydrophilic membranes.

Therefore, to realize an evaporator and a condenser, there were needed respectively 3 and 2 hydrophilic units (34.5x34.5 cm each). As 3 stages were implemented for each distiller, a total of 15 membranes were employed in the construction of each distillation device.

Some elastomeric material was also cut in hollow rectangular shapes, with external dimensions of 59.5x42 *cm* and an internal one of 55.5x38.5 *cm*, and strips of either dimensions of 56.5x2 *cm* or 38x2 *cm*. This component was used as a gasket to interpose between the PMMA panel and the solar absorber, to further decrease convective thermal loss and to avoid any accidental compression of the hydrophilic layers. On the other hand, to prevent any water evaporation outside the panel area, the cloths connecting the apparatus to the environment were covered with some PP layer, previously sealed together through a MACOM VAC2060 sealing machine (shown in figure 2.6d). These envelopes were then employed to contain the protruding strips at the evaporator and the condenser. In the evaporator strips, in fact, evaporation would have caused an increase in the membrane salt concentration, thus leading to a performance decaying. In the condenser strips, instead, water evaporation would have resulted in a direct loss of produced distilled water.

(a) Yielded sealing

(b) System input cover

(c) System output cover

(d) MACOM VAC2060.

Figure 2.6: Plastic protection to prevent evaporation in the protruding strips.

Other crafting operations, regards the realization of the plywood supports, the smaller one with dimensions 16.3x4.3x4.3 *cm*, the taller ones 27x4.3x4.3 *cm*. These were realized through the help of a rotary saw. A slope of ~16 ° was set at the tip of the supports to allow the cross-flow configuration functioning. Furthermore, a 6 *mm* hole was realized at the tip center of each support, to create space for a screw plug to insert (as shown in figure 2.7a). This, coupled with the bolts, enabled the supports assembling to the last stage of the device. Overall, the main inclined support purposes are to establish a hydraulic head between the seawater and distillate basins, and to ensure the water flows gravity's aid.

Lastly, the catheters, used as freshwater basin, were carved (as shown in figure 2.7b) in order to suitably be coupled with the outgoing condenser strips. To work as freshwater basins, catheters resulted as an ideal solution. The first design, conceived to attach to the protruding strips of the condensers to some silicone rubber tubes that could ease the freshwater collection. However this solution showed different problematics; it resulted very unhandy, and it did not enable a sealed freshwater basin, which would have then been at risk from any external contamination. The expedient of using catheters not only solved many of these problems, but they also provided a neat low-cost solution to withdraw freshwater at the end of each working day, by exploiting the embodied throttling valves.

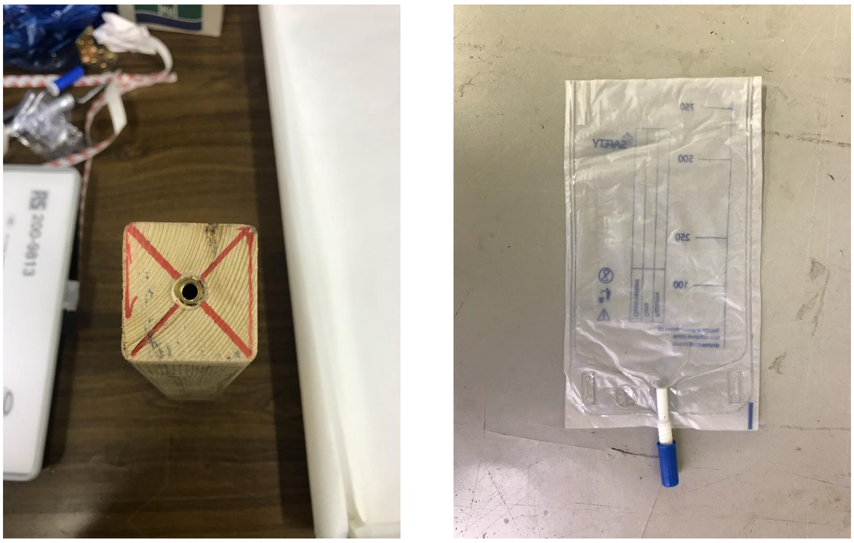

(a) (b)

Figure 2.7: How the screw plug inserted in the supports (a), and how the catheters were adapted to be used as freshwater bags (b).

2.4.2 Device assembling

After having customized most of the components, some further fixed assembling procedures needed to be executed to obtain the modular parts. After, these had to be coupled together, in order to form the final working device. In this section, there are then going to be described both of these processes. It is important to point out that while the fixed assembling does not have to be repeated every time the system is newly put into operation, the modular one it is.

Device fixed assembling

To form the ultimate solar absorber component, the aluminum sheet covered by TiNOX® had to be coupled with the transparent cover. The goal of this latter, is not only to reduce convective heat loss, but also to work as a shield to protect the panel from salt and powder, which if deposited on the TiNOX® surface, would otherwise reduce the solar power absorbed. At this point, it is worth to highlight that this technology is designed so that condensation of water drops does not influence the transmittance of the transparent cover. In typical solar stills, in fact, this is usually considered a big limitation of the technique. However, the transparent cover is not directly in contact with the TiNOX®, as this configuration would not be completely sufficient to avoid air infiltration at the borders. The rectangular rubber shape is then here placed, so to work a gasket. The three components are fixed together by means of 10 M5 bolts. The final result is shownw in figure 2.8a.

After, evaporators and condensers are built on the aluminum sheets, by attaching over the hydrophilic layers. It is important to notice that as in the evaporators flows just seawater, this might actually corrode the aluminum, thus causing an higher need of maintenance. To overcome this problem, some LDPE, is secured over the sheets by means of a biadhesive tape, as shown in figure 2.8b. Although it may seem that this expedient introduces some additional thermal resistance, created by either the air gaps between the aluminum and the plastic or the plastic itself, the necessary consideration have been made. By laying the LDPE as flat as possible, the thermal losses due to the air gaps staying in between are negligible. For what concerns the plastic itself, this layer is extremely thin (in the order of ~10 mu m). Even though thermal conductivity of the LDPE is low (0.33 W m^{-1} K^{-1} at 20°C [115]) then, the exchanged heat will encounter a negligible resistance by crossing this layer.

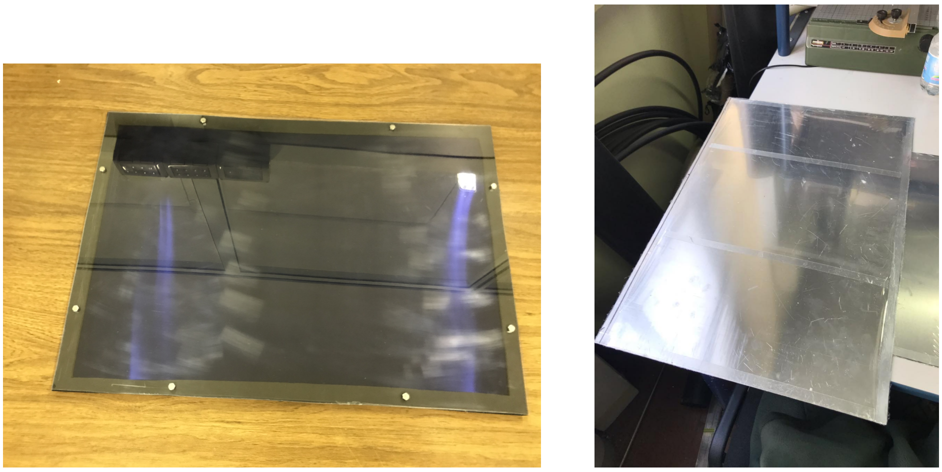

(a) Solar panel (b) Aluminum sheet

Figure 2.8: Assembled solar panel and example of a shaped aluminum sheet covered in a plastic.

As it could first be noticed from figure 2.2, of the 3 aluminum sheets needed for each device, one of them hosts one evaporator (the first one from the top), two of them host an evaporator on one side and a condenser on the other, and the last hosts a condenser (the last from the top). In particular, in the working device all the evaporators are always collocated below the aluminum sheet to which they are attached (they face downwards), while the condenser are above (they face upwards). To allow the laying of an aluminum layer one over the other, without compressing the hydrophobic membrane that will stay in between, some additional rubber strips are glued at the side of each condenser by means of some silicon. By doing so, the characteristic distance of the hydrophilic membranes is still kept low, thus enabling an efficient multiple complete evaporation/condensation cycle at ambient pressure. Moreover, lateral thermal losses are also kept minimized. Lastly, the hydrophilic membranes are properly attached to the respective sides of the aluminum layers, by means of both biadhesive tape and silicon, to finally form the complete evaporator and condenser components. Each mounted together in a very compacted manner, keeping each membrane very stretched, in order to avoid any additional air gap which would act as an other thermal resistances. A picture of the final result is shown in figure 2.9a and figure 2.9b.

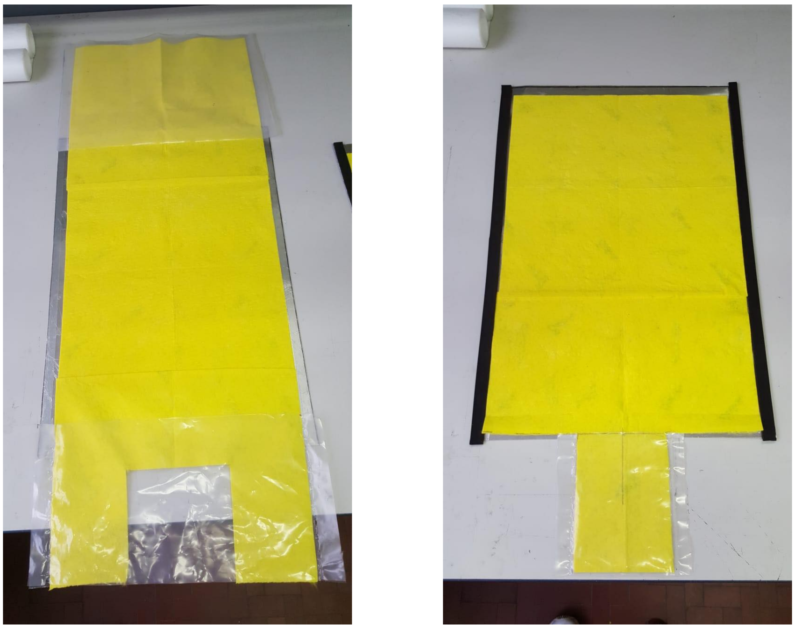

(a) Evaporator (b) Condenser

Figure 2.9: Representation of the constructed of evaporator and condenser components.

The last fixed mounting process regards the coupling of the plywood supports with the last stage of the device, the coupling of the aluminum tape shield with the protruding in going strips at the evaporators, and the freshwater bags incorporation. These latters were simply attached to the membrane strips by means of biadhesive tape, positioned internally respect to the bags, as shown in figure 2.10a.

The aluminum tape shield was built by partially overlapping some tape strips and fixing them together. The component was then attached on top of the first evaporator protruding feeding membrane, as depicted in figure 2.10b. The goal of this system is to do not concede water solar heating before it enters in the system, as it would otherwise cause unwanted evaporation (here the water vapor flux would go dispersed, also increasing salt concentration, and thus reducing the device productivity).

Finally, on the last condenser, 4 holes were executed at the corners of the panel. These were built as a space to insert the 4 remaining A2-70 bolts, useful to attach the last stage of the device to the plywood supports, as represented in figure 2.10c. This solution provides a robust, cheap and light apparatus able to impose the desired slope, and at the same time able to leave the bottom of the last condenser in contact with open air. This last part works then as a heat sink. Convection is enhanced, and an higher thermal gradient will lead to an higher vapor flux, and thus an higher productivity of the system. The plywood supports are exposed in this section as their assembling is definite. However, they are also eventually easily removable, thus to be carried separately, thus the system transport more effortless.

(a) Freshwater bag coupled (b) Aluminum tape shield (c) Coupled plywood support

Figure 2.10: Additional operation performed on the prototype construction.

Device modular assembling

After having executed the fixed mounting processes, assembling of the modular components is a simple repeatable operation, which can be performed within a couple of minutes. This aspect results very advantageous whenever a scenario where the distiller needs to be transported and mounted by a single person occurs. The processes which will now be described needs thus to be executed every time the system is newly put into operation.

The composition of the system starts from the bottom. Having the first condenser mounted on the plywood support, the first hydrophobic membrane is laid over, by keeping it stretched in order to minimize the occurrence of eventual air gaps. It is worth to point out, the PTFE membranes are hydrophobic only on one side, which thus needs to be faced upwards, towards the evaporator. Next, another aluminum sheet is laid over, having the first evaporator facing downwards on one side, and the second condenser facing upwards on the other. After, an additional hydrophobic membrane is laid over, and the whole process is repeated once again. The last evaporator is then positioned on top the stack, it is then left a bare aluminum sheet in contact with air on its other side. It is here that it is laid the solar panel. A composition of these steps in showed in figure 2.12, while on figure 2.11, it is presented how the final stratigraphy will look like.

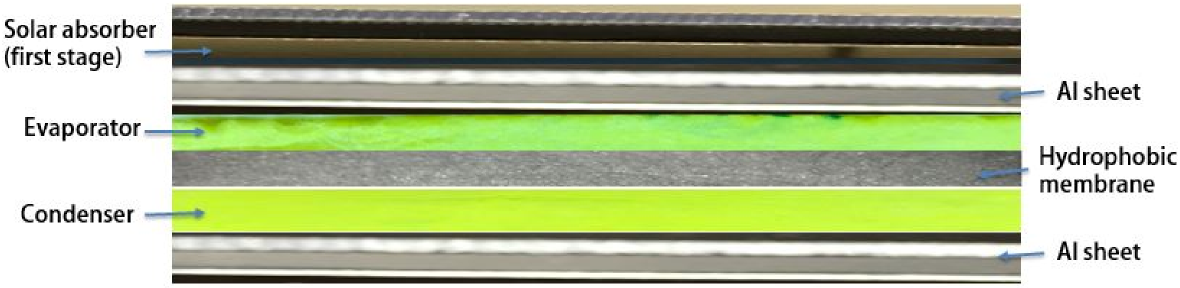

Figure 2.11: Representation of the device stratigraphy.

.

It is important to mention that although the modular assembling is practically an easy operation to perform, it needs to be done carefully, as the system productivity or the water quality may depend on it. For example, both the hydrophilic and hydrophobic membranes need to be very stretched to maximize the heat transport efficiency. Moreover, attention must be paid also to the condition of the PTFE membrane. This material is in fact hydrophobic but just as long as it stands within certain pressures. If the membrane is randomly subjected to an high compression (e.g. during mounting), it will get punctured and water will be able to pass through. In this case, as freshwater is at risk of being contaminated, the membrane needs thus to be changed.

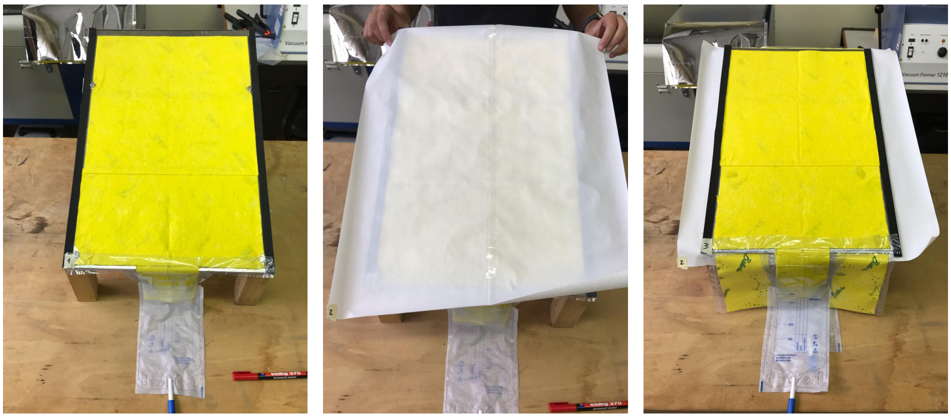
(1) First condenser mounted on the wooden support

(2) First membrane laid over the first condenser er

(3) First evaporator laid downwards, and second condenser facing upwards on the other side.

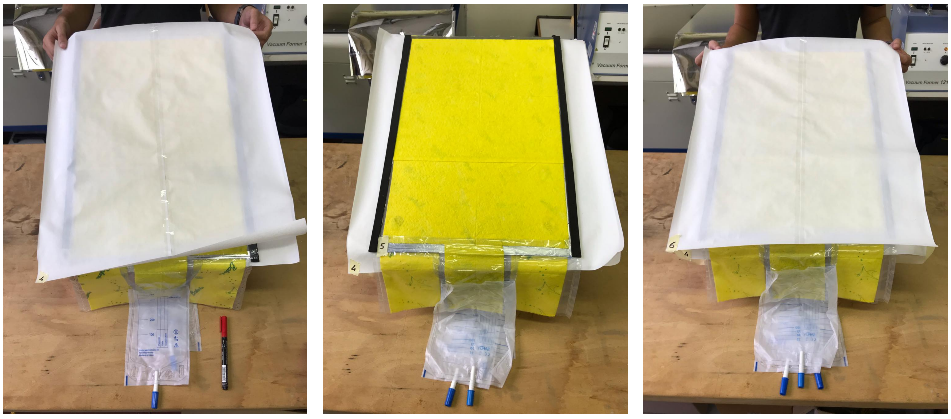
(4) Second membrane laid over the second condenser er

(5) Second evaporator laid downwards, and third condenser facing upwards on the other side.

(6) Third membrane laid over the third condenser er

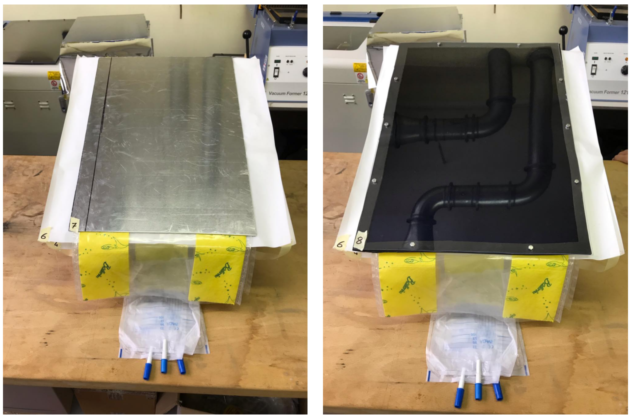
(7) Third evaporator laid downwards, a bare aluminum sheet left upwards.

(8) Solar absorber laid on the aluminum sheet

Figure 2.12: Set-up steps of the device modular components.

Lastly, the device should be coupled with each respective basin. In particular that would be the seawater basin upstream, and the undistilled seawater basin downstream. This latter is not strictly required unless there exits a the brine discharged issue. The seawater basin should also be covered by some reflecting sheets, in order to avoid free evaporation of water in the environment. Evaporation in the upstream basin would in fact increase the salt concentration of the feed water, thus decreasing the distiller productivity. In a working day, the mounted distillation device theoretically will produce 1 l/day; being its RE of 5, that means it must treat at least 5 l/day of saltwater. The user must then always ensure the seawater basin is fulfilled till providing this amount. Moreover, to benefit from the optimal performances of the distiller, the device is supposed to be placed on a flat surface with good sun exposure. In the Boreal Hemisphere, that would be facing the South direction.

Figure 2.13: Completely assembled distiller: the old version on the upper left is compared to the new version depicted on the upper right and its lateral view at the bottom.

2.4.3 Device features and characteristics

As previously discussed, throughout the whole designing process, an objective was to undergo the criteria imposed by the OHDC, not only to join the challenge but also to use their guidelines as a mean to assure the device appealingness. In this section it will then be analyzed how the distiller prototype meets the competition criteria, along with some of its most particular characteristics.

1. Low cost

Being the prototype a passive device, the operating costs are almost negligible. The only expenses may derive from the possible manpower which is needed to assemble the device and to refill the seawater basin. However, these operations are extremely simple, so also in this case such costs would be very low. Therefore, the price of the system relies only on the one of its components realization. In detail, as already shown, theses processes are not complicated as they mainly comprehend simple operations such as cutting, gluing, holing metal or customizing the plastic parts. For this reason, the cost of the device is very close to the one of the raw materials which compose its different parts. These have in turn be carefully chosen so to be relatively cheap. In table 2.1 it is shown the estimated cost of the whole desalination device. The prices of the units where taken from the respective wholesale supplier, namely *Alibaba*. The prices considered were also chosen assuming a large orders of raw materials was going to be requested.

	Unit cost	**Amount**	**Actual cost**	**Reference**
Hydrophilic membranes	0.65 $\$/m^2$	1.50 m^2	0.98 $	Alibaba wholesale
Plastic envelope	1.80 $\$/kg$	0.15 kg	0.27 $	Alibaba wholesale
Aluminum sheet	2.00 $\$/m^2$	0.85 m^2	1.70 $	Alibaba wholesale
TiNOX® panel	5.00 $\$/m^2$	0.25 m^2	1.26 $	Alibaba wholesale
Transparent cover	1.76 $\$/m^2$	0.25 m^2	0.44 $	Alibaba wholesale
Hydrophilic membranes	1.00 $\$/m^2$	0.76 m^2	0.76 $	Alibaba wholesale
Adhesive aluminum tape	0.50 $\$/m^2$	0.10 m^2	0.05 $	Alibaba wholesale
Rubber curbs	0.07 $\$/m^2$	4.48 m^2	0.31 $	Alibaba wholesale
Tilted support	0.12 $\$/L$	1.55 m^2	0.18 $	Alibaba wholesale
Freshwater bags	0.11 $\$/units$	3 units	0.33 $	Alibaba wholesale
M5 bolts	0.001 $\$/units$	14 units	~0.01 $	Alibaba wholesale

Table 2.1: Estimation of the production costs for one desalination device.

On the other hand, the analysis of the costs of the raw materials only, needed for the construction of device components, is represented in table 2.2. The prices considered were taken once again assuming a large order demand. This estimation is further from the real one as constructing new components from scratch would require the adequate machinery and manpower; however,it also allows to take a cue about eventually new source of savings, if the device is going to be produced in large quantities in the future.

	Material	**Unit cost** *[\$/kg]*	**Weight** *[kg]*	**Actual cost** *[\$]*	**Reference**
Hydrophilic membranes	Microfiber	1.50	0.35	0.53	Alibaba wholesale
Plastic envelope	PP	0.60	0.20	0.12	Alibaba wholesale
Aluminum sheet	Aluminum	0.99	1.70	1.68	Made in China wholesale
TiNOX® panel	Aluminum + TiNOX®	-	0.35	1.26	Alibaba wholesale
Transparent cover	PMMA	0.55	0.73	0.40	Alibaba wholesale
Hydrophilic membranes	PTFE	7.00	0.05	0.36	Alibaba wholesale
Adhesive aluminum tape	Aluminum + Acrylic adhesive	-	0.01	0.03 \$	Alibaba wholesale
Rubber curbs	Elastomer	0.40	0.10	0.04	Made in China wholesale
Tilted support	Plywood	0.08	0.75	0.06	Alibaba wholesale
Freshwater bags	Silicon and plastic	-	0.05	0.33	Alibaba wholesale
M5 bolts	A2-70 steel	-	0.10	~0.01	Alibaba wholesale

Table 2.2: Weight and estimation of the raw material costs for one desalination device.

Overall, one desalination device result costing ~6.29 \$. A proof that this cost is really close to the one of the raw materials used is given by a comparison with this latter. The cost of the raw material employed in the construction of one device is in fact ~4.82 $. However, as already mention, one device is able to produce about 1 L day^{-1} of freshwater, thus, to pursue the initial goal of 3 l/day, 3 devices need to work in parallel. In this case, the cost of the device composition needs to be multiplied. It then reaches ~18.87 $, or considering the cost of the only raw material ~14.46 $. As the initial goal was to withstand a 20$ budget, it can be safely affirmed that the employment of this technology would respect such criteria. Lastly, it is relevant to highlight that amongst the initially cited device components, the seawater and brine basin were not mentioned. That is because the device would not actually comprehend these parts, but they need to be separately added for its use. Anyway, as no particular restriction are related to these components, any shallow basin would actually accomplish the task.

2. Handheld-size

Overall, the dimensions of the desalination device are 60x42x3 cm, in length, width and thickness respectively. Its weight amount instead to 4.4 kg (13.3 kg, account for all 3 devices). These characteristic allows the system to be practically very handy. Moreover, a proper envelope design could actually be developed to further ease the device manageability. However, it must to be also pointed out that when the system is carried at the end of a working day, it will be wet and thus heavier. In detail, it was experimentally noticed that the membranes can host an intrinsic volume of 0.7 kg. In this case, the system would weight up to 5.1 kg (15.3 kg, account for all 3 devices), which is still a manageable load to carry for a man though.

3. Easy to use

The assembling of the modular parts can be performed within minutes. The relatively low weight allows the operator to transport it even for long distances. To keep the system simple, throughout the whole designing process, the principles of frugal engineering were followed. As a result, the desalination device is composed by a low number of spare parts, and it is very easy to start-up, to operate and to maintain. Furthermore, its use does not employ any material or chemical which could be otherwise toxic to the ambient and/or operator.

4. Robust

As there are no moving parts, wires or chemicals in the desalination device, it is very unlikely for it to break. In the worst case scenario, the hydrophobic membrane (the most delicate component) would get punctured, thus causing contamination in the product. However, this is also very unlikely to happen as these components, in working condition, are kept in between two soft porous membranes,that protect the PTFE from accidentally tears or being cut. Moreover, the rubber curbs help avoiding any accidental compression of the hydrophobic layer. On the other hand, the resilience of the device stands on its ability to work even if the layers are misaligned, or some small damage concerning their planetary occurs. The composition of the system also ensure a corrosion resistant property. Aluminum alloys are in fact are extremely resistant to seawater corrosion, because, when aluminum does corrode, the thin coating of aluminum oxide that forms, creates a protective shield that inhibits any further corrosion. Furthermore, a LDPE coating was applied to the evaporator side of the aluminum sheet as a further protection from corrosion. Lastly, in order to ensure a long shelf-life, the number of layers employed in the system were minimized. Only 8 layers are in fact designed, and all of them are big enough to make the device transport handy, with no risk of loosing some auxiliary component which would compromise the device usage.

5. Easily transportable

When the system is completely dried out, it weights 4.4 kg (13.3 kg acounting for all 3 devices). This characteristic allow the system to be easily transportable and very handy. Eventually, it could be designed a proper envelope to deliver along with the device, embodied with an handle, to further ease its manageability.

6. Minimum rate of production

The multi-stage concept allows to re-use the solar energy up to three times (once for each stage), thus yielding a higher productivity and smaller surface area, especially respect to traditional solar stills. During the experimental campaign (which will be lately discussed), a single desalination unit has demonstrated to produce an average of 0.57 L kWh^{-1}. In a city like Muscat, Oman, where on average the solar irradiation amounts to 199 kWh m^{-2} per each month (data grabbed from the online software PVGIS), that would then allow the device to produce up to 1.15 L day^{-1} on average. In detail, it is 0.87 L day^{-1} in the worst scenario (namely, when stagnant air is in the proximity of the device) and 1.42 L day^{-1} in the best scenario (namely, in light wind condition). In fact, a better natural convection is preferable to enhance the heat flux through the different distillation stages. To meet to the requirement of 3 L day^{-1} (more than a single person drinkable water needs), 3 desalination units are then required. Although this solution may seem cumbersome, it intrinsically owns the big advantage of being extremely resilient. In fact, even if one desalination units gets damages, the user would still benefit from the distilled water produced by the other two devices.

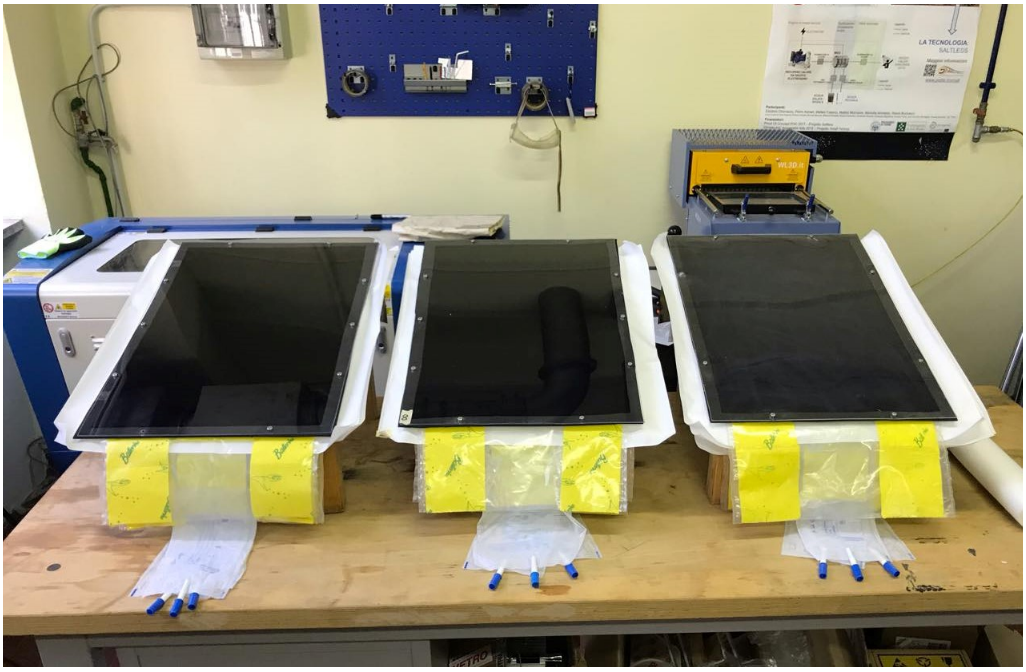

Figure 2.14: Ultimate presentation of 3 desalination units.

7. Stand-alone

The desalination device is completely solar-driven. Any evaporation and condensation processes are guided by the thermal gradient induced by the thermal solar energy. No need of any other external power source is then required, which is a big advantage not only economically but also pollution-wise. Moreover, the system can work during the day with no need of supervision a part from re-filling the seawater basin, thus making the device practically independent. Eventually, solar position could also be tracked to move the device accordingly, to maximize its performance, but this is not a strict requirement.

8. Water quality

Salt removal is a key argument for all distillation technologies. Most devices employing thermal distillation technique inherently provide high-quality products. According the experimental experience, a result of 0.0 g L^{-1} of salt concentration is in fact mostly obtained. Actually, although this device is designed to distillate seawater, it was proved that it can practically work also with higher level of salinity (at a lower production rate though). However, salt removal is not the only requirement needed to obtain good water quality. Theoretically, as the hydrophobic membrane are crossed by only water vapor, also other particles contained in the feed water should be inhibited from passing through. It was then executed a laboratory test to prove that the turbidity of the seawater does not influence the quality of the freshwater produced, namely that it has no effect on the selectivity of the hydrophobic membrane. The test is represented in figure 2.15.

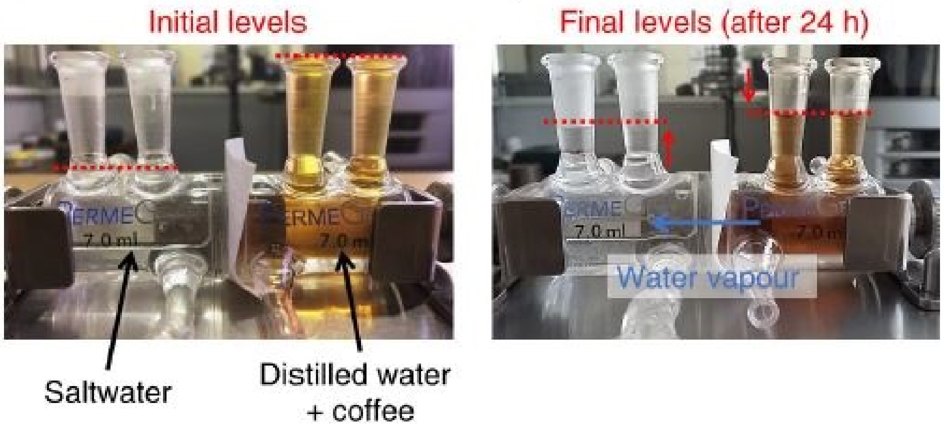

Figure 2.15: Testing the effect of turbidity on the selectivity of the hydrophobic membrane.

At first, two chambers, filled at different levels, one with saltwater and one with distilled water and coffee (left and right respectfully), were separated by a PTFE hydrophobic membrane. After 24 hours, water had flown into the saltwater chamber, guided by the osmotic gradient. It was then observed no contamination of coffee in the saltwater, thus proving that that solid particles could not permeate through the membrane. Concerning the contamination due to bacteria (according to the WHO standard), the same considerations hold as well. Furthermore, the re-generating operation which is supposed to be done at the end of each device working day, and the temperature to which the membranes are subjected (usually between 40°C and 60°C), both help also to prevent the accumulation of particles and the partial pasteurization of bacteria, allowing to never reach particularly high level of turbidity.

9. Short-term use

As long as the salinity of the hydrophilic membrane at the evaporator is regenerated every day, experimental experience has shown the ability of this device to work for even long-term periods. However, the regeneration step is fundamental, not only to re-establish the right vapor pressure within the system, but also to prevent the hydrophilic membranes from drying out. This phenomenon would in fact cause the generation of a transient at the begin of each working day, which would then cause a decrease in the device daily productivity.

2.4.4 Experimental layout

In order to carry out the experimental campaign, auxiliary devices were coupled with the desalination system, in order to detect the quantities of interest to be studied. Experiments were practiced mainly outdoor due to difficulties encounter in replicating the same conditions indoor. However, before arriving to this conclusion, also indoor trials were carried out. Only few differences occurred in the aiding instrumentation employed between the two cases. In this section it will then be extensively discussed the instruments that have been used for the complete experimental layout, employed during the experimental campaign. As it can be noticed from figure 2.16a and figure 2.17a many components were common to both types of experiments. Amongst the few differences, many were not due to the diverse environment but were adopted at different stages of the prototyping phase (in figure 2.16a it is how the device looked in July, in figure 2.17a in October). As already mention, in fact, the system was sometimes improved in parallel with the experimental campaign; an example of such differences is the installation of catheters, employed lately, rather than polymeric tubes. Overall, the auxiliary instrumentation used during the campaign can be summed up in the following items (in italic the additional components used during the indoor tests):

1. **Laptop**: for data storage and post-processing elaboration.
2. **DAQ**: data acquisition board, to connect the laptop to the measurement instruments.
3. **Thermocouples**: to detect the temperature profile in the device studied areas.
4. **Digital refractometer**: for salinity measurements.
5. **Digital scale**: for distillate mass measurements.
6. **Modular distiller**: objective of this study.
7. **Pipette**: to extract water samples.
8. ***Quartz light lamp***: to emulate the solar irradiance.
9. ***Pyranometer***: to verify the adequacy of the irradiance emitted by the lamp.

Figure 2.16: Indoor experimental layout

Figure 2.17: Outdoor experimental layout.

(1) Laptop (2) DAQ (3) Thermocouples

(4) Digital refractometer (5) Digital scale (6) Modular distiller

(7) Pipette (8) Quartz light lamp (9) Pyranometer

Figure 2.18: Auxiliary instrumentation employed during the experimental campaign.

Laptop, DAQ and thermocouples worked in sync, to gather the device working temperature profile over time. In particular, 6 thermocouples of the type K, NiCr composed, were employed. These are characterized by a very low thermal mass and a low cost, thus resulting particularly suitable for the equipment assemblies. They exploit the thermoeletric effect of Ni and Cr, to produce a temperature dependent voltage. This signal is then transmitted to the data acquisition system. In detail, this is an hardware, able to convert the analogical signal coming from the environment into a digital one, that can then be processed by the calculator. For the purpose of the experimental campaign, a "TB-9212" DAQ was adopted, mounted on the compact DAQ chassis "cDAQ-9174". Both these components are ideal to work in series with the software used for data analysis, namely LabVIEW, as all these products are come from the same company; the "National Instrument".

The digital refractometer is used for measuring the salinity concentration of the feed water, the distilled water produced, the remaining water in the membranes (before and after the experiments) and finally in brine. In detail, the refractomer employed was an "HI96821", by the "Foodcare line". This device is primarily designed to detect water salinity, by analyzing the refractive index of the solution. Its resolution amounts to 1 g L^{-1}, while its accuracy is ± 0.3 g L^{-1} at 20°C. To gather the water samples, the glass pipette shown in figure 2.187 was used.

Finally, a digital scale was employed to keep track of the distillate mass measurement; a "PCB 1000-2" digital scale, by "KERN", was adopted. This device ensured a resolution of 0.01 g.

During the outdoor experimental campaign, other than the device itself, no other additional components were engaged. Summing up, in fact, the parameters of interest studied have been the distillate mass production, the salt concentration and the device temperatures. Of course, also the solar irradiance is a very relevant parameter, from which the whole system performance depend on. This information was not detected in field only for a commodity matter; it was in fact possible to simply use the data offered by the PVGIS online software, a tool primarily created to estimate the solar electricity production of photovoltaics, storing every day the irradiance of many parts of the world. However, the same considerations do not apply to the indoor experiments case. As already mention, in fact, here two additional components resulted necessary in order to conduct the tests. As shown in figure 2.188 and 2.189, these are the quartz light lamp and the pyranometer. The first one, in detail, is a QL-1000, a professional quartz light head, working at a maximum of 1000 W. This component was thus used to replicate sunlight in an indoor environment. To verify the adequacy of the irradiance emitted by the lamp a "LPPYRA08 Second Class Pyranometer" was used. This device is able to measure the global irradiance (direct irradiance plus diffuse irradiance) on a flat surface, with a sensitivity of 10 mV kW^{-1} m^{-1}. This component was coupled in parallel with the same DAQ linked to the thermocouples, and its data were processed through a slightly different code in LabVIEW.

2.5 Theoretical model

In this section it is going to be exposed the theoretical model supporting the system working principle. Although this latter may seem relatively simple, the physics behind it is not elementary. It is then important to have a deep understanding of the laws which allow the device to work, in order to get a full panoramic of what its limitations are and where instead it could be actually improved. Furthermore, the theoretical approach helps to lay down the foundation about the basic concepts on which the simulations, which will be lately discussed, are based.

The driving force of the each stage of the distiller dwells in the vapor pressure difference existing between each evaporator and condenser respectively. As already mention, this latter is given by the differences in water activities (inversely proportional to water salinity) and vapor pressures (directly proportional to temperature), at the two sides of the hydrophobic membrane. Equation 2.1 previously allowed to understand how these quantities were correlated. Now it is interesting to better perceive their meaning by deeper analyzing the physic. As a start, the water activity can be described more accurately, assuming ideal conditions by equation 2.2.

$$a = \frac{M_{NaCl}(1-Y)}{M_{NaCl}(1-Y) + N_{ion}M_{H_2O}} \tag{2.2}$$

where M_{NaCl} and M_{H_2O} are the molar mass of of sodium chloride and water, respectively. In detail, they are $M_{NaCl} = 58.44$ g mol^{-1} and $M_{H_2O} = 18,015$ g mol^{-1}. Moreover, the number of ions in a sodium chloride molecules is $N_{ion} = 2$. It is then possible to compute the exact value of the water activity both at the condenser and the evaporator, using their respective values of water salinity Y (where $Y = m_{salt}/m_{solution}$). As for seawater $Y = 0.035$, water activity in the evaporator will be $a_e = 0.978$. On the other hand, in the condenser water salinity is supposed to be null, thus water activity will be $a_c = 1$.

On the other hand, the other parameter influencing the difference in vapor pressure at the two sides of the hydrophobic membrane, is the vapor pressure itself. This can be hystorically estimated through different equations that correlates this parameter with temperature. For this case of study it is here used Antoine's semi-empirical correlation, shown as following:

$$\log\left[p_v\right] = A - \frac{B}{C + T - 273.15} \tag{2.3}$$

where p_v is the vapor pressure in mmHg, A,B and C are material constants, and T is the temperature in Kelvin. This equation is valid for not a very large temperature range, corresponding to the pressure interval of 0.01-2 *bar*. Outside of this range, Antoine equation looses its physical meaning; however, it is more than suitable to be used in this application. In this case, while temperatures keep changing during the device working hours, the material constant are respectively $A = 8.07$, $B = 1,730.63$ and $C = 233.42$ [116].

It results now interesting to provide an analytical solution to the produced specific mass flow rate of freshwater (J). To do so, the same steps carried out by Chiavazzo et al. [113] for the smaller device are retraced. The same models are in fact considered to be still valid for the scale-up version. In this piece of literature they have combined the "Maxwell–Stefan model" and the "dusty-gas model", to derive a produced specific mass flow rate equation. While the first one takes in account both the chemical potential and molecular diffusion phenomena, the second one considers the interaction between gas molecules (occurring with porous walls as well) and the viscous flow, usually present in membrane distillation technologies, generated by the total pressure gradient coexisting across the membrane. Afterwards, they have applied some reasonable assumptions in order to simplify the model; these are in order:

- Approximate the mixture of water vapor, hydrogen and nitrogen to the binary mixture of water vapor and air.
- Ideally the air particles are stuck in the pores of the medium, as air is low soluble in water. The air molar flux is then null.
- The viscous flow is considered to be null as there is no total pressure difference between the two sides of the membrane. The whole system works in fact an ambient pressure.
- Ideal gas are taken in consideration; it is then possible to compute the chemical potential of water vapor as $\mu_w = \mu_{w,pure} + RT \ln[x_w]$; being μ_w water vapor chemical potential, $\mu_{w,pure}$ pure water vapor chemical potential, R the ideal gas constant (8.314J K^{-1} mol^{-1}), T the temperature in Kelvin, and x_w water mole fraction.
- When used membrane with porous size of 0.1 μm, pure Knudsen regime may be considered; it in fact takes place when the mean free path of the moleculus is comparable or higher with the scale of the system (the porous walls in this case). For membranes with larger pores (e.g 3 μm), a series of Knudsen and molecular resistors is instead approximated. This aspect will better be exposed, when the total diffusion coefficient will be computed, as a contribution of both Knudsen and molecular diffusion.
- By computing the ratio between the water vapor partial pressure (by means of Antoine equation) and the total pressure (atmospheric pressure), it is possible to compute the water mole fraction, which then results is much smaller than 1. It can be thus assumed $x_w << 1$. In detail, that is especially because condensation is downstream the pore, and not within the membrane where also air is present.

Through this consideration, it was possible to approximate, through a 1^{st} order Taylor series, the specific mass flow rate of freshwater with:.

$$J = K\Delta p_v \tag{2.4}$$

where it is possible to obtain Δp_v from equation 2.1, while K is the permeability coefficient of the gap between each of the two hydrophilic layers. This latter can be approximated as the sum of the contribution of the membrane permeability. In detail, this is given by a term, which refers to the interaction between vapor and vapor, a term which refers to the interaction between vapor and pore wall (being it less effective as higher is the pore dimension) and the last term which refers to interaction with vapor and air in the air gap; namely:

$$\frac{1}{K} = \frac{1}{\frac{\varepsilon_m P D_{wa} M_{H_2O}}{p_a \tau R T d_m}} + \frac{1}{\frac{2\varepsilon_m r M_{H_2O}}{3RT d_m \tau}\sqrt{\frac{8RT}{\pi M_{H_2O}}}} + \frac{1}{\frac{P D_{wa} M_{H_2O}}{p_a R T d_a ir}} \tag{2.5}$$

where ε_m is the membrane porosity, P is the total pressure, D_{wa} is the diffusion coefficient of water vapor in air, p_a is the arithmetic mean of the air partial pressure, τ is the tortuosity (here it can be described as the pores tendency to be tilted), d_m is the membrane thickness, $d_a ir$ is the air layer thickness and r is the average pore radius of the membrane. In detail, Chiavazzo et al. have already empirically estimated the product $PD_{wa} = 1.19 * 10^{-4} T^{1.75}$, which is still valid for this application [113]. They have also developed less approximated functions, which, however, are not necessary to the scope of this work. Furthermore, the Mackie–Meares equation can be adopted to estimate the correlation between the tortuosity and porosity of the membrane:

$$\tau = \frac{(2-\varepsilon_m)^2}{\varepsilon_m} \tag{2.6}$$

The approach described by equation 2.4 and 2.5 is an already affirmed method, as the multiple applications found in the literature support [117, 118]. Moreover, it was already verified in the study concerning the smaller device, that the results yielded by equation 2.5, are in good accordance with experimental data.

Finally, it is also interesting to analyze the specific heat flux (q) occurring between the evaporator and the condenser. This can simply be yielded by the following equation:

$$q = \frac{k_{eff,g}}{d_g ap}(T_E - T_C) + J\Delta h_{LV} + q_1 \tag{2.7}$$

Being $k_{eff,g}$ the effective thermal conductivity represented in the gap within the air and the membrane, $d_g ap$ the thickness of each stage, $\Delta h_L V$ the enthalpy of vaporization and q_1 the specific heat loss occurring at the borders of each stage. It is then possible to construct a 1D lumped parameter system to represent the thermal resistance circuit, equivalent to the distillation system:

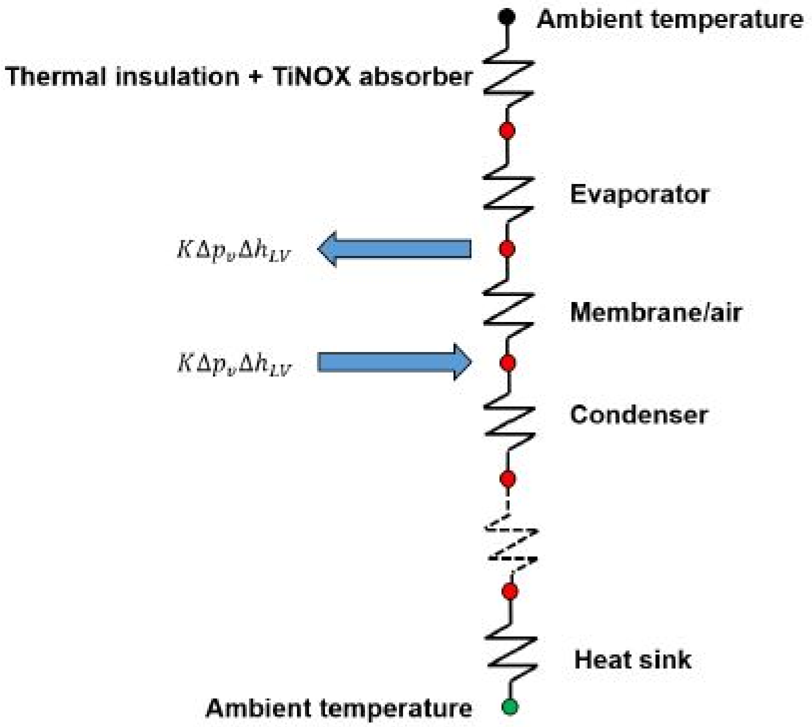

Figure 2.19: Lumped parameters, 1D distiller thermal circuit [113] (adapted with permission).

It is relevant to point out that, in steady-state conditions, the water flow taking place within the hydrophilic membranes is driven exclusively by the hydraulic head imposed on the tilted system, and no more by also the capillary forces. However, velocities are still not very high, thus, as it was for the smaller device, the flow can be considered typically laminar. Convection phenomena within the membranes are then negligible, and the whole heat transfer process is mainly given by conduction. These considerations are particularly important also to be used in the COMSOL simulations that will be exposed in the next chapter.

Chapter 3

Results

3.1 Introduction

After having concluded the designing and prototyping processes, the system was tested both numerically and experimentally, in order to better analyze its operating conditions. In detail, it was interesting to observe if the model predictions obtained by the already developed older theoretical approach were in accordance with the new device performance. In this chapter, it will first be exposed the numerical analysis, conducted by means of the COMSOL Multiphysics® software. Then, the results of the extensive in-field experimental campaign, prosecuted on the roof of Politecnico di Torino, will be reported and discussed. Finally, a comparison between the two numerical and experimental results will be exposed, in order to validate the results and to eventually analyze the source of any discrepancy between the two of them. While investigating the device results, it will be important to keep in mind that the prototype is not a pure scale-up of the smaller desalination system; as in fact it was extensively discussed in the previous chapter, the changes that were adopted during the designing process have caused slight changes on the device functioning; for instance the cross-flow configuration. However, also these aspects will be deeply analyzed along the description of the the simulation set-up.

3.2 Numerical analysis

3.2.1 Basic concepts

The numerical analysis was carried out by means of the COMSOL Multiphisics® software. This platform exploits the finite element analysis to solve a various type of problems involving different physics, that can then be applied to numerous case of studies (e.g. stationary, transient). COMSOL gives the possibility to in-build the geometry and to select the relative materials from a library, but it is also very suitable to communicate with other CAD software. After these preliminary processes, it is possible to enter the physic environment, where the choice of the governing equations and the definition of the boundary condition is set. Other than a very intuitive environment, one of the biggest advantage of COMSOL is the ability to modify such governing equations. After meshing, the solution is obtained by exploiting either a segregated or fully coupled approach. Lastly, a wide set of post-processing process can be performed. In this specific case of study, it was developed a 3D model of the distiller, objective of this thesis. In detail, it was created a multilayer structure, not comprehending any of the protruding strips linked to the evaporators and condenser, but only involving the core of the device. The main developed simulation was based then on the 3-stage device, that will now be analyzed in this section. However, also other variant of this model have been created in order to have a deeper understanding of the device potentialities and limitations; these results will instead be later analyzed in the **Discussion** section.

3.2.2 Simulation set-up

Geometry & Material

The 3-stage distiller geometry was built as a simple composition of rectangular layers. In detail, the first stage is composed by 8 blocks, namely the solar absorber (TiNOX® plate), the evaporator support (thin aluminum sheet), the evaporator (microfiber layer), the hydrophobic membrane (PTFE layer, with pore size 0.1 μm), the condenser (microfiber layer), the condenser support (thin aluminum sheet) and the two rubber lateral rubber supports (CR - polychloroprene). The remaining two stages are instead constituted by 6 blocks, namely the same of the first stage but with no solar absorber and no evaporator support, as after the first stage each evaporator share the same support of the preceding stage condenser. According to the real dimensions sizes, each block was modelled 1 mm thick, a part from the rubber components, which are thick 3 mm. The upper area of the panel and the aluminum sheets was set to 56.5x38 cm, the hydrophobic and hydrophilic membrane are instead 56.5x34.5 cm; lastly, rubber components are 56.5x1.75 cm.

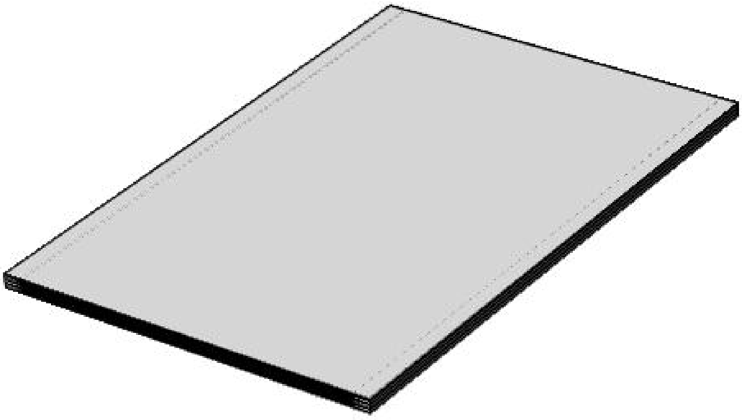

Figure 3.1: Overview of the device 3D model.

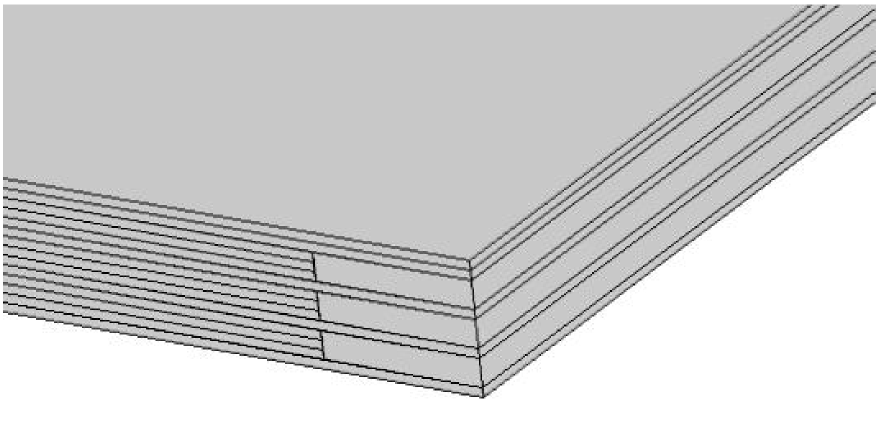

Figure 3.2: Zoom-in on one edge to observe the multilayer structure.

The microfiber layers composing both evaporators and condensers are modelled as water layers, with a thermal conductivity computed as a weighted average between their constituent; namely they are made for 30% of microfiber and 70% of water:

$$k_{hphi} = k_{microfiber} * 0.3 + k_w * 0.7 \tag{3.1}$$

being $k_{microfiber} = 0.04$ W m^{-1} K^{-1} and $k_w = 0.6$ W m^{-1} K^{-1}. Cotton has in fact very similar thermal property respect microfiber; on the other hand the quantity of water retrieved at saturation was estimated by comparing the weights of the dry and wet membranes. The hydrophobic membranes, were modelled in parallel with the air gap standing between each evaporator and the condenser. In detail, the gap thickness (d_{gap}) is the sum between the membrane's ($d_m = 0.15$mm) and the air gap's ($d_{air} = 0.85$mm) ones. The thermal conductivity of such layer was then estimated as:

$$\frac{1}{k_{gap}} = \frac{1}{\left[k_{air}\ \varepsilon_m + (1-\varepsilon_m)\ k_{PTFE}\right] \frac{d_{gap}}{d_m}} + \frac{1}{k_{air}\ \frac{d_{gap}}{d_{air}}} \tag{3.2}$$

being k_{gap} the overall thermal conductivity of the gap, k_{air} the air thermal conductivity (equal to 0.026 W m^{-1} K^{-1}), k_{PTFE} the PTFE thermal conductivity (about to 0.25 W m^{-1} K^{-1}), ε_m the membrane porosity (being it 0.9), d_{gap} the total gap thickness (1 mm overall). This latter is then formed for 0.85 mm by d_{air}, and 0.15 mm by d_m. Given the majority of the gap is composed by air the final thermal conductivity results ~0.028 W m^{-2} K^{-1}. Finally the remaining aluminum and rubber supports are modelled according their proper material properties found in the software library.

Physics & Boundary conditions

The problem is set stationary. As the main objective is to find water vapor flux and the temperature profile, the transient is of no interest. To solve the numerical problem 3 different physics had to be employed; namely these are "transport of diluted species", "heat transfer in porous media" and "laminar flow". While heat transfer takes place in the whole system, the mass transfer occurs only within the porous membrane; for this reason, the related physic is constrained to this domain. On the other hand, for the sake of simplicity, the laminar flow was modelled separately only in the evaporators, as it was not interesting to observe water behaviour in the condensers as the main goal of the simulation was to detect the water vapor flux. Furthermore, the assumption of consiering static condenser is reasonable as the velocities are negligible ($Re < 10^{-5}$). Therefore, the Navier-Stokes equations, related to this latter were solved independently of the water vapor flux. The other two sets of equations belonging to the remaining physics were solve by employing the "fully coupled approach", thus letting the system solve a single big system of equations. To this objective, the heat transfer, generated by the water vapor flux through the membrane, was modelled as two boundary heat sources, positioned at the respective membrane surface. These were solved numerically through the help of the Lagrangian multiplier; namely:

$$Q_{boundary} = \pm J * \Delta h_{LV} = \lambda * \Delta h_{LV} \tag{3.3}$$

where $Q_{boundary}$ is the heat source, J is the water vapor flux, λ is the lagrangian multiplier, and Δh_{LV} is the enthalpy of the liquid-vapor phase change. This weak constraint is then exploited in the fully coupled approach to connect the physics through the Lagrangian function, namely the function that connects the heat equation 2.7, through the above weak constraint, in a stationary regime, to the mass transport equation 2.4.

The mass transport within the porous membrane can be described by the following equation:

$$N = -D_{eff} \nabla c = -D_{eff} \nabla (\frac{p_v}{RT}) \tag{3.4}$$

being N the diffuse molar flux (mol m^{-2} s^{-1}), D_{eff} the effective diffusion coefficient and c the molar concentration. In detail, the diffusion coefficient, is accounted considering both Knudsen and molecular transport. However, being the membrane modelled within the air gap, also its contribution had to be accounted for. By also considereding the linear assumption yielded by having $x_w << 1$, it is to compute the equivalent diffusion coefficient as:

$$\frac{1}{D_{eff}} = \frac{1}{D_{wK}} + \frac{1}{D_{wa}} + \frac{1}{D_{wa,air}} \tag{3.5}$$

where:

$$D_{wK} = \frac{8r}{3} * \sqrt{\frac{RT}{2\pi M_w}} * \frac{\varepsilon_m d_{gap}}{\tau d_m} \tag{3.6}$$

$$D_{wa} = 1.19 * 10^{-4} * \frac{T^{1.75}}{P} * \frac{\varepsilon_m d_{gap}}{\tau d_m} \tag{3.7}$$

$$D_{wa,air} = 1.19 * 10^{-4} * \frac{T^{1.75}}{P} * \frac{d_{gap}}{d_{air}} \tag{3.8}$$

being D_{wK} the Knudsen diffusion coefficient, D_{wa} the molecular diffusion coefficient and $D_{wa,air}$ the molecular diffusion coefficient in the air layer, where Knudsen regime is not effective. As the temperatures differ in each stage, the overall diffusion coefficient value to assign to all membranes was given as an arithmetic average of the different D_{eff} computed at the different temperatures. On the other hand, the initial molar concentration (c_0) to be used in the equation can be computed as:

$$c_0 = \frac{\phi_{rel} \rho_{max}}{M_w} \tag{3.9}$$

where ϕ_{rel} is the relative humidity, assumed 0.2, and ρ_{max} is the maximum amount of water, at ambient temperature, for a $\phi_{rel} = 1$; namely 0.0172 kg m^{-3}.

The heat fluxes within the system were instead modelled through different boundary conditions. For instance, the solar irradiance itself was modelled as an in-going heat flux through the solar absorber (first layer). It was assumed then, an heat flux of 650 W m^{-2}, in accordance with the irradiance's data gathered during the experimental campaign. This value was then lowered than 0.95 and 0.93, respectively the solar absorbance of the TiNOX® and the transparency of the PMMA panel. Convective heat fluxes act instead on each external surface of the device, thus causing thermal losses. On the top surface, the convective heat flux was modelled in series with the thermal resistance furnished by the PMMA layer and the air layer standing in between this latter and the TiNOX®; namely:

$$\frac{1}{h_{top}} = \frac{1}{\frac{k_{air}}{d_{air,top}}} + \frac{1}{\frac{k_{PMMA}}{d_{PMMA}}} + \frac{1}{h_{conv,top}} \tag{3.10}$$

being $d_{air,top}$ the thickness of the air layer between the PMMA and the TiNOX® (2 mm), k_{PMMA} the PMMA thermal conductivity (equal to 0.19 W m^{-2} K^{-1}), d_{PMMA} the PMMA panel thickness (3 mm) and h_{conv_top} the convective heat transfer coefficient generated by convection, caused by wind speed at 2 m s^{-1} (it was then assumed 10 W m^{-2} K^{-1}). The heat flux acting on the bottom of the system, working as an heat sink, is instead purely convective, the related heat transfer coefficient was then assumed slightly lower than the one at the top, as this side is supposed to be more sheltered. In detail it was assumed to be 80% of the upper connective heat flux coefficient (8 W m^{-2} K^{-1}). On the lateral sides of the device, instead, the h_{conv} was set to 3 W m^{-2} K^{-1}, as, by assuming wind blows on a steady direction, one of the four edge will not even be subjected to any air flow. However, the contribution of this losses is minimal, as the aspect ratio of the device geometry is very high. The ambient temperature is assumed to be 32 °C, based on experimental experience. Other source of heat loss are generated by radiation. To simulate them it was then necessary to assume each of the device surface emissivities. In detail, the top surface emissivity is 0.04, the one of TiNOX®; the bottom surface emissivity is 0.1, the one of aluminum; and on the lateral one is estimated as a weighted average of the rubber, aluminum, microfiber and PTFE emissivity, which yielded 0.362.

Lastly, the laminar flow within the evaporator was modelled through two simply inlet and outlet boundary conditions. At the inlet, both the temperature and the inlet velocities were imposed. The inflow temperature is the ambient temperature itself, while the inlet velocity was computed knowing that the device consumes on average 5 litres of water per day (where a day is about 8 sunny hours). Knowing then the section of the evaporator it was possible to obtain the inlet velocity, namely 5.91×10^{-4} m s^{-1}. The outlet condition imposed was instead given by the ambient pressure. The effect of gravity was also included.

Mesh

Due to the high aspect ratio of the device, a uniform mesh resulted to much computational expensive to be performed. It was then adopted a sweep mesh. In detail, the outlet face of the system was first meshed with a "extra-fine" mesh size (element sizes ranging from 8.48×10^{-4} m to 0.0198 m), the distribution was then swept along the longitudinal length of the device, over 9 intervals. Overall, the simulations were solved for 147191 degrees of freedom plus 119958 internal degrees of freedom.

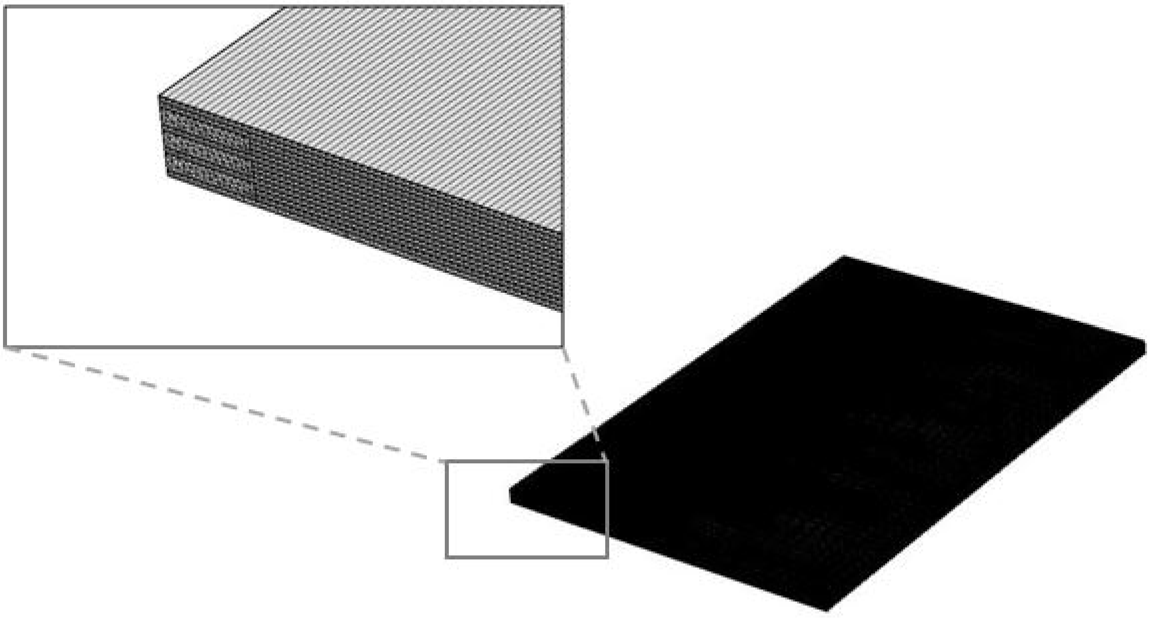

Figure 3.3: Detailed view of the mesh structure.

The expedient of a sweep mesh resulted very useful to perform simulation with different thickness of the hydrophobic membrane. Eventually, in fact, the thickness of the membrane could have gotten smaller then the minimum element size of the mesh. Adopting this solution allowed to decrease the element size without increasing the computational cost, but just loosing some accuracy on the transverse results, the direction considered less interesting to study.

3.2.3 Numerical results

As meshing was the last step of the simulation set-up, in this section it will now be extensively discussed the yielded results. These are strongly dependent on the input parameters, which have then been carefully chosen before simulating. The resultant computational cost of the process resulted relatively low, thanks to the fully coupled approach. Convergence was in fact reach within 3 iterations:

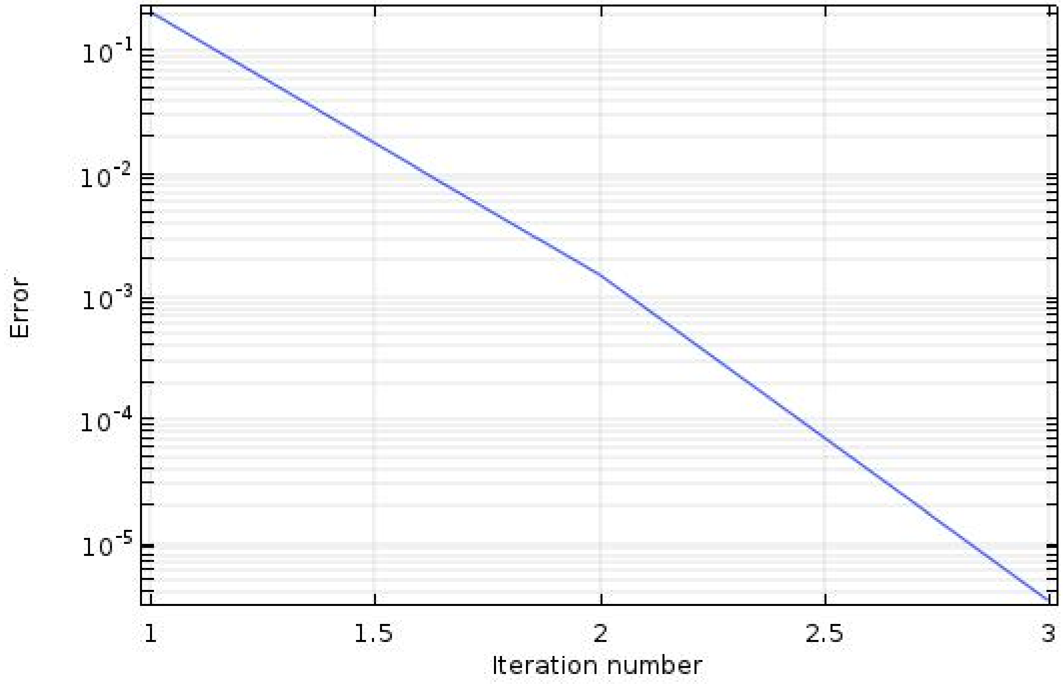

Figure 3.4: Error plot.

The most important result yielded from the simulations is with no doubt the water vapor flux; according the simulation results a diffusive molar flux of 1.9575×10^{-3} mol s^{-1} was obtained. This result can be easily converted into more familiar units easier to analyze. In detail, such flux corresponds to 127.2 g h^{-1}, or rather 0.65255 L m^{-2} h^{-1}. This result is surely lower than the one obtained with the 3-stages smaller device (1.462 L m^{-2} h^{-1}), as in fact also the efficiency analysis of the system supports:

$$\eta = \frac{N M_w \Delta h_{LV}}{q_{solar}} \approx 13\% \tag{3.11}$$

against the 32% referring to the smaller device. However, this result seems understandable as in the scaled-up version the distiller employs the accumulated energy not only to cause water evaporation, but also to heat up the undistilled flow. Moreover, the older version was tested with an higher average irradiance. However, a better analysis, involving also a sensitivity analysis, will also be later exposed.

It is now interesting to analyze in which measure the solar energy get dissipated in heat loss channels. To this goal it is possible to observe table 3.1.

Heat loss channel	**Convective flux [mW]**	**Radiative flux [mW]**	**Total flux [mW]**
TiNOX®, top	25,249	1,705	26,954
TiNOX®, lateral	131.7	119.8	251.52
Aluminum	430.2	381.2	811.4
Evaporator	/	89.3	89.33
Membrane	95.1	85.5	180.59
Condenser	92.4	82.1	174.45
Rubber	660.5	579.4	1,239.9
Bottom	28,765	2,545	31,310
Water heating	/	/	71,870

Table 3.1: Heat losses in the device.

Relating these quantities to Q'_{solar}, (the solar heat flux diminished from the optical losses, which account for 11.65% of Q'_{solar}), it can be estimated the weight of each heat loss source:

Heat loss channel	**Convective flux [%]**	**Radiative flux [%]**	**Total flux [%]**
TiNOX®, top	20.48	1.38	21.86
TiNOX®, lateral	0.11	0.1	0.21
Aluminum	0.35	0.31	0.66
Evaporator	/	0.07	0.07
Membrane	0.08	0.07	0.15
Condenser	0.07	0.07	0.14
Rubber	0.54	0.47	1.01
Bottom	23.33	2.06	25.39
Water heating	/	/	50.51

Table 3.2: Heat losses related to Q'_{solar} in the device.

So it can be observed on what level the heat transferred to the brine is a a new source of thermal losses. However, it is inevitable to renounce to this cross-flow configuration, as this is crucial in order to allow any scale-up of the system (which would otherwise dry out if only driven by capillary forces), and to avoid an excessive salt concentration during the single working day, which would otherwise cause a drop in the distiller productivity.

Having already given the total water vapor flux, it results now interesting to study its distribution within the stages, along with their temperature profiles. These observation can be carried out by looking at the following plots:

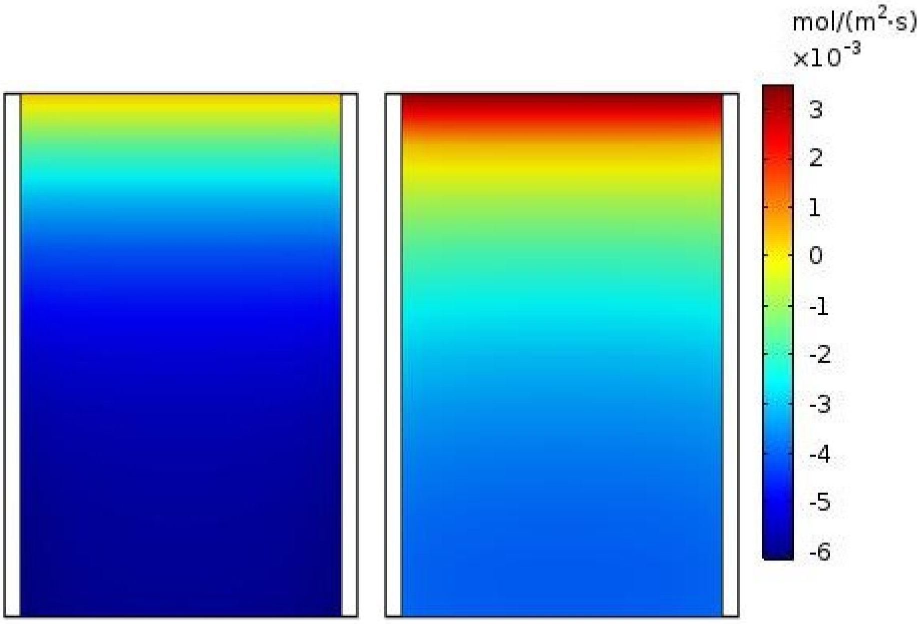

(a) Top view (b) Bottom view (c)

Figure 3.5: Distilled flow rate distribution on top and bottom of the device.

As it can be noticed it results an opposite water vapor flux at the entrance of the last stage (directed upwards). Here in fact, the temperature difference between evaporator and condenser is too low in order to contrast the chemistry; the difference in the water vapor pressure is driven mainly by the difference in the salinities, and not by the water vapor pressure, as the temperature is about constant in this region. Overall, as expected the most performing stage is the first one, furnishing a distilled flow rate of 56.4 g h^{-1}; the second one instead reaches 41.9 g h^{-1} and the last one 28.9 g h^{-1}. Therefore the respective contribution of each stage, with respect the final productivity is respectively about 44.3%, 32.9% and 22.8%.

As expected, the distilled flow rate behaves accordingly the temperature profiles:

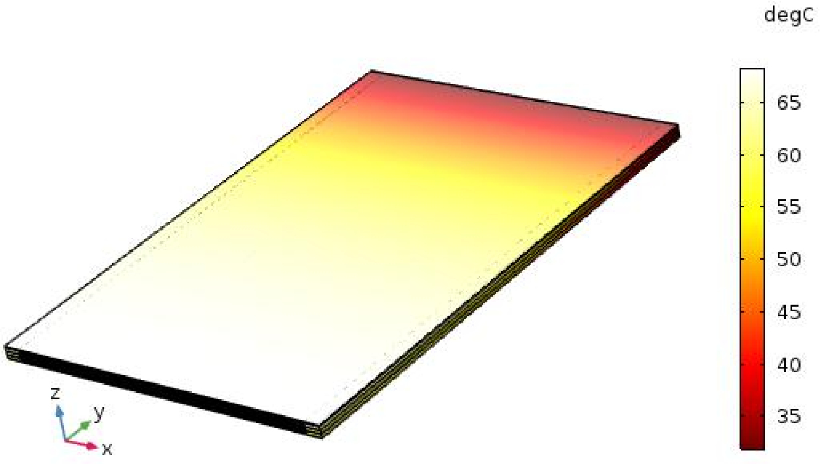

Figure 3.6: 3D representation of the device temperature distribution.

More in detail, the temperature drop across the device height near the entrance region, in the middle and near the exiting region, behaves as:

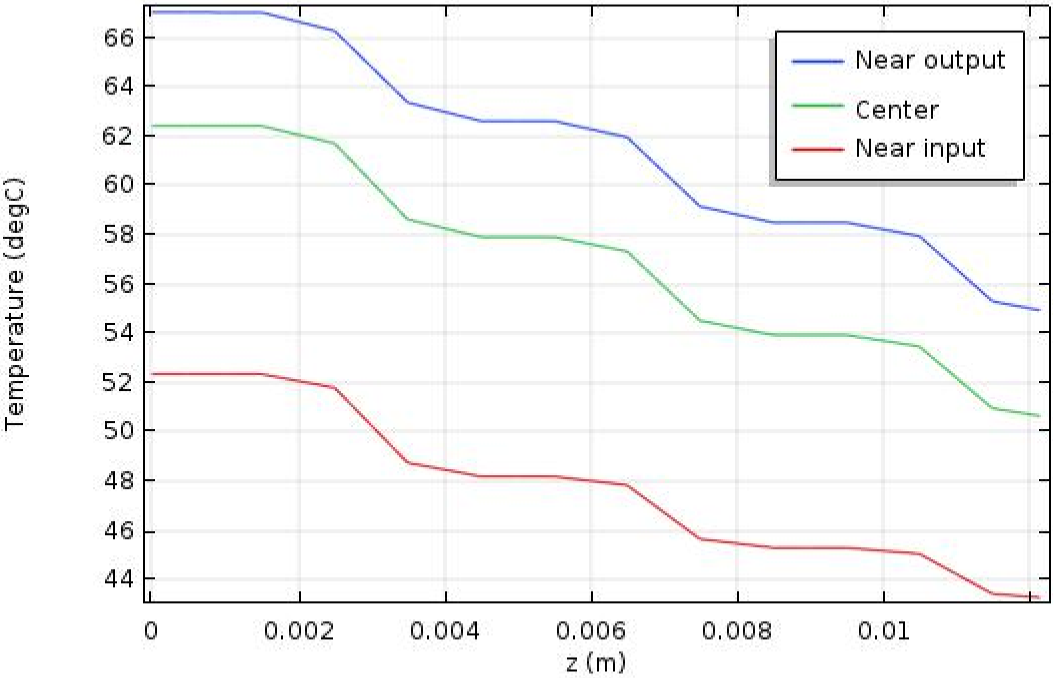

Figure 3.7: Temperature drop across the device height, studied at the water entrance region, at the center and the water exititing region.

While the temperature profile along each evaporator length behaves as:

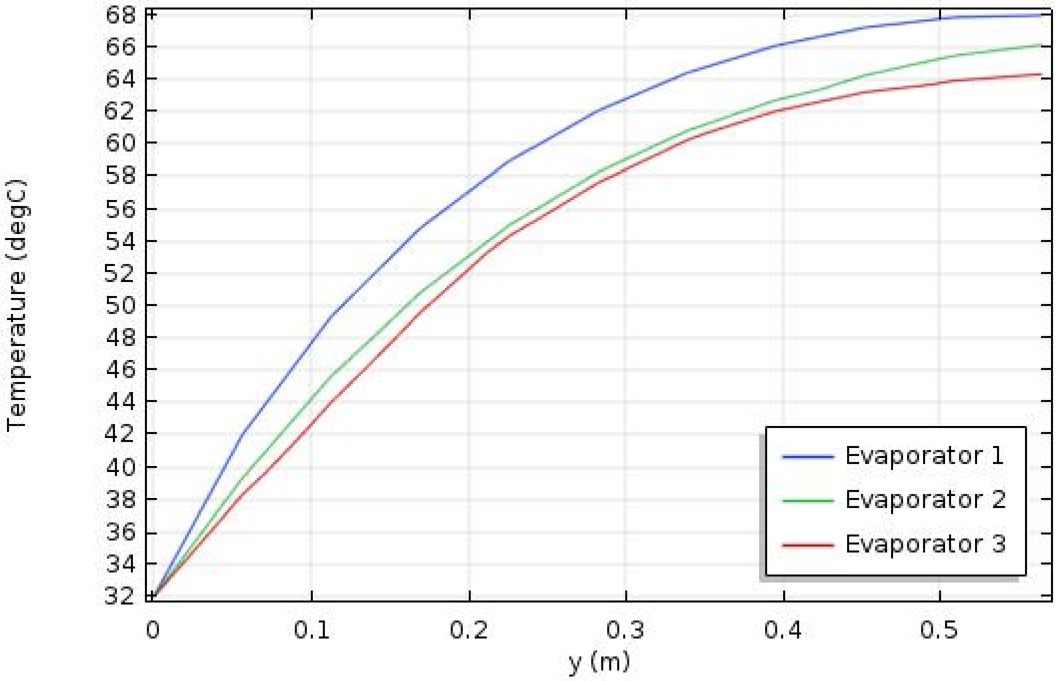

Figure 3.8: Temperature drop across the first evaporator length.

From figure 3.7 it is appreciable the temperature drop caused by the different thermal conductivity. In the hydrophobic membrane, where this parameter is the lowest, the temperature drops the most; in the aluminum, where instead it is the highest, temperature remain about constant. It is also interesting to notice the relation between these last two plots. Figure 3.8 testifies how the temperature gradient is higher near the water entrance region, and lower towards the exit; therefore, in figure 3.7 the gap between the functions is higher when comparing the central region to the entrance region.

Finally, it is is interesting to observe in detail, the temperature drop and the vapor heat flux behavior within the multilayer structure:

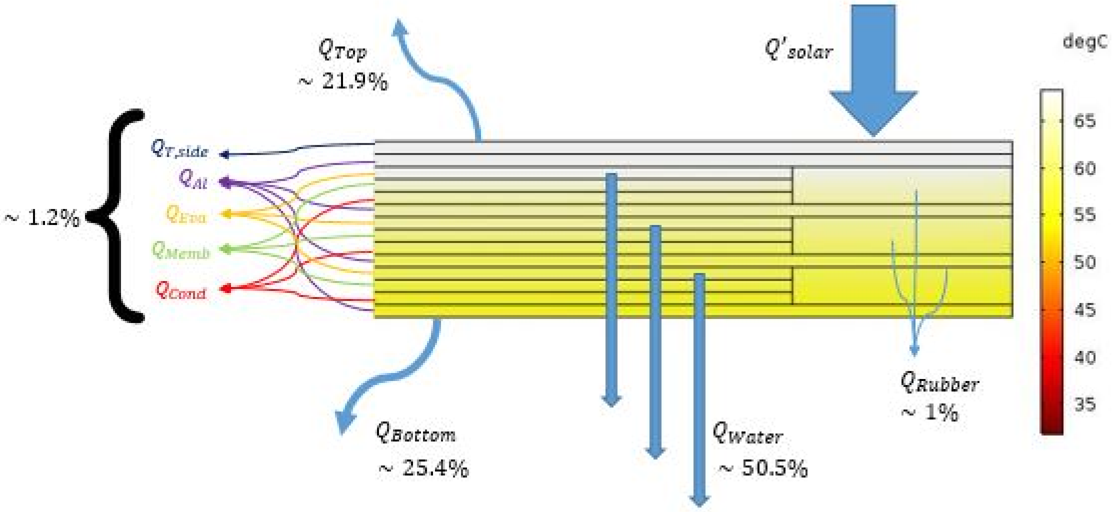

Figure 3.9: Representation of the temperature distribution across the layers studied on a downstream edge and thermal loss channels representation.

Figure 3.10: Water vapor flux through the hydrophobic membranes, studied on a downstream edge.

As the simulation is performed in a stationary regime, the temperature distribution is about uniform along the transversal device length. On the other hand, in figure 3.10, it can further be appreciated the different contribution of each stage in the distilled water production.

3.3 Experimental campaign

3.3.1 Basic concepts

The experimental campaign was carried out mainly outdoor, on the roof of Politecnico di Torino, employing artificially made seawater with a typical salt concentration of 35 g L^{-1}. During testing the detected quantity of interest were mainly 3: the *distilled mass*, the *temperatures* and the *water salinity*.

The distilled water mass was detected manually, through the help of the digital scaled previously described. Measurements were performed about every 30 minutes, over each working day, considered on average about 5 hours. It is important to highlight that many tests conducted during the experimental campaign were discard due to the unsatisfactory results obtained from the distilled mass measurement or the water salinity. In detail, that is due to the lately employed expedient of the distilled water bags. As already mention, in fact, for most of the experimental campaign some polymeric tubes, which lead freshwater to a separate basin, were employed as distilled water collective system. This solution was correlated by some problematics, amongst which, mainly evaporation of water from the basin (usually tried to be prevented through an aluminum lid) and contamination of the produced water, caused by some salty water drops dripping from the evaporators to the tubes exterior and thus to the freshwater basin. When this phenomenon occurred, it could have been noticed not only from the final water salinity higher than 0.0-0.1 g L^{-1}, but also from the increased distilled produced water mass itself.

Temperatures were gathered through the help of thermocouples, the DAQ and the LABview code generated for the data analysis. In detail, of the 6 thermocouples, 2 were place at the bottom of the last stage aluminum sheet (TC0 and TC1) and 2 at the top of the solar absorber panel (TC2 and TC3), to observe the temperature drop across the profile, namely the implicit driving force of whole distillation process. Of the remaining two thermocouples 1 was placed in air, right below the the last system stage (TC4), and one always in air, but far from the device (TC5), respectively to observe the environmental temperatures to be used for the estimation of the convective heat loss given by the heat sink and the one at the system edges. Overall, the thermocouples positioning can be deducted by looking at figure 3.11. As it can be observed in the figure, each thermocouple was covered with some adhesive aluminum tape, to help increase the measurement accuracy, as it would otherwise be influenced by natural convection.

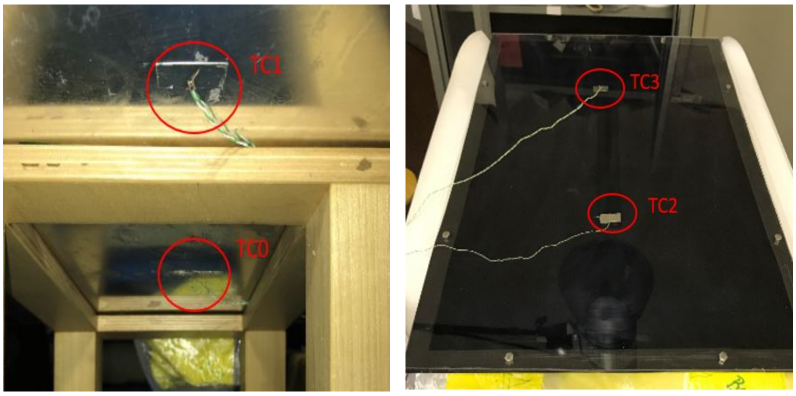

(a) TC0 and TC1 (b) TC2 and TC3

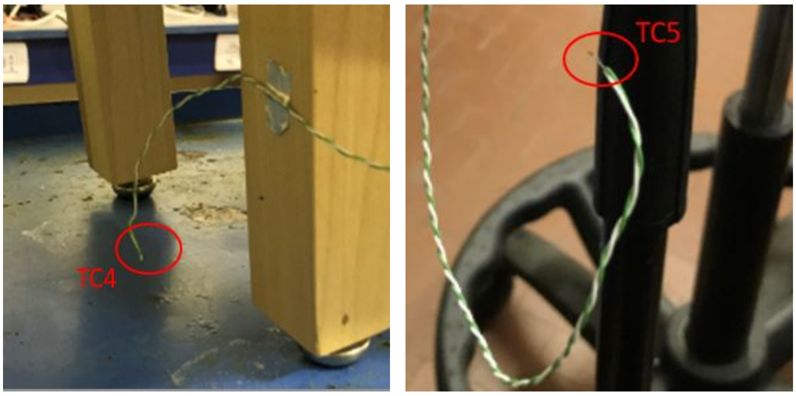

(c) TC4 (d) TC5

Figure 3.11: Thermocouples positioning.

Lastly, salinity measurements were performed both at the beginning and the end of each working day, through the help of the pipette and the refractometer previously exposed. In particular, salinity was studied in the following components:

- **Feed water basin**: to mimic the correct salt concentration and to ensure this was kept constant throughout all the process.
- **Evaporators**: at the beginning of each working day the evaporators should have had

a null (or very low) salt concentration if the transient was going to be studied as well. If not, the system should have had the typical seawater concentration, by being first initialized, by saturating it with some additional seawater first. At the end of each working day, instead, the salinity was expected to be higher than 35 g/l, due to evaporation. Measuring the salinity at the end thus enabled to understand in which stage the most water evaporation occurred.

- **Condensers**: salinity in each condenser should have always been kept null. At the beginning of each working day, this was then detected to ensure the right working condition were reached. At the end instead, it was verified to confirm that no contamination of saltwater had occurred (e.g. eventually due to an hydrophobic membrane puncturing).
- **Brine basin**: salinity in the brine basin was always detected in order to understand the level of salt present in the production "waste". As already mention, in fact, brine discharge is usually a problem in an environmental prospective, proportional to the salt concentration itself.
- **Distilled water basin**: Measuring the salinity level in the distilled water was the ultimate step to verify the device effectiveness. If it was higher than ~0.0-0.1 g L^{-1}, that would have a been a proof some external contamination had occurred, and thus most of the data collected during the test had to be discarded.

When looking at such data, it is important to keep in mind the refractometer resolution is 0.1 g L^{-1}. This feature is fundamental in fact when studying the condensers or the freshwater salinity, as it is in these cases that value close to zero are approached, and therefore, the instrument error is more influential.

Although distilled mass, temperatures and water salinity were the only parameters supervised during the experiments, these are not the only ones important. During each test, in fact, at least two other very important factor had a big influence on the results; these are the *direct solar irradiance* and the *wind speed*. Solar irradiance can be considered mainly of 3 types: *global irradiance*, *direct normal irradiance* and *diffusive horizontal irradiance*. This latter is the irradiance that is scattered from molecules and particles in the atmosphere and thus arrives from all directions; the direct irradiance, on the other hand is the one which has not been scattered, and thus arrives on the solar panel on a direct path from the sun; global irradiance is instead simply the sum of these two. Considering the irradiance arriving on the solar absorber, it seems then fait to consider only the direct irradiance as the one causing the main heating. The effect of wind speed is instead less intuitive to observe. This variable is closely correlated to the convective heat transfer coefficient between the environment and the device. In detail, the best ambient condition considered a convective heat transfer coefficient of 10 W m^{-2} h^{-1} (light wind), the worst one instead between ~0 and 5 W m^{-2} h^{-1} (stagnant air). A better natural convection was in fact preferable to enhance the heat flux through the different stages, as it contributed to increase the temperature difference between top and bottom of the system. However, no proper instrumentation to monitor these quantities was employed for the sake of the experimental layout simplicity. It was in fact possible to obtain such values from some online software. In particular, for solar irradiance, it was used the "PVGIS" online tool, an ideal software created to estimate the solar electricity production of a PVs. In detail, amongst its various feature, it was possible to detect the daily average solar irradiance profile of any month in any part of the world, by also taking in account the device inclination and azimuth angle. Depending on the different hours in which the distiller was employed, the average irradiance was then computed by considering clear sky conditions. According Khan et al. in fact, *"When the amount of diffuse radiation reaching the earth's surface is less than or equal to 25% of global radiation, the sky is termed as clear sky"* [119]; thus, considering about the 20-25% of the global irradiance, it was possible to obtain the direct irradiance on the solar absorber. In figure 3.12 the results yielded by such consideration are shown.

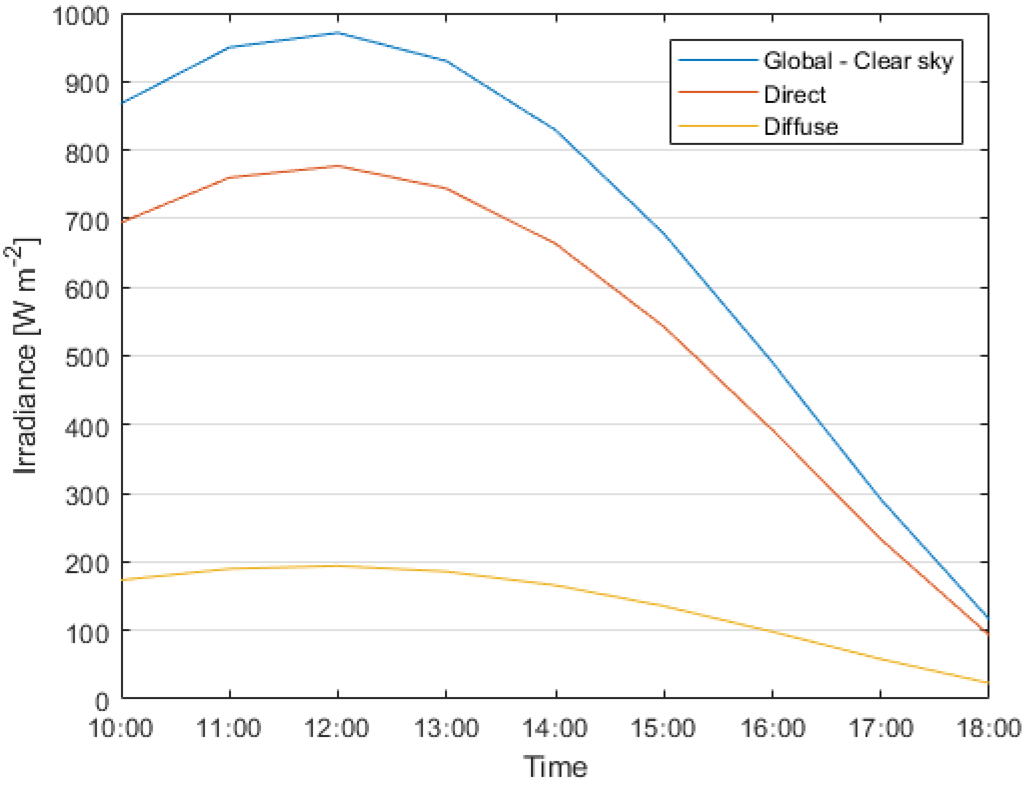

Figure 3.12: Average daily irradiance in July.

The wind speed, data refer instead to the "NASA Surface meteorology and Solar Energy database", which is accessible through another online tool. This service stores various every day's climate variables, for every part of the world, amongst which indeed the wind speed.

Lastly, another not quantitative feature to highlight, is the quality of the assembling. Although the system is easy and quick to mount, it is important to ensure all the layers are well positioned, each with its membrane as more stretched as possible, so to avoid the presence of any air gaps that would otherwise act as additional thermal resistances. Overall, a compact assembling also enhances the heat flux taking place through the different distillation stages. Having a not excellent repeatability of the process is another important factor to take in account when analyzing the distiller performance.

3.3.2 Indoor test

As already mention, the experimental campaign was practised mainly outdoor. However, as the weather condition were not as always optimal to perform the tests (mainly due to the cloudy weather), it was also tried to carry out some experiments indoor. In order to perform such tests, it was adopted the previously introduced 1000 W quartz light. Although this lamp did not mimic properly the sun waveband irradiance (it works mostly in the infrared), the integral over the whole spectral irradiance was considered similar enough to the one of the sun. It is worth to point out that in the SMaLL lab, it was also present an ISOSun machine, able to perfectly mimic the sun irradiance. However, although this was employed to test the smaller distiller, it was not possible to use it on the scaled-up version due to the exasperated increased size of the unit.

In figure 3.13, figure 3.14 and table 3.3 it is presented an experimental data set related to a successful test carried out indoor.

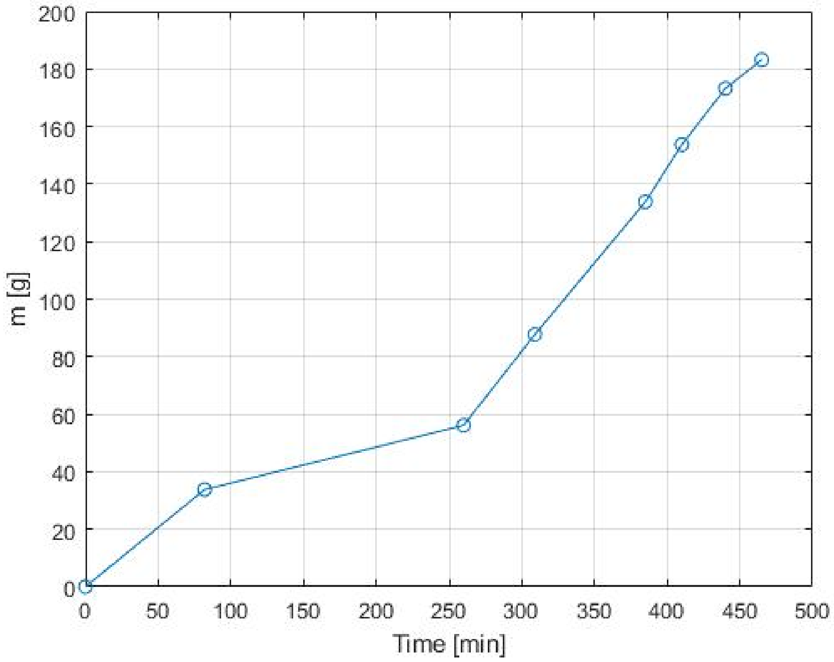

Figure 3.13: Distillate mass over time for one of the indoor experiment.

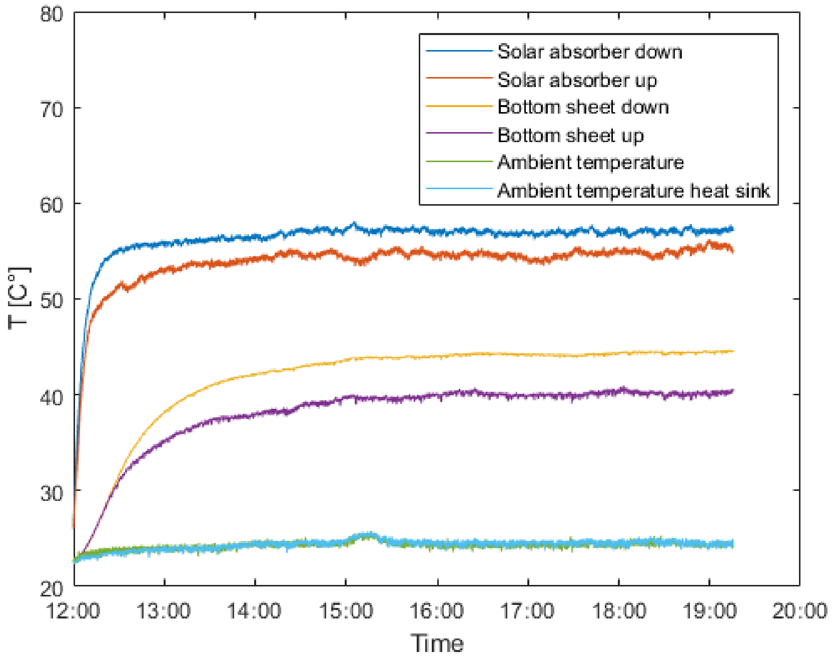

Figure 3.14: Temperatures over time for one of the indoor experiment.

[g/l]	**Before test**	**After test**
Feed water	35	/
Evaporator 1	1	27
Condenser 1	0	1
Evaporator 2	1	31
Condenser 2	0	1
Evaporator 3	1	32
Condenser 3	0	1
Brine	/	33
Distilled water	/	1

Table 3.3: Salinities in the device before and after testing.

Results are consider positive as the system worked properly, reporting a good level of salinity in the distilled product, over a period of 5 hours. It is interesting to observe how the temperature got steady, after a transient corresponding to the system initialization. The transient of the system was in fact also analyzed and it resulted to last about 35 minutes; a short time then, probably influenced by the residual wetting left from the previous experiments. The steadiness of the temperature and thus the one of the produced distilled water mass, is given by the ideal indoor condition, where randomness phenomena are less likely to happen. However, the most important parameter to examine is the distilled mass flow rate; this amounts to ~37 g h^{-1} (from when it got steady), and was thus considered unsatisfying, as not in accordance with the theoretical model predictions, from which it was expected to produce at least ~100 g h^{-1}. The source of such a negative result was not found in the device itself but in the lamp. To verify the irradiance the lamp was able to mimic, a system composed by the previously described pyranometer, the DAQ and a different LabVIEW code was mounted. Positioning the pyranometer in different positionsof the panel, it was possible to construct a map of the irradiance received by the solar absorber, as shown in figure 3.15.

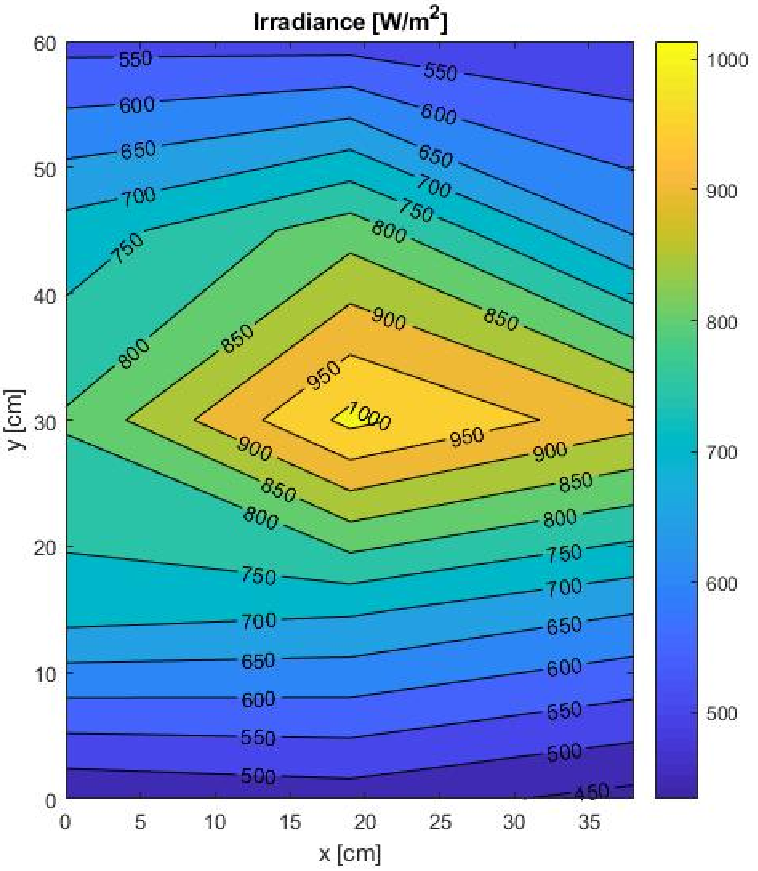

Figure 3.15: Panel received irradiance during indoor experiment.

This result showed the average solar irradiance, delivered to the solar absorber was about 640 W m^{-2}. Although this value seemed fair with respect the solar irradiance detected through PVGIS, its distribution over the panel was not uniform (ranging from 500 W m^{-2} to 1000 W m^{-2}), thus preventing the layers to work uniformly. The difference between the irradiance exploited in indoor and outdoor conditions stood also in the behaviour of the irradiance over time. In indoor condition a constant value of irradiance was reached, which although it is good to work when the weather does not allow it, it is also unfavourable as no high peak are ever reached during the day. These are very important as they allow to further heat up the system, increasing its productivity, even after they are passed, thanks to the system thermal inertia. For all these reasons, the idea of testing the device indoor had been discarded ever since.

3.3.3 Data set 1

Data set 1 refers to a test with average irradiance of 559 W $m^{-2}$and wind speed of 2 m s^{-1}:

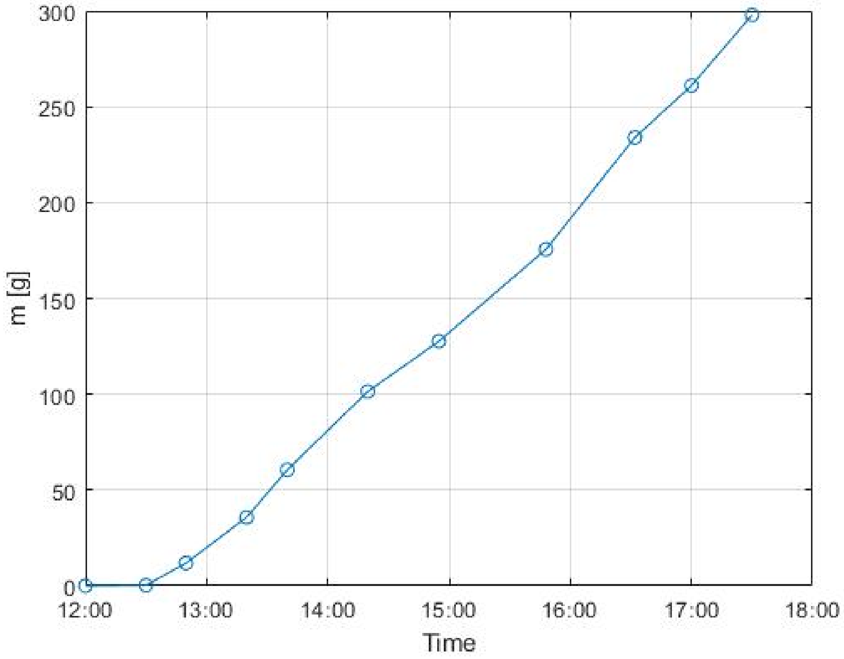

Figure 3.16: Distillate mass over time for the first data set experiment.

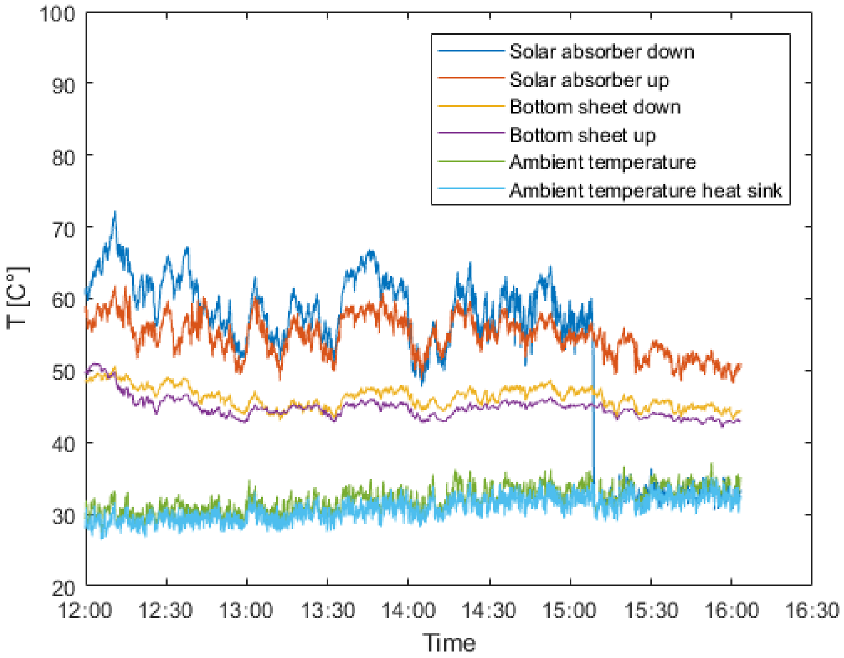

Figure 3.17: Temperatures over time for the first data set experiment experiment.

[g/l]	**Before test**	**After test**
Feed water	35	/
Evaporator 1	1	36
Condenser 1	1	1
Evaporator 2	1	36
Condenser 2	1	0
Evaporator 3	1	34
Condenser 3	1	1
Brine	/	43
Distilled water	/	2

Table 3.4: Salinities in the device before and after testing for the first data set experiment experiment..

In this first data set the experiment was carried out for 5 and an half hours, more precisely from 12:00 to 17:30. At the beginning of the test the membranes were still wet from the previous experiment, thus was very short; it lasted about 30 minutes. The freshwater production rate is almost steady throughout the whole experiment. An average 80 g h^{-1} distilled water flow rate is achieved. Although this result is not fully satisfying, it can be still considered acceptable, as the system worked at an average irradiance relatively low (as indoor experiments). As it can be seen from the temperature in fact, after an initial peak of about 70 degrees, at the top surface, the system has constantly cool down. The system thermal inertia is appreciable as the production rate is about constant although the cooling. This phenomena can be observed also comparing the temperatures detected by the thermocouples TC0/TC1 and TC2/TC3. While the temperatures at the top are subject to oscillation, the one at the bottom are steadier. At the end, the experiment was considered mostly successful, also under the produced water quality aspect. In detail, the salt concentration in the product is 2 g L^{-1}, which although it does not fell within the expected salt concentration range (<1 g L^{-1}), its very close to it, also considering that the refractometer resolution of 1 g L^{-1}.

3.3.4 Data set 2

Data set 1 refers to a test with average irradiance of 624 W m^{-2} and wind speed of 1.75 m s^{-1}:

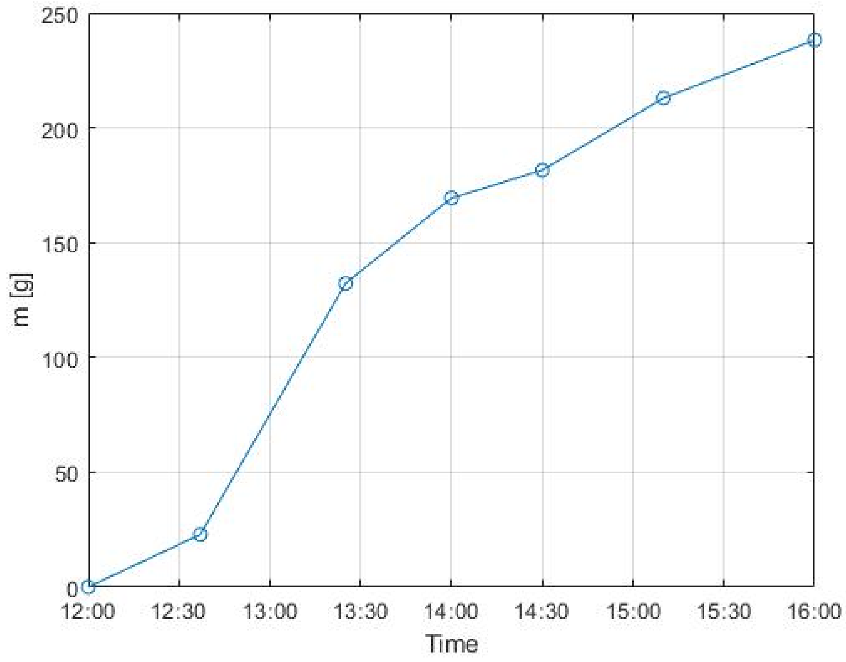

Figure 3.18: Distillate mass over time for the second data set experiment.

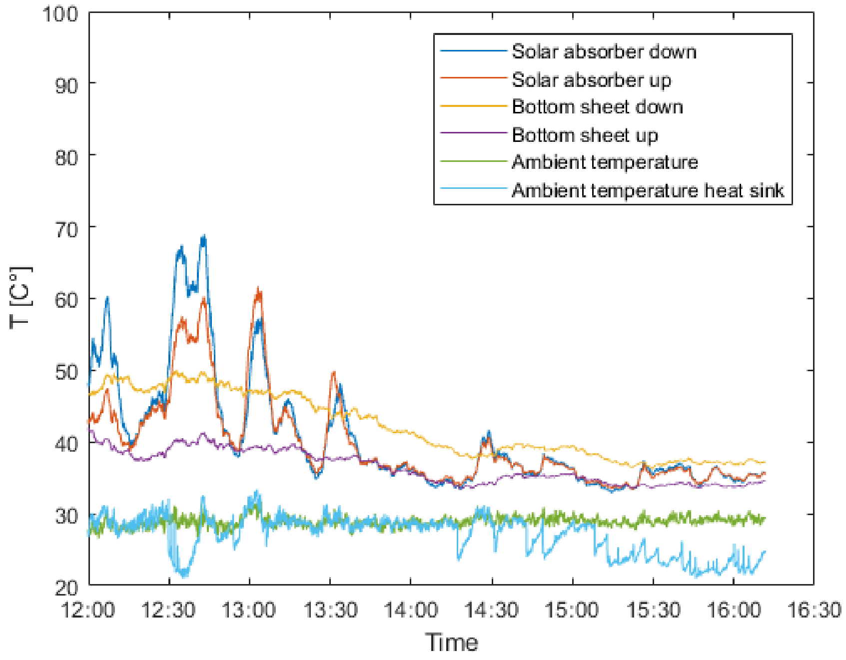

Figure 3.19: Temperatures over time for the second data set experiment.

[g/l]	**Before test**	**After test**
Feed water	35	/
Evaporator 1	4	33
Condenser 1	1	1
Evaporator 2	1	30
Condenser 2	1	1
Evaporator 3	1	32
Condenser 3	1	0
Brine	/	39
Distilled water	/	1

Table 3.5: Salinities in the device before and after testing for the second data set experiment experiment.

The second data set refers to an experiment carried out for 4 hours; from 12:00 to 16:00. As it can be noticed from the first part of the distilled water mass function, also in this case no transient was present. Moreover, although the average irradiance is higher than the previous case, the produced freshwater behaviour is less steady. This phenomenon can be confirmed by the system temperature profiles, which now oscillates in a wider range. It is in fact very interesting to observe how well the distilled flow rate (namely, the produced mass function slope), behaves accordingly to the temperatures. The maximum flow rate achieved is about 89 g h^{-1}, while the average one amounts just to 55 g h^{-1}. However, the experiment can still be considered successful as salt concentrtion in the distilled is now <1 g L^{-1}. The missing flow rate required to reach the expected amount is then caused by a large variation in the solar irradiance during the working day. As a lower flow rate was achieved, it is interesting to observe how also the final salinities in the evaporators are lower. Lastly, it can be once again observed the effect of the system thermal inertia, for which the temperature on the lower bottom (TC0), gets even higher than the one at the top, due to a combination of an immediate drop in the solar irradiance and natural convection.

3.3.5 Data set 3

Data set 3 refers to a test with average irradiance of 654 W m^{-2} and wind speed of 2.07 m s^{-1}:

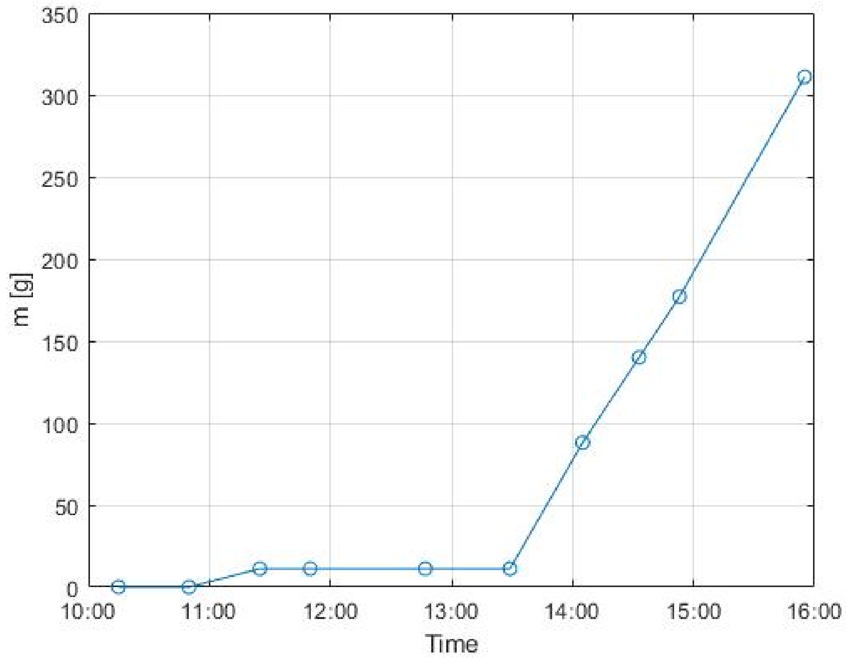

Figure 3.20: Distillate mass over time for the third data set experiment.

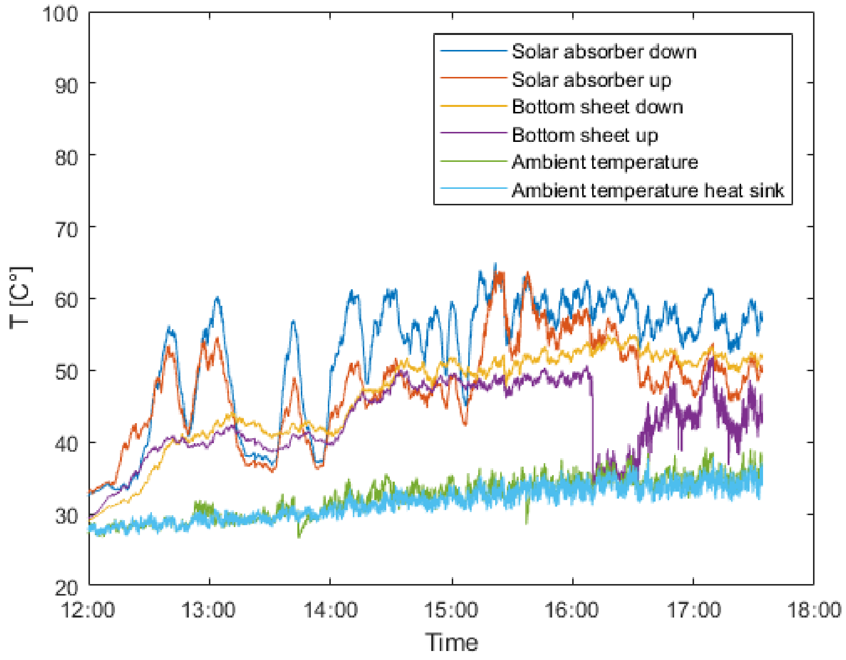

Figure 3.21: Temperatures over time for the third data set experiment.

[g/l]	**Before test**	**After test**
Feed water	35	/
Evaporator 1	1	35
Condenser 1	0	0
Evaporator 2	1	36
Condenser 2	0	0
Evaporator 3	1	39
Condenser 3	0	1
Brine	/	42
Distilled water	/	2

Table 3.6: Salinities in the device before and after testing for the third data set experiment experiment.

The third data set refers to the test with the highest average irradiance ever detected during the experimental campaign. This test, was carried out for 5 hours and 45 minutes, from 10:15 to 16:00. In this case, also the system transient was studied, as the assembling was performed without initializing the membranes (dry membranes). After one hour from the beginning of the experiment, a small amount of water was obtained, but the process then suddenly stopped. This phenomenon can be explained by looking at the temperatures reached at that same time. Due to the presence of clouds the system drastically could down, thus interrupting the production of distilled water. As long as the system had the time to heat up again, the production rate re-start steadily and it was so kept until the end of the experiment. Due to the very high irradiance, a very satisfactory flow rate was finally obtained. This amounted to even 129 $\mathrm{g\,h^{-1}}$, thus more than the device's goal of 100 $\mathrm{g\,h^{-1}}$ (about a liter per day overall, considering each working day to last between the 8 and 10 hours). To state the goodness of this proof, also the salt salinities are found to be in a very acceptable range. On the other hand, not very much consideration can be done on the transient, due to the unexpected momentarily accumulation of clouds.

3.3.6 Data set 4

Data set 4 refers to a test with average irradiance of 621 W m^{-2} and wind speed of 2.26 m s^{-1}:

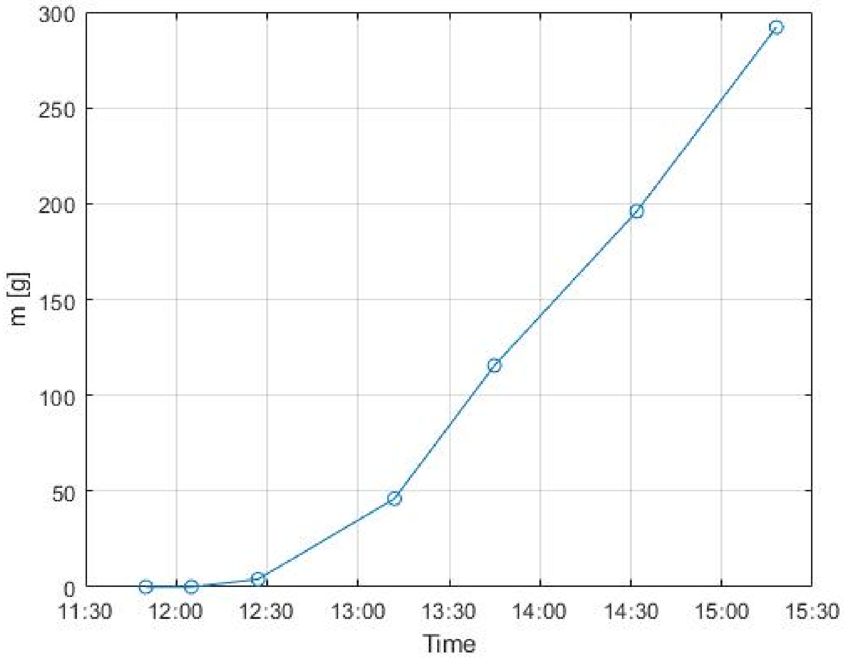

Figure 3.22: Distillate mass over time for the fourth data set experiment.

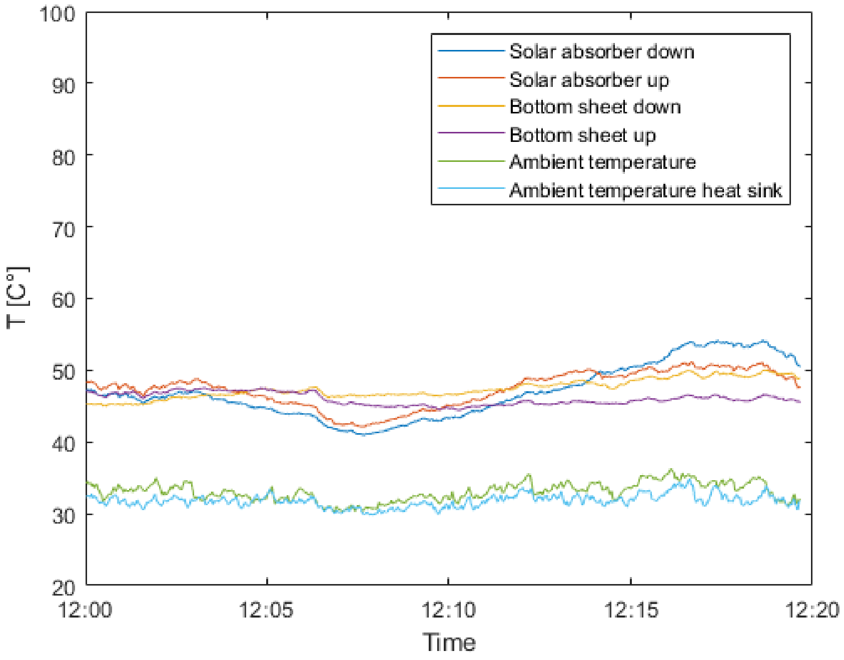

Figure 3.23: Temperatures over time for the fourth data set experiment.

[g/l]	**Before test**	**After test**
Feed water	35	/
Evaporator 1	1	39
Condenser 1	0	0
Evaporator 2	1	36
Condenser 2	0	0
Evaporator 3	1	36
Condenser 3	0	1
Brine	/	40
Distilled water	/	1

Table 3.7: Salinities in the device before and after testing for the fourth data set experiment experiment.

The fourth data set refers to an experiment executed for 4 hours and 40 minutes, from 11:50 to 16:30. In origin, this test lasted 1 hours and an half longer, but after 11:30 some external salt contamination in the produced water was found. The results belonging to this part of the experiment were then erased, and the rest of the experiment was carried on. Also in this case, the membranes were assembled by being mostly dry, in order to investigate also the transient required before freshwater production occurred. In detail, for this experiment the transient lasted about 50 minutes. Although the average irradiance registered was not as high as in the third data set, the distilled water mass production rate showed very good result. The average flow rate amounts to 117 g h^{-1}, and a peak of 129 g h^{-1} was registered between 13:12 and 13:45. Such good result may be attributed to the light wind condition, which, as already mention, allow to enhance the heat transfer through the different distillation stages. Unfortunately, temperatures data were not fully collected due to a not correct functioning of the DAQ component in the middle of the experiment; however, also from this fewer data it can be recognized how the temperature between the top and the bottom of the condenser are closer than in the other cases, thus confirming an high heat transfer within the device.

3.3.7 Data set 5

Data set 5 refers to a test with average irradiance of 598 W m^{-2} and wind speed of 1.92 m s^{-1}:

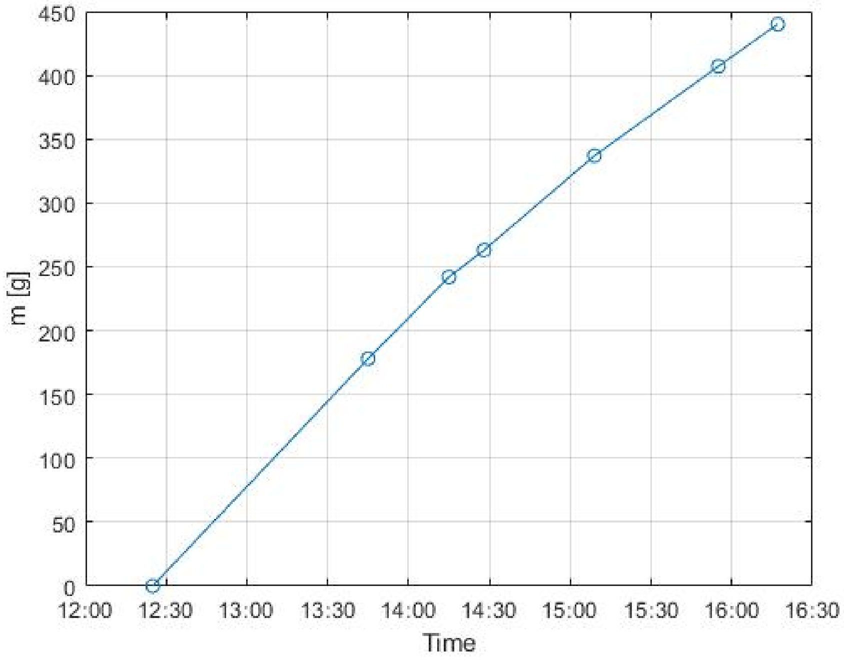

Figure 3.24: Distillate mass over time for the fifth data set experiment.

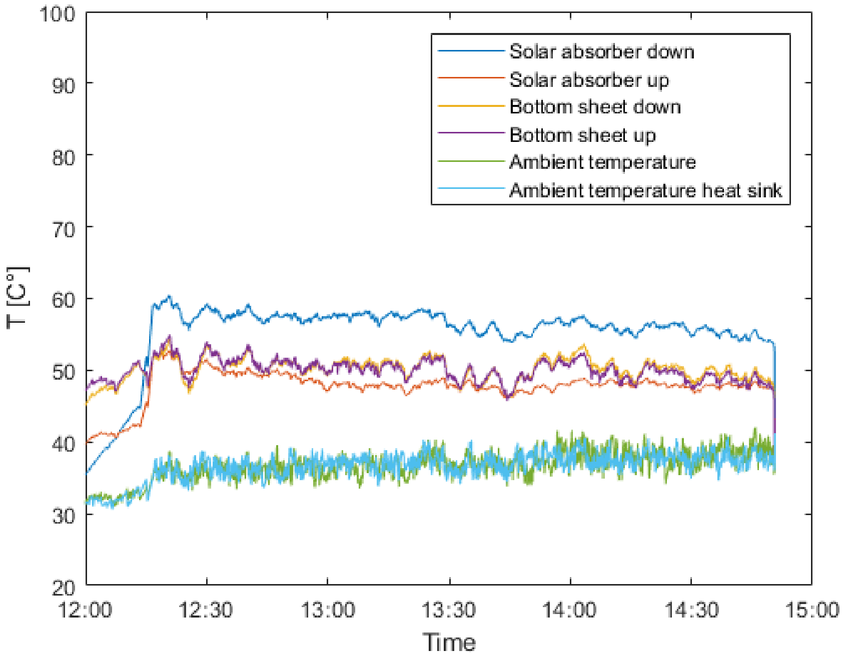

Figure 3.25: Temperatures over time for the fifth data set experiment.

[g/l]	**Before test**	**After test**
Feed water	35	/
Evaporator 1	1	33
Condenser 1	0	1
Evaporator 2	2	32
Condenser 2	0	1
Evaporator 3	4	32
Condenser 3	1	1
Brine	/	40
Distilled water	/	2

Table 3.8: Salinities in the device before and after testing for the fifth data set experiment experiment.

The fifth and last data set shown in this work refers to a test performed for 3 hours and 55 minutes, from 12:25 to 16:20. In this experiment the membranes were fully initialized, so no trace of a transient is present. For this reason, an higher initial level of salinity in the third evaporater was considered irrelevant. The second highest average irradiance detected throughout the whole experimental campaign belong to this test. An average distilled water mass flow rate of 114 g h^{-1} was measured, with a peak of 135 g h^{-1}. A reduction of the flow rate then slowly occurred, as the system slightly cooled down throughout the rest of the day. However this aspect can not fully be proven by the temperature profiles, as there were once again problems with the data acquisition system during the last hour and half of the experiment. The temperature detected at the lower side of the top layer shows an uncommon behaviour; it results lower, from the beginning, than the temperatures at the bottom. This phenomenon could be explained by the not perfect mounting of the relative thermocouple, which had probably been effected by some natural convection. Overall, the results yielded by this final test are considered very important, as they allow to further validate that a production higher than 110 g h^{-1} can be easily obtained when the proper ambient conditions are present.

3.4 Results discussion

In this section it will deeply discussed the major result yielded by this thesis and their significance. In detail, as both numerical and experimental data were successfully gathered, it results interesting to carry out a parallel analysis between the two, in order to have a fully understanding of the device potentialities and limitations.

At a first insight, to have a better understanding of the device performance, and thus of new potential inputs to future works, simulations were carried out in order to study the overall effect of the number of stages. In detail, the distilled flow rate and the temperature were analyzed in dependence of a number of stages ranging from 1 to 5. An uncertainty analysis was carried out along the model, in order to ensure the reliance of such results. To develop the previous simulations the required parameters were in fact singularly chosen, but it was proven by the experimental campaign that such variables are subjected to a wide range of perturbation during the working day. Therefore, in order to take in account their effect, upper and lower variable bounds were chosen in order to create a more accurate estimation of the performances. In detail, the variables of interest are: the convective heat transfer coefficient (h), the membrane porosity (ε_m) and the air gap present between each of the hydrophobic membranes and their respective hydrophilic layer (d_{air}). The convective heat transfer coefficient considered refers to the convection occurring between the top of the device and the ambient only; then at the bottom the coefficient was consequently approximated as the 80% of the upper case. On the edges this was left at a constant value of 3 $\mathrm{W\,m^{-2}\,K^{-1}}$, as here the heat losses are much less relevant due to the smaller area involved in the heat transfer. The convective heat transfer coefficient range was then set between 5 $\mathrm{W\,m^{-2}\,K^{-1}}$ and 15 $\mathrm{W\,m^{-2}\,K^{-1}}$, in accordance with real life wind condition. On the other hand, the porosity of the membrane was assumed to vary between 0.8, as a lower bound, and 0.9 as a upper bound; and the air gap thickness was chosen between 0.5 mm and 1 mm; these are the ranges in which the real prototype is most likely to withstand. The numerical results yielded by such considerations are exposed in figure 3.26 and figure 3.27.

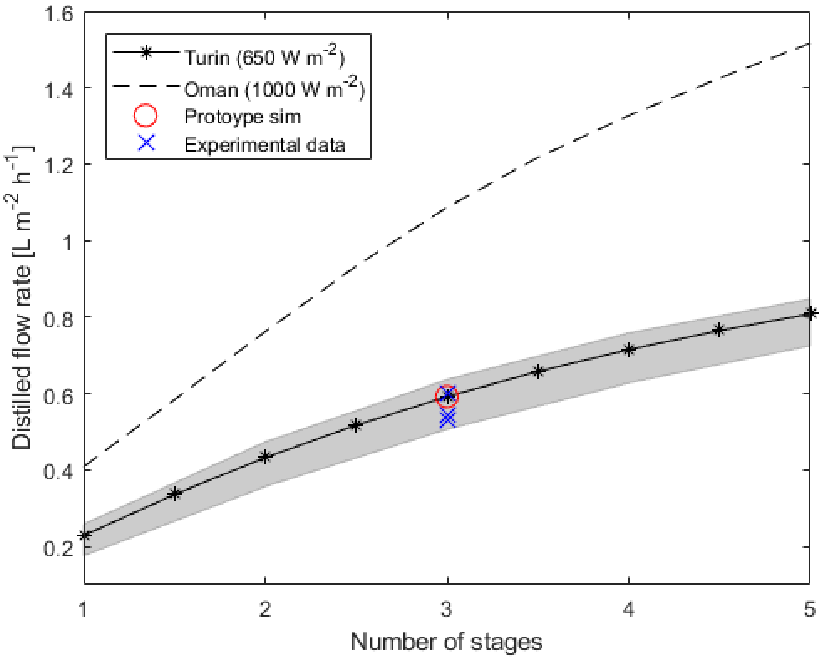

Figure 3.26: Representation of the numerical result obtained studying the distilled flow rate vs the number of stages, considering the uncertainties. The results from the experimental campaign and the foreseen performance at higher irradiance are also depicted.

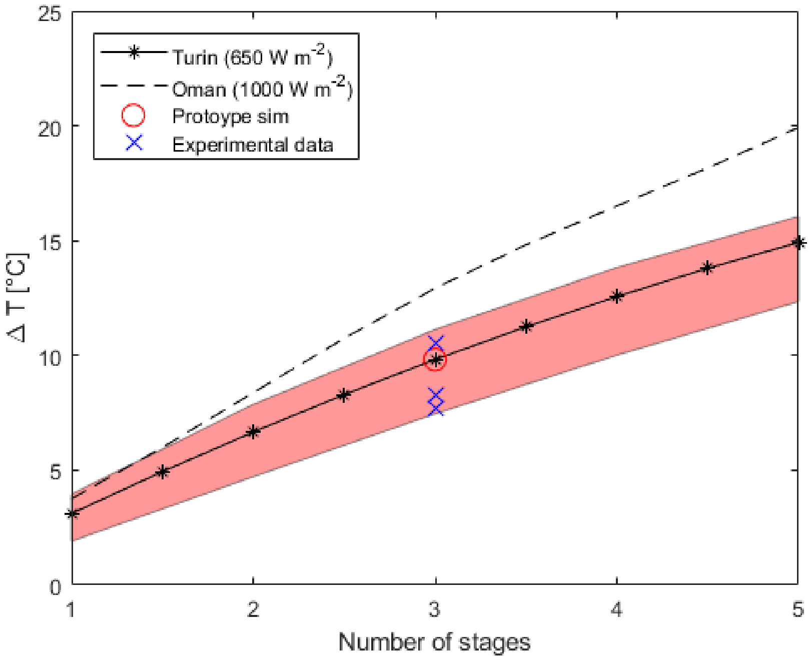

Figure 3.27: Representation of the numerical result obtained studying the temperature drop across the device height vs number of stages, considering the uncertainties. The results from the experimental campaign and the foreseen performance at higher irradiance are also depicted.

The results brought by the best tests in the experimental campaign are also depicted. As expected, they fall within the uncertainty band, thus verifying the goodness of such experiments. It is also interesting to notice the performance predicted under an higher irradiance, namely 1000 W m^{-2}. This value is chosen as it represents clear sky condition, during summer, when the sun reaches its maximum height, namely at noon, around the equator. It is then fair to assume this level of irradiance is the one most likely to be reached in countries like Oman (in principle the region where the device was supposed to work). The productivity reached under this heat flux respects the one predicted by the already developed theoretical model, namely ~1.462 L m^{-2} h^{-1}. Thanks to these results it is possible not only to appreciate the advantages brought by the multistage configuration, but also to observe the further improvements that can be easily reached by increasing the number of stages. However, it is important to keep in mind that this device is supposed to work in remote areas, and so to be most likely employed by individual users. Increasing the number of stages would then result also more unhandy, as it would follow an higher encumbrance and weight, thus making the system less suitable for this type of applications. This is also why no more then 5 stages were studied in the simulations. Therefore, a 5 stage distiller, although it should yield $J \approx 175 \pm 10$ g h^{-1}, would already weight as much as 22 *kg* when dry, 25.5 *kg* when wet; thus an high load to transport for long distances, especially by a single person.

A study concerning also the system efficiency in dependence of the number of stages was also carried out in order to better observe the gain brought by the multistage configuration. Also in this case the effect of the uncertainties was accounted in the model. Results are depicted in figure 3.28.

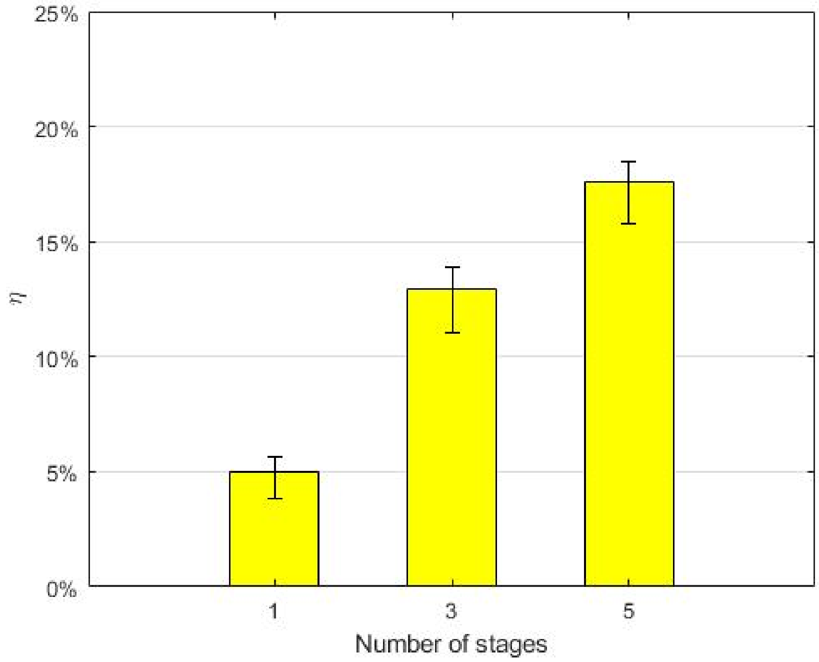

Figure 3.28: Plot of the device efficiency vs the number of stages; the effect of uncertainties is represented through the related error bars.

A 5 stages device would then work at an efficiency as high as 17.5% ± 1%. Although this value is still lower than the one yielded by the study of the smaller device, it represents a fair increase with respect the 3 stages cross-flow distiller, namely 12.9% ± 0.9%. Moreover, it is worth to highlight the efficiency computed in the best experimental tests accounted to about 12.43%, 12.53% and 13.09%. These values perfectly fall in the uncertainty range, thus once again confirming the goodnessess of such results.

Furthermore, also the effect of the membrane thickness was studied with respect to the distiller performances. Although this parameter is theoretically a constraint imposed by the membrane supplier, it was interesting to observe the level of drop in the performances, as this would on the other hand also make the membranes robuster, and thus less subjected to puncturing phenomena. Also in this study the effect of uncertainties was taken in account. Resulted are exposed in figure 3.29 and 3.30.

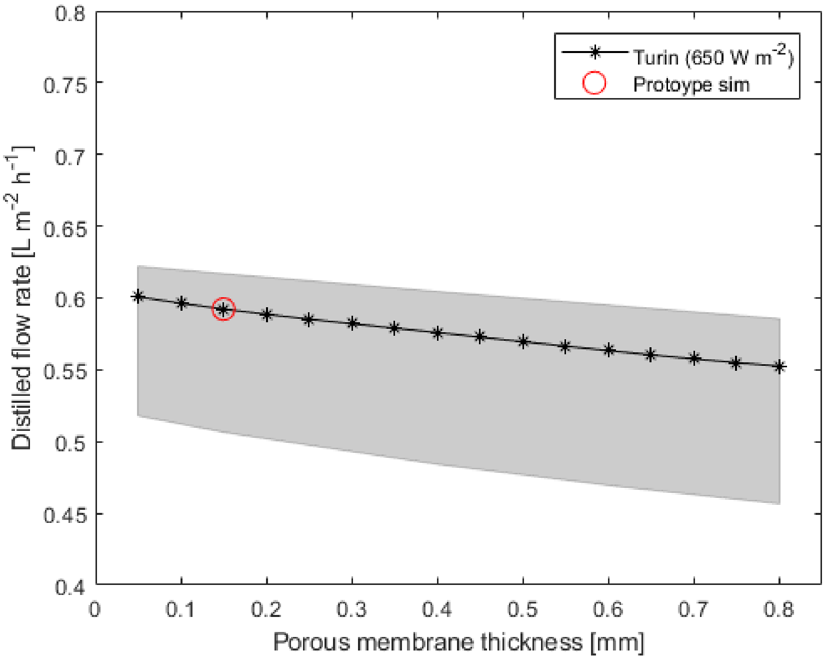

Figure 3.29: Representation of the numerical result obtained studying the distilled flow rate vs the membrane thickness.

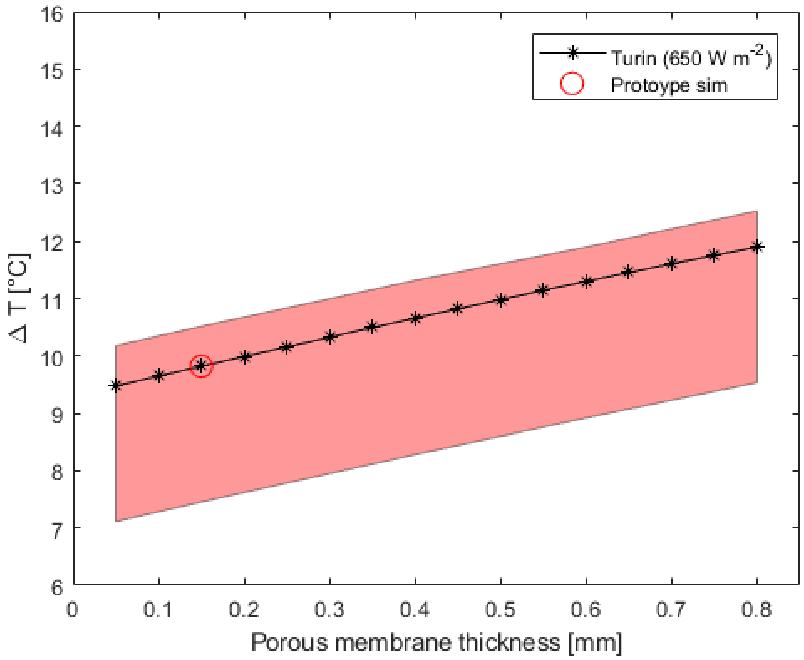

Figure 3.30: Representation of the numerical result obtained studying the temperature drop across the device height vs the membrane thickness.

Lastly, amongst the uncertainty variables, the effect of the air gap layer thickness resulted the most relevant to study. Simulations on this topic were then conducted in order to have a better understanding of the device performance dependence on this variable. The results obtained are shown in figure 3.31.

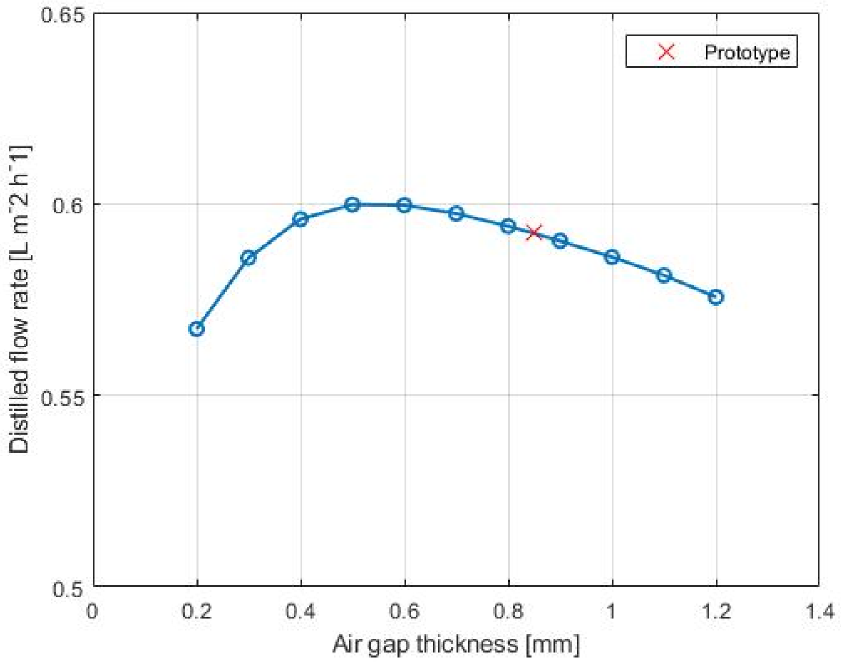

Figure 3.31: Representation of the numerical result obtained analyzing the distilled flow rate to the air gap thickness.

The function shows a maximum around 0.45 *mm*. Such behaviour was predictable, as on one side the air gap positively allows to reduce the heat loss by conduction (minimizing heat transport), on the other, the air itself acts also as a resistance, thus negatively reducing the water vapor flux (minimizing the mass transport); an optimal configuration had then to exist. In the prototype the air layer thickness amounted to about 0.85 *mm*; this parameter was in fact enforced by the constructing limitation brought in by the rubber supports. However, although this result could be exploited, the optimal air gap thickness may depend also on other parameters. Therefore, further studies should be conducted in order to have a better understanding of this phenomenon.

Chapter 4

Conclusions and future works

4.1 Conclusions

As it is every year more of a common sense, water scarcity is a fundamental problem that humanity is already facing around the world. In order to prevent droughts and crisis (and to fight the ones already occurring), the research concerning new methods to furnish freshwater is striking, mainly basing its developments on saltwater desalination. Of particular attention are the achievements lately reached in regards of the passive technologies. Two of the main drawback of desalination are in fact the high energy requirement and the environmental issue related to both the brine discharge and the energy sources exploited. Passive technology implicitly solve both of this problem, yielding in contrast lower productivity. These types of techniques are thus ideal to be employed in remote areas, where a smaller scale production is usually required. Amongst them, the *Passive solar high-yield seawater desalination by modular and low-cost distillation*, developed in Politecnico di Torino by Chiavazzo et al. is one of the most promising technology to be employed on a large scale, as it unlocks productivity levels before considered prohibitive for passive systems, by exploiting exclusively clean solar energy. The goal of this thesis was then to design, realize and test a scale-up version of the aforesaid device, in order to confirm the positive results already predicted by the theoretical model, and to eventually improve the system configuration. The design process was carried out basing it on the some guidelines imposed by a world wide desalination challenge, namely the *Oman Humanitarian Desalination Challenge*. Adopting this expedient the requirements needed to create a competitive device have been implicitly respected, these are: low cost, handled-size, easiness of use, robustness, easiness of transport, competitive distilled water production rate, passivity, water quality and possibility of short-term-use. After a successful prototyping process, the performances of the device were investigated by means of both numerical simulations and extensive experimental campaign. Results brought up by the simulations have shown a slight decrease in the specific productivity, due to the changes implemented in the scaled-up version (for instance, the cross-flow configuration), exasperated by the increased dimensions of the unit. However, the yielded results are still above the state-of-the-art performances. The consequences brought by increasing the number of stages were also numerically analyzed. A relevant gain in the system efficiency can thus be reached, but this is contrasted by the higher weight and encumbrance of the device, which would then make it less handy to be transported. In detail, the results have been analyzed also accounting for the effect related to uncertainties, such as the convective heat transfer coefficient, the porosity and the air gap layer thickness. The productivity dependence on this latter was also separately studied, thus bringing out there exist an optimal thickness for which the best performances are obtained. Results brought by the experimental campaign were instead obtained by testing the device on the rooftop of Politecnico di Torino, mainly on the month of July, employing artificially made seawater. The main quantities analyzed have been the distilled productivity, the device temperatures and the initial and final salinities. Other important parameters such as the solar irradiance and the wind speed where detected through the help of online tools such the "PVGIS" software and the "NASA Surface meteorology and Solar Energy database". The experimental set-up employed, was composed by: type-K thermocouples, DAQ, laptop, refractometer, pipette, digital scale and the modular distiller itself. A quartz light lamp and a pyranometer were also employed to carry out few indoor experiments, which however resulted unsuccessful due to the impossibility to mimic the uniformity and intensity of the sun solar irradiance. During the outdoor experimental campaign, in detail, although the device was subject to a lower direct solar irradiance than the one expected (650 W m^{-2} vs 1000 W m^{-2}), the results collected by those tests considered successful, were in accordance with the one predicted by the theoretical model. Productivity as high as 129 g h^{-1} was reached, despite the adverse condition. Numerically, it was proven that much higher productivity can be achieved when exposing the system to one sun, as it would occur in a practical test in Oman.

4.2 Future works

The optimization of other features of the device need to further be developed, by also withstanding the low cost and weight requirements, which are considered fundamental in order to realize a competitive distiller. An example, it would be to study the air gap thickness behaviour, in relation with the other device parameters, in order to find an optimal configuration to employ for the different device working conditions. Moreover, an optimal inclination of the device, should be studied, in order to increase the device performance with no increase in the device cost. The results furnished by the experimental campaign were also limited by the adverse weather condition that have been encountered during the progress of this thesis. Therefore, these results could be just considered preliminary towards a more extensive experimental campaign that would ultimately validate the in-field device tested performances. Finally, as exposed by the prediction estimated in the numerical model, it would be interesting to validate the performance of a 5-stages device. The drawbacks brought by the further increased size of the unit and its higher weight are in fact not to be considered prohibitive; they may be worth the gain that would be obtained on the device efficiency, also in perspective of slightly different type of applications.

References

[1] Colin P Kelley, Shahrzad Mohtadi, Mark A Cane, Richard Seager, and Yochanan Kushnir. Climate change in the fertile crescent and implications of the recent syrian drought. *Proceedings of the National Academy of Sciences*, 112(11):3241–3246, 2015.

[2] Rutger Willem Hofste, Paul Reig, and Leah Schleifer. Wri: 17 countries, home to one-quarter of the world's population, face extremely high water stress. https://www.wri.org/blog/2019/08/17-countries-home-one-quarter-world-population-face-extremely-high-water-stress, Aug 2019.

[3] WWAP (World Water Assessment Programme). *The United Nations World Water Development Report 4: Managing Water under Uncertainty and Risk*, volume 1. United Nations Educational, Scientific and Cultural Organization, Paris, France, 2012.

[4] Martina Floerke. The key effects of climate change. http://news.bbc.co.uk/2/hi/sci/tech/7821082.stm, Dec 2009.

[5] David Seckler, Randolph Barker, and Upali Amarasinghe. Water scarcity in the twenty-first century. *International Journal of Water Resources Development*, 15(1-2):29–42, 1999.

[6] Malin Falkenmark, Anders Berntell, Anders Jägerskog, Jan Lundqvist, Manfred Matz, and Håkan Tropp. *On the verge of a new water scarcity: a call for good governance and human ingenuity*. Stockholm International Water Institute (SIWI), 2007.

[7] Malin Falkenmark, Jan Lundqvist, and Carl Widstrand. Macro-scale water scarcity requires micro-scale approaches: Aspects of vulnerability in semi-arid development. In *Natural resources forum*, volume 13, pages 258–267. Wiley Online Library, 1989.

[8] Brian D Richter, David Abell, Emily Bacha, Kate Brauman, Stavros Calos, Alex Cohn, Carlos Disla, Sarah Friedlander O'Brien, David Hodges, Scott Kaiser, et al. Tapped out: how can cities secure their water future? *Water Policy*, 15(3):335–363, 2013.

[9] Igor A Shiklomanov. The world's water resources. In *International symposium to commemorate the*, volume 25, pages 93–105, 1991.

[10] Igor A Shiklomanov. World freshwater resources. water in crisis: A guide to the world's fresh water resources, 1993.

[11] Food and Agriculture Organization of the United Nations. *Review of World Water Resources by Country*, volume 23. FAO, Rome, Italy, 2003.

[12] Jason J Gurdak. Groundwater: Climate-induced pumping. *Nature Geoscience*, 10(2):71, 2017.

[13] Kuai Fang, Xinye Ji, Chaopeng Shen, Noel Ludwig, Peter Godfrey, Tasnuva Mahjabin, and Christine Doughty. Combining a land surface model with groundwater model calibration to assess the impacts of groundwater pumping in a mountainous desert basin. *Advances in Water Resources*, 130:12–28, 2019.

[14] Iman Janghorban Esfahani, Jouan Rashidi, Pouya Ifaei, and ChangKyoo Yoo. Efficient thermal desalination technologies with renewable energy systems: A state-of-the-art review. *Korean Journal of Chemical Engineering*, 33(2):351–387, 2016.

[15] Nikolay Voutchkov. Desalination – Past, Present and Future. *International Water Association*, Aug 2017.

[16] Sammy Roth. California's last resort: Drink the pacific. *Desert Sun*, 2015.

[17] Wei He and Jihong Wang. Feasibility study of energy storage by concentrating/desalinating water: Concentrated water energy storage. *Applied energy*, 185:872–884, 2017.

[18] Hila Frank, Eyal Rahav, and Edo Bar-Zeev. Short-term effects of swro desalination brine on benthic heterotrophic microbial communities. *Desalination*, 417:52–59, 2017.

[19] Ihsan Ullah and Mohammad G Rasul. Recent developments in solar thermal desalination technologies: A review. *Energies*, 12(1):119, 2019.

[20] Simon Gottelier. A desalination boom in california could help it deal with 'exceptional' drought. *The Guardian*, 2014.

[21] Jenny Lindblom. *Solar thermal technologies for seawater desalination: state of the art*. Luleå tekniska universitet, 2003.

[22] H Sharon and KS Reddy. A review of solar energy driven desalination technologies. *Renewable and Sustainable Energy Reviews*, 41:1080–1118, 2015.

[23] Pei Xu, Tzahi Y Cath, Alexander P Robertson, Martin Reinhard, James O Leckie, and Jörg E Drewes. Critical review of desalination concentrate management, treatment and beneficial use. *Environmental Engineering Science*, 30(8):502–514, 2013.

[24] PG Youssef, RK Al-Dadah, and SM Mahmoud. Comparative analysis of desalination technologies. *Energy Procedia*, 61:2604–2607, 2014.

[25] Pinar Cay-Durgun and Mary Laura Lind. Nanoporous materials in polymeric membranes for desalination. *Current opinion in chemical engineering*, 20:19–27, 2018.

[26] Jay R Werber, Akshay Deshmukh, and Menachem Elimelech. The critical need for increased selectivity, not increased water permeability, for desalination membranes. *Environmental Science & Technology Letters*, 3(4):112–120, 2016.

[27] PS Goh, WJ Lau, MHD Othman, and AF Ismail. Membrane fouling in desalination and its mitigation strategies. *Desalination*, 425:130–155, 2018.

[28] Manjula Nair and Dinesh Kumar. Water desalination and challenges: the middle east perspective: a review. *Desalination and Water Treatment*, 51(10-12):2030–2040, 2013.

[29] Muhammad Qasim, Mohamed Badrelzaman, Noora N Darwish, Naif A Darwish, and Nidal Hilal. Reverse osmosis desalination: A state-of-the-art review. *Desalination*, 459:59–104, 2019.

[30] J Kucera. Reverse osmosis design, processes, and applications for engineers. 2010.

[31] RM Garud, SV Kore, VS Kore, and GS Kulkarni. A short review on process and applications of reverse osmosis. *Universal Journal of Environmental Research & Technology*, 1(3), 2011.

[32] Ali Al-Karaghouli and Lawrence L Kazmerski. Energy consumption and water production cost of conventional and renewable-energy-powered desalination processes. *Renewable and Sustainable Energy Reviews*, 24:343–356, 2013.

[33] S Jamaly, NN Darwish, I Ahmed, and SW Hasan. A short review on reverse osmosis pretreatment technologies. *Desalination*, 354:30–38, 2014.

[34] Tzyy Haur Chong, Siew-Leng Loo, Anthony G Fane, and William B Krantz. Energy-efficient reverse osmosis desalination: effect of retentate recycle and pump and energy recovery device efficiencies. *Desalination*, 366:15–31, 2015.

[35] Joseph A Cotruvo. Desalination guidelines development for drinking water: Background. *Nutrients in Drinking Water*, 13, 2005.

[36] Muhammad Wakil Shahzad, Muhammad Burhan, and Kim Choon Ng. Pushing desalination recovery to the maximum limit: Membrane and thermal processes integration. *Desalination*, 416:54–64, 2017.

[37] Thomas M Missimer and Robert G Maliva. Environmental issues in seawater reverse osmosis desalination: Intakes and outfalls. *Desalination*, 434:198–215, 2018.

[38] Quantum J Wei, Ronan K McGovern, et al. Saving energy with an optimized two-stage reverse osmosis system. *Environmental Science: Water Research & Technology*, 3(4):659–670, 2017.

[39] Erica DeNicola, Omar S Aburizaiza, Azhar Siddique, Haider Khwaja, and David O Carpenter. Climate change and water scarcity: the case of saudi arabia. *Annals of global health*, 81(3):342–353, 2015.

[40] Amjad Aliewi, Essam El-Sayed, Adnan Akbar, Khaled Hadi, and Muhammad Al-Rashed. Evaluation of desalination and other strategic management options using multi-criteria decision analysis in kuwait. *Desalination*, 413:40–51, 2017.

[41] Muhammad Tauha Ali, Hassan ES Fath, and Peter R Armstrong. A comprehensive techno-economical review of indirect solar desalination. *Renewable and Sustainable Energy Reviews*, 15(8):4187–4199, 2011.

[42] Victor Yangali-Quintanilla, Zhenyu Li, Rodrigo Valladares, Qingyu Li, and Gary Amy. Indirect desalination of red sea water with forward osmosis and low pressure reverse osmosis for water reuse. *Desalination*, 280(1-3):160–166, 2011.

[43] Tzahi Y Cath, Sherwin Gormly, Edward G Beaudry, Michael T Flynn, V Dean Adams, and Amy E Childress. Membrane contactor processes for wastewater reclamation in space: Part i. direct osmotic concentration as pretreatment for reverse osmosis. *Journal of Membrane Science*, 257(1-2):85–98, 2005.

[44] Khaled Touati, Fernando Tadeo, and Hamza Elfil. Osmotic energy recovery from reverse osmosis using two-stage pressure retarded osmosis. *Energy*, 132:213–224, 2017.

[45] Jennifer Leijon and Cecilia Boström. Freshwater production from the motion of ocean waves–a review. *Desalination*, 435:161–171, 2018.

[46] Mark Wilf and Craig Bartels. Optimization of seawater ro systems design. *Desalination*, 173(1):1–12, 2005.

[47] Noreddine Ghaffour, Thomas M Missimer, and Gary L Amy. Technical review and evaluation of the economics of water desalination: current and future challenges for better water supply sustainability. *Desalination*, 309:197–207, 2013.

[48] Ammar Alsheghri, Saad Asadullah Sharief, Shahid Rabbani, and Nurzhan Z Aitzhan. Design and cost analysis of a solar photovoltaic powered reverse osmosis plant for masdar institute. *Energy Procedia*, 75:319–324, 2015.

[49] Ibrahim S Al-Mutaz and Abdullah M Al-Namlah. Characteristics of dual purpose msf desalination plants. *Desalination*, 166:287–294, 2004.

[50] Dhananjay Mishra. Desalination for cost-effective water production. *Advisian Worley Group*, 2017.

[51] Mohammad Abdul-Kareem Al-Sofi. Fouling phenomena in multi stage flash (msf) distillers. *Desalination*, 126(1-3):61–76, 1999.

[52] Lourdes Garcia-Rodriguez and Carlos Gomez-Camacho. Conditions for economical benefits of the use of solar energy in multi-stage flash distillation. *Desalination*, 125(1-3):133–138, 1999.

[53] Ali M El-Nashar. Cogeneration for power and desalination—state of the art review. *Desalination*, 134(1-3):7–28, 2001.

[54] Yousef Al-Wazzan and Faisal Al-Modaf. Seawater desalination in kuwait using multi-stage flash evaporation technology—historical overview. *Desalination*, 134(1-3):257–267, 2001.

[55] Junjie Zhao, Minghui Wang, Haitham MS Lababidi, Hamad Al-Adwani, and Karen K Gleason. A review of heterogeneous nucleation of calcium carbonate and control strategies for scale formation in multi-stage flash (msf) desalination plants. *Desalination*, 442:75–88, 2018.

[56] OK Buros. *The ABCs of desalting*. International Desalination Association Topsfield, MA, 2000.

[57] Ruh Ullah, Majeda Khraisheh, Richard J Esteves, James T McLeskey Jr, Mohammad AlGhouti, Mohamed Gad-el Hak, and H Vahedi Tafreshi. Energy efficiency of direct contact membrane distillation. *Desalination*, 433:56–67, 2018.

[58] David Warsinger, Karan Mistry, Kishor Nayar, Hyung Chung, V Lienhard, et al. Entropy generation of desalination powered by variable temperature waste heat. *Entropy*, 17(11):7530–7566, 2015.

[59] Kim Choon Ng, Kyaw Thu, Seung Jin Oh, Li Ang, Muhammad Wakil Shahzad, and Azhar Bin Ismail. Recent developments in thermally-driven seawater desalination: Energy efficiency improvement by hybridization of the med and ad cycles. *Desalination*, 356:255–270, 2015.

[60] Muhammad Wakil Shahzad, Kim Choon Ng, Kyaw Thu, Bidyut Baran Saha, and Won Gee Chun. Multi effect desalination and adsorption desalination (medad): a hybrid desalination method. *Applied Thermal Engineering*, 72(2):289–297, 2014.

[61] Ali A Al-Karaghouli and LL Kazmerski. Renewable energy opportunities in water desalination. *Desalination, Trends and Technologies*, pages 149–184, 2011.

[62] Hui Tong Chua and Bijan Rahimi. *Low Grade Heat Driven Multi-effect Distillation and Desalination*. Elsevier, 2017.

[63] Ibrahim S Al-Mutaz and Irfan Wazeer. Current status and future directions of med-tvc desalination technology. *Desalination and Water Treatment*, 55(1):1–9, 2015.

[64] Tongwen Xu and Chuanhui Huang. Electrodialysis-based separation technologies: a critical review. *AIChE journal*, 54(12):3147–3159, 2008.

[65] Inamuddin. *Applications of Adsorption and Ion Exchange Chromatography in Waste Water Treatment*. Materials Research Forum LLC, 2017.

[66] ASTOM Corporation. About electrodyalisis reversal. http://www.astom-corp.jp/en/product/04.html, 2013.

[67] Fernando Valero, Angel Barceló, and Ramón Arbós. Electrodialysis technology-theory and applications. In *Desalination, trends and technologies*. IntechOpen, 2011.

[68] Kevin Westerling. Ed vs. ro: The benefits of electrodialysis for desalination, 2015.

[69] GJ Doornbusch, M Tedesco, JW Post, Z Borneman, and K Nijmeijer. Experimental investigation of multistage electrodialysis for seawater desalination. *Desalination*, 464:105–114, 2019.

[70] R Singh. Chapter 5-design, energy and cost analyses of membrane processes. *Membrane Technology and Engineering for Water Purification*, pages 339–368, 2015.

[71] Fourth Edition. Guidelines for drinking-water quality. *WHO chronicle*, 38(4):104–8, 2011.

[72] Robert A Johnson and Minh H Nguyen. *Understanding membrane distillation and osmotic distillation*. John Wiley & Sons, 2017.

[73] Lies Eykens, Kristien De Sitter, Chris Dotremont, Luc Pinoy, and Bart Van der Bruggen. How to optimize the membrane properties for membrane distillation: a review. *Industrial & Engineering Chemistry Research*, 55(35):9333–9343, 2016.

[74] Abdulaziz M Alklaibi and Noam Lior. Membrane-distillation desalination: status and potential. *Desalination*, 171(2):111–131, 2005.

[75] Andrea Cipollina and Giorgio Micale. Coupling sustainable energy with membrane distillation processes for seawater desalination. In *2010 1st International Nuclear & Renewable Energy Conference (INREC)*, pages 1–6. IEEE, 2010.

[76] Chennan Li, Yogi Goswami, and Elias Stefanakos. Solar assisted sea water desalination: A review. *Renewable and Sustainable Energy Reviews*, 19:136–163, 2013.

[77] Jean-Pierre Mericq, Stéphanie Laborie, and Corinne Cabassud. Evaluation of systems coupling vacuum membrane distillation and solar energy for seawater desalination. *Chemical Engineering Journal*, 166(2):596–606, 2011.

[78] Mohammadali Baghbanzadeh, Dipak Rana, Christopher Q Lan, and Takeshi Matsuura. Zero thermal input membrane distillation, a zero-waste and sustainable solution for freshwater shortage. *Applied energy*, 187:910–928, 2017.

[79] Fawzi Banat and Nesreen Jwaied. Economic evaluation of desalination by small-scale autonomous solar-powered membrane distillation units. *Desalination*, 220(1-3):566–573, 2008.

[80] N Akther, A Sodiq, A Giwa, S Daer, HA Arafat, and SW Hasan. Recent advancements in forward osmosis desalination: a review. *Chemical Engineering Journal*, 281:502–522, 2015.

[81] Muhammad Qasim, Naif A Darwish, Sarper Sarp, and Nidal Hilal. Water desalination by forward (direct) osmosis phenomenon: A comprehensive review. *Desalination*, 374:47–69, 2015.

[82] Akshay Deshmukh, Ngai Yin Yip, Shihong Lin, and Menachem Elimelech. Desalination by forward osmosis: Identifying performance limiting parameters through module-scale modeling. *Journal of membrane science*, 491:159–167, 2015.

[83] OASYS Water. Clearflo membrane brine concentrator. http://oasyswater.com/solutions/technology/, 2019.

[84] Tai-Shung Chung, Sui Zhang, Kai Yu Wang, Jincai Su, and Ming Ming Ling. Forward osmosis processes: yesterday, today and tomorrow. *Desalination*, 287:78–81, 2012.

[85] Ming Ming Ling, Kai Yu Wang, and Tai-Shung Chung. Highly water-soluble magnetic nanoparticles as novel draw solutes in forward osmosis for water reuse. *Industrial & Engineering Chemistry Research*, 49(12):5869–5876, 2010.

[86] Hasan F Makki, Majid I Abdul Wahab, and Rana Raheem Said. Forward osmosis process for the treatment of wastewater from textile industries. *Journal of Engineering*, 19(12):1557–1565, 2013.

[87] Bruce E Logan and Menachem Elimelech. Membrane-based processes for sustainable power generation using water. *Nature*, 488(7411):313, 2012.

[88] Voltaire Sant'Anna, Ligia Damasceno Ferreira Marczak, and Isabel Cristina Tessaro. Membrane concentration of liquid foods by forward osmosis: process and quality view. *Journal of Food Engineering*, 111(3):483–489, 2012.

[89] PP Bhatt. Osmotic drug delivery systems for poorly water soluble drugs, pharmaventures ltd, 2004.

[90] Tzahi Y Cath, Amy E Childress, and Menachem Elimelech. Forward osmosis: principles, applications, and recent developments. *Journal of membrane science*, 281(1-2):70–87, 2006.

[91] Yiben Gao, Yi-Ning Wang, Weiyi Li, and Chuyang Y Tang. Characterization of internal and external concentration polarizations during forward osmosis processes. *Desalination*, 338:65–73, 2014.

[92] R Valladares Linares, Z Li, V Yangali-Quintanilla, N Ghaffour, G Amy, T Leiknes, and Johannes S Vrouwenvelder. Life cycle cost of a hybrid forward osmosis–low pressure reverse osmosis system for seawater desalination and wastewater recovery. *Water research*, 88:225–234, 2016.

[93] Sameer Tadros. Desalination plant integration with cogeneration systems for eor/commercial/industrial applications. *Desalination*, 87(1-3):137–147, 1992.

[94] Or Rabinowitz. Nuclear energy and desalination in israel. *Bulletin of the Atomic Scientists*, 72(1):32–38, 2016.

[95] Faisal Mandani, Hisham Ettouney, and Hisham El-Dessouky. Libr h2o absorption heat pump for single-effect evaporation desalination process. *Desalination*, 128(2):161–176, 2000.

[96] Akili D Khawaji, Ibrahim K Kutubkhanah, and Jong-Mihn Wie. Advances in seawater desalination technologies. *Desalination*, 221(1-3):47–69, 2008.

[97] Mahmoud Shatat and Saffa B Riffat. Water desalination technologies utilizing conventional and renewable energy sources. *International Journal of Low-Carbon Technologies*, 9(1):1–19, 2012.

[98] Mohammad Shafiur Rahman, Mushtaque Ahmed, and X Dong Chen. Freezing-melting process and desalination: I. review of the state-of-the-art. *Separation & Purification Reviews*, 35(02):59–96, 2006.

[99] Toshikatsu Sata. *Ion exchange membranes: preparation, characterization, modification and application*. Royal Society of chemistry, 2007.

[100] Merck KGaA. Water in the laboratory - ion exchange. http://www.merckmillipore.com/IT/it/water-purification/learning-centers/tutorial/purification-techniques/ion-exchange/Y2eb.qB.k.EAAAFAw5twFMvS,nav?ReferrerURL =https%3A%2F%2Fwww.google.com%2F, 2019.

[101] George M Ayoub and Lilian Malaeb. Developments in solar still desalination systems: A critical review. *Critical reviews in environmental science and technology*, 42(19):2078–2112, 2012.

[102] Hiroshi Tanaka and Koji Iishi. Experimental study of a vertical single-effect diffusion solar still coupled with a tilted wick still. *Desalination*, 402:19–24, 2017.

[103] Amimul Ahsan, M Imteaz, Ukwuani A Thomas, M Azmi, Ataur Rahman, and NN Nik Daud. Parameters affecting the performance of a low cost solar still. *Applied energy*, 114:924–930, 2014.

[104] Angela Hausmann, Peter Sanciolo, Todor Vasiljevic, Mike Weeks, and Mikel Duke. Integration of membrane distillation into heat paths of industrial processes. *Chemical engineering journal*, 211:378–387, 2012.

[105] Tsung-Ching Chen and Chii-Dong Ho. Immediate assisted solar direct contact membrane distillation in saline water desalination. *Journal of Membrane Science*, 358(1-2):122–130, 2010.

[106] L Martinez-Diez and Mi I Vazquez-Gonzalez. Temperature and concentration polarization in membrane distillation of aqueous salt solutions. *Journal of membrane science*, 156(2):265–273, 1999.

[107] Pratiksha D Dongare, Alessandro Alabastri, Seth Pedersen, Katherine R Zodrow, Nathaniel J Hogan, Oara Neumann, Jinjian Wu, Tianxiao Wang, Akshay Deshmukh, Menachem Elimelech, et al. Nanophotonics-enabled solar membrane distillation for off-grid water purification. *Proceedings of the National Academy of Sciences*, 114(27):6936–6941, 2017.

[108] Xiuqiang Li, Weichao Xu, Mingyao Tang, Lin Zhou, Bin Zhu, Shining Zhu, and Jia Zhu. Graphene oxide-based efficient and scalable solar desalination under one sun with a confined 2d water path. *Proceedings of the National Academy of Sciences*, 113(49):13953–13958, 2016.

[109] Danil W Boukhvalov, Mikhail I Katsnelson, and Young-Woo Son. Origin of anomalous water permeation through graphene oxide membrane. *Nano letters*, 13(8):3930–3935, 2013.

[110] Andrej Lenert and Evelyn N Wang. Optimization of nanofluid volumetric receivers for solar thermal energy conversion. *Solar Energy*, 86(1):253–265, 2012.

[111] Todd P Otanicar, Patrick E Phelan, Ravi S Prasher, Gary Rosengarten, and Robert A Taylor. Nanofluid-based direct absorption solar collector. *Journal of renewable and sustainable energy*, 2(3):033102, 2010.

[112] Hadi Ghasemi, George Ni, Amy Marie Marconnet, James Loomis, Selcuk Yerci, Nenad Miljkovic, and Gang Chen. Solar steam generation by heat localization. *Nature communications*, 5:4449, 2014.

[113] Eliodoro Chiavazzo, Matteo Morciano, Francesca Viglino, Matteo Fasano, and Pietro Asinari. Passive solar high-yield seawater desalination by modular and low-cost distillation. *Nature Sustainability*, 1(12):763, 2018.

[114] Peter H Gleick. Basic water requirements for human activities: meeting basic needs. *Water international*, 21(2):83–92, 1996.

[115] GoodFellow. Online catalogue. http://www.goodfellow.com/E/Polyethylene-Low-Density.html.

[116] Bruce E Poling, John M Prausnitz, John P O'connell, et al. *The properties of gases and liquids*, volume 5. Mcgraw-hill New York, 2001.

[117] Mohamed Khayet and Takeshi Matsuura. *Membrane distillation: principles and applications*. Elsevier, 2011.

[118] Kevin W Lawson and Douglas R Lloyd. Membrane distillation. *Journal of membrane Science*, 124(1):1–25, 1997.

[119] M Maroof Khan and M Jamil Ahmad. Estimation of global solar radiation using clear sky radiation in yemen. *Journal of Engineering Science & Technology Review*, 5(2), 2012.

Acknowledgments

In these few lines i would like to thank all the people that allowed and contributed, directly or not, to work of this thesis.

In the first place, I would like to thank my academic supervisor, Prof. Pietro Asinari, that gave me the chance to work to this project, which i have enjoyed so much. I would like also to thank my research advisor, Dr. Matteo Morciano, which has guided me throughout the whole preparation of this work. Its help and availability have been extremely important to me in order to progress towards always more satisfying results.

Huge gratitude goes to my family, they are the foundation of the person i am today. They have always to guide me towards becoming a better person. They supported and respected all my decisions and this has been of extremely importance to me throughout the years. I owe you everything.

Thank you to my all my friends, closer and further. Thank you to the "xXx", the guys who have been been like a second family to me since I was 13. Thank you to the "Torino is the new Palermo", the people which have lived next to me all the joys and sorrows that this master degree has brought along. Thank you to all my friends in Palermo, which have always supported me also from far. Thank you to all the guys from Maidstone, you accompanied me during one of the most important year of my life. Thank you to the people from UIUC for letting me live such a different and amazing year oversea that greatly contributed to my professional and human formation.

This work could have never be done without your support, thank you.